

Development of Low-Cost Sensors for Structural Health Monitoring Applications

Doctoral thesis performed by:
[Seyedmilad Komarizadehasl](#)

Directors:
[Prof. Dr. Jose Turmo Coderque](#)
[Prof. Dr. Jose-Antonio Lozano Galant](#)

Doctoral program:
[Construction engineering](#)

Barcelona, Spain [October 2022](#)



UNIVERSITAT POLITÈCNICA DE CATALUNYA
BARCELONATECH
Departamento de Ingeniería Civil y Ambiental

DoctoralThesis



UNIVERSITAT POLITÈCNICA
DE CATALUNYA
BARCELONATECH

PhD program in Construction Engineering

Development of Low-Cost Sensors for Structural Health Monitoring Applications

Doctoral thesis by:

Syedmilad Komarizadehasl

Thesis advisor:

Jose Turmo, Jose Antonio Lozano

Department of Civil and Environmental Engineering

Barcelona, October 2022

Dedication

Acknowledgments

I want to express my most gratitude and respect to my supervisors, professor Jose Turmo and Jose Antonio Lozano-Galant, who fully trusted my research and provided me with the needed material, knowledge, and guidance throughout my doctorate. In addition, they supervised and helped me in every single step of my thesis.

I would also like to show appreciation to my parents, who believed in me and sent me to another country to pursue a better life and satisfy my research admissions. Furthermore, I must express my profound gratitude toward my girlfriend, Gabriela Beug, who stood beside me in times of despair and gave me self-belief, courage and hope. Finally, I would like to extend thanks to engineer Pierre Huguenet for helping me with the operational modal analysis of bridges.

A special thanks to Mr. Tomas Garcia, the director of the "Lluís Agulló" Laboratory from the Technical University of Catalonia (UPC), for aiding in calibrating the hydraulic jack and for his assistance throughout this project. I want to say a special thank you to Dr. Nirvan Makoond for helping with the experimental laboratory analysis. A special thanks to my research assistant, Mahyad Komary, who helped me with my research. Finally, I would like to thank my collages Behnam Mobaraki, Dr. Tian Peng, Edison Atencio, and Josep Farrèl, who collaborated with me on several projects resulting in several publications.

This work was funded by the Spanish Ministry of Economy and Competitiveness provided through the research project BIA2013-47290-R, BIA2017-86811-C2-1-R directed by José Turmo and BIA2017-86811-C2-2-R. All these projects were funded with FEDER funds. The author is also indebted to Spanish Agencia Estatal de Investigación del Ministerio de Ciencia Innovación y Universidades grant and the Fondo Social Europeo grant (PRE2018-083238).

Abstract

There is increasing interest in developing low-cost sensors for economical structural health monitoring of civil engineering infrastructures. In addition to their price, they have the additional benefit of being easily connected to low-cost microcontrollers such as Arduino. A reliable data acquisition system based on Arduino technology can further lower the cost of data collection and monitoring, enabling long-term monitoring at an affordable cost. This thesis proposes the following four high-precision low-cost monitoring systems.

Firstly, to correctly measure structural responses, a **Cost Hyper-Efficient Arduino Product (CHEAP)** has been developed. CHEAP is a system made up of five synchronized accelerometers connected to an Arduino microcontroller that works as a data collecting device. CHEAP is a uniaxial MEMS accelerometer with a sampling frequency of 85 Hz. To validate its performance, laboratory experiments were carried out and the results were compared with those of two high-precision accelerometers (PCB393A03 and PCB 356B18).

Secondly, a unique low-cost inclinometer is presented, the **Low-cost Adaptable Reliable Angle-meter (LARA)**, which measures inclination through the fusion of different sensors: five gyroscopes and five accelerometers. LARA combines a microcontroller based on Internet of Things technology (NODEMCU), allows wireless data transmission, and free commercial software for data collection (SerialPlot). To confirm the precision and resolution of this device, its measurements under laboratory conditions were compared with the theoretical ones and with those of a commercial inclinometer (HI-INC). Laboratory results of a load test on a beam demonstrate LARA's remarkable accuracy. It is concluded that the accuracy of LARA is sufficient for its application in detecting bridge damage.

Thirdly, **the effect of combining similar range sensors** to investigate the increase of the accuracy and mitigation of the ambient noises, is also elucidated. To investigate the sensor combination theory, a measuring equipment composed of 75 contactless ranging sensors controlled by only two microcontrollers (Arduinos), was built. The 75 sensors are 25 HC-SR04 (analog), 25 VL53L0X (digital), and 25 VL53L1X (digital). In addition, the impact of various environmental conditions on the standard deviation, distribution functions, and error level of these sensors (HC-SR04, VL53L0X, and VL53L1X) is determined.

Finally, **a novel remote versatile data acquisition system** is presented that allows the recording of time with microsecond resolution for the subsequent synchronization of the acquired data of the wireless sensors located at various points of a structure. This functionality is what would allow its application to static or quasi-static load tests or to the modal analysis of structures. The system developed has a noise density of 51 g/Hz and a sampling frequency of 333 Hz. This device was used to identify the eigenfrequencies and modal analysis of several structures (polvorín footbridges in Barcelona and Andoain Bridge, Donostia-San Sebastian). The comparison of the modal analysis of the Andoain Bridge using the acquired data of the developed accelerometer and data acquisition equipment with those of commercial accelerometers (PCB 607A61) were satisfactory.

The low-cost accelerometer, inclinometer and data acquisition system developed and validated in this thesis can make SHM and infrastructure damage detection a reality at low cost, long term and remotely.

IX

Keywords: Low-cost sensors, Operational Modal analysis, Arduino, Raspberry, post synchronization.

Resumen

Cada vez hay más interés en desarrollar sensores baratos para conocer de manera económica el estado de las infraestructuras civiles. Además de su precio, estos sensores tienen la ventaja añadida de poder conectarse fácilmente a microcontroladores de bajo coste como Arduino. Un sistema fiable de adquisición de datos basado en la tecnología Arduino puede disminuir aún más el coste de la recogida de datos y la monitorización, lo que permitiría una monitorización a largo plazo a un coste asequible. Esta tesis propone los cuatro siguientes sistemas de monitorización de alta precisión y bajo coste.

En primer lugar, para medir correctamente las respuestas estructurales, se ha desarrollado el **Cost Hyper-Efficient Arduino Product (CHEAP)**. CHEAP es un sistema compuesto por cinco acelerómetros sincronizados de bajo coste conectados a un microcontrolador Arduino que hace el papel de dispositivo de recogida de datos. CHEAP es un acelerómetro MEMS uniaxial con una frecuencia de muestreo de 85 Hz. Para validar su rendimiento, se efectuaron unos experimentos de laboratorio y sus resultados se compararon con los de dos acelerómetros de alta precisión (PCB393A03 y PCB 356B18).

En segundo lugar, se presenta un inclinómetro de bajo coste, un **Low-cost Adaptable Reliable Angle-meter (LARA)**, que mide la inclinación mediante la fusión de distintos sensores: cinco giroscopios y cinco acelerómetros. LARA combina un microcontrolador basado en la tecnología del Internet de las Cosas (NODEMCU), que permite la transmisión inalámbrica de datos, y un software comercial gratuito para la recogida de datos (SerialPlot). Para confirmar la precisión y resolución de este dispositivo, se compararon sus mediciones en condiciones de laboratorio con las teóricas y con las de un inclinómetro comercial (HI-INC). Los resultados de laboratorio de una prueba de carga en una viga demuestran la notable precisión de LARA. Se concluye que la precisión de LARA es suficiente para su aplicación en la detección de daños en puentes.

En tercer lugar, también se dilucida el **efecto de la combinación de sensores de rango similar** para investigar el aumento de la precisión y la mitigación de los ruidos ambientales. Para investigar la teoría de la combinación de sensores, se construyó un equipo de medición compuesto por 75 sensores para la medición de distancias acoplados a dos microcontroladores de Arduino. Los 75 sensores son 25 HC-SR04 (analógicos), 25 VL53L0X (digitales) y 25 VL53L1X (digitales). Además, se determina el impacto de diversas condiciones ambientales en la desviación estándar, las funciones de distribución y el nivel de error de estos sensores.

Por último, se presenta un novedoso y versátil **sistema de adquisición de datos a distancia** que permite el registro del tiempo con una resolución de microsegundos para la sincronización posterior de las lecturas de los sensores inalámbricos situados en diversos puntos de una estructura. Esta funcionalidad es lo que permitiría su aplicación a pruebas de carga estáticas o quasi-estáticas o al análisis modal de las estructuras. El sistema desarrollado tiene una densidad de ruido de 51 g/Hz y una frecuencia de muestreo de 333 Hz. Este dispositivo se utilizó para identificar las frecuencias propias y los modos de vibración de varias estructuras (pasarela polvorín en Barcelona y Puente de Andoain, Donostia-San Sebastian). Los modos calculados en una de ellas, el Puente de Andoain, a partir de los datos obtenidos con el acelerómetro y sistema de adquisición de datos desarrollado se comparan satisfactoriamente con los de sensores comerciales (PCB 607A61).

XI

El acelerómetro, el inclinómetro y el sistema de adquisición de datos de bajo coste desarrollados y validados en esta tesis pueden hacer realidad la SHM y la detección de daños en infraestructuras a bajo coste, a largo plazo y de forma remota.

Palabras clave: Sensores de bajo coste, análisis modal, Arduino, Raspberry, post-sincronización.

TABLE OF CONTENTS

Chapter 1 Introduction	1
1.1 MOTIVATION	1
1.2 OBJECTIVES	3
1.3 THESIS ORGANIZATION	4
1.4 METHODOLOGY	5
Chapter 2 : State of the art	7
2.1 STRUCTURAL HEALTH MONITORING	7
2.1.1 ACCELEROMETERS	9
2.1.2 INCLINOMETERS	14
2.1.3 NONCONTACT DISTANCE MEASURING SENSORS	15
2.1.4 LOW-COST MICROCONTROLLERS	18
2.2 THE GAPS DETECTED AND PROPOSED SOLUTIONS.	23
Chapter 3 : Development and laboratory validation of a Low-Cost System for the Accurate Measurement of Structural Vibrations	26
3.1 INTRODUCTION	26
3.2 SIGNAL ACQUISITION AND PROCESSING SYSTEM	26
3.3 A COST HYPER-EFFICIENT ARDUINO PRODUCT (CHEAP)	26
3.4 CONTROL SYSTEMS DESCRIPTION	30
3.5 LABORATORY TEST AND RESULTS	33
3.5.1 LABORATORY TEST	33
3.5.2 RESULTS AND DISCUSSIONS	35
Chapter 4 : A Novel Wireless Low-Cost Inclinometer Made from Combining the Measurements of Multiple MEMS Gyroscopes and Accelerometers	44
4.1 INTRODUCTION	44
4.2 CONTROL SYSTEM AND THE PROPOSED INCLINOMETER	44
4.2.1 LOW-COST ADAPTABLE RELIABLE ANGLE-METER (LARA) SYSTEM	44
4.2.2 CONTROL SYSTEM DESCRIPTION	48
4.3 STATISTICAL REPRESENTATION OF COMBINING DYNAMIC-SENSOR THEORY	49
4.3.1 NOISE REDUCTION OF INCLINOMETERS	49
4.3.2 STUDY OF ALLAN VARIANCE	51

XIII		
4.4	LABORATORY EXPERIMENTS	52
4.4.1	ACCURACY EVALUATION	52
4.4.2	COMBINATORY ANALYSIS	54
4.4.3	LARA RESOLUTION AND ACCURACY VERIFICATION	56
Chapter 5 : Low-Cost Sensors Accuracy Study and Enhancement Strategy		60
5.1	INTRODUCTION	60
5.2	MATERIAL AND METHOD	60
5.2.1	LOW-COST DISTANCE SENSOR	61
5.2.2	MICROCONTROLLER SECTION AND DATA ACQUISITION	62
5.2.3	CONSTRUCTION OF THE MEASUREMENT DEVICE	63
5.3	LABORATORY VALIDATION	66
5.4	RESULT AND DISCUSSION	67
5.4.1	ERROR RECOGNITION	67
5.4.2	BENEFICIAL EFFECT OF COMBINING SIMILAR SENSORS	70
5.4.3	EFFECT OF COUPLED SIMILAR SENSORS	72
5.4.4	STATISTICAL EVALUATION	77
Chapter 6 : Low-Cost Wireless Structural Health Monitoring of Bridges		88
6.1	INTRODUCTION	88
6.2	TRIAXLE WIRELESS LOW-COST ADAPTABLE RELIABLE ACCELEROMETER (LARA) WITH THE POST-SYNCHRONIZATION CAPABILITY	88
6.3	LABORATORY TESTS AND RESULTS	92
6.3.1	SENSITIVITY, ND AND RESOLUTION EVALUATION	94
6.3.2	FREQUENCY VALIDATION	98
6.3.3	ACCELERATION AMPLITUDE VALIDATION	101
6.4	REAL STRUCTURE TEST AND RESULTS	105
6.4.1	EIGENFREQUENCY VALIDATION OF A FOOTBRIDGE	105
6.4.2	MODAL ANALYSIS VALIDATION OF A BRIDGE	109
Chapter 7 : Conclusions and future research		114
7.1	CONCLUSIONS	114
7.2	FUTURE STEPS	116
7.3	RELATED WORKS AND PUBLICATIONS	117

XIV	
Bibliography	122
<hr/>	
Appendix 1: Publications	136

LIST OF TABLES

Table 2-1. Summary of the characteristics of the accelerometers commonly used in the literature. _____	11
Table 2-2. Some of the low-cost vibration acquisition applications of the civil engineering literature. _____	13
Table 2-3. Characteristics of some of the commercially available inclinometers. _____	15
Table 2-4. Specifications of different low-cost range sensors. _____	17
Table 2-5. Characteristics of the Arduino products _____	20
Table 2-6. Characteristics of several Raspberry Pi products. _____	22
Table 3-1. Characteristics of introduced Waves. _____	34
Table 3-2. Frequency extracted from the acquired accelerometers together with their error. ___	36
Table 3-3. Amplitudes extracted from the accelerometers together with their error. _____	37
Table 3-4. Price comparison of the three systems _____	41
Table 4-1. Accuracy comparison of LARA with HI-INC. _____	53
Table 4-2. Comparing the inclination estimation of LARA and HI-INC _____	57
Table 5-1. Characteristics of the performed tests. _____	67
Table 5-2. The normalized values of similar sensors. _____	69
Table 5-3. Statistical analysis of VL53L0X for tests with ambient light. _____	78
Table 5-4. Statistical analysis of VL53L0X for tests with no excessive ambient light. _____	79
Table 5-5. Statistical analysis of VL53L1X for tests with ambient light. _____	81
Table 5-6. Statistical analysis of VL53L1X for tests with no excessive ambient light. _____	83
Table 5-7. Statistical analysis of HC-SR04 values. _____	86
Table 5-8. price comparison of the devices made from coupled sensors. _____	86
Table 6-1. comparison of commercial triaxial MEMS accelerometers with LARA. _____	97
Table 6-2. Frequency validation of the accelerometers _____	101

XVI

Table 6-3. Comparison of the first three mode steps frequencies of LARA with HI-INC. ____ 109

Table 6-4. Modal analysis outputs of LARA and the PCB 907A61 accelerometers. _____ 112

Table 6-5. Comparing the modal and eigenfrequency analysis of LARA and PCB 907A61
accelerometers _____ 113

LIST OF FIGURES

Figure 2-1. Key elements of SHM applications _____	8
Figure 2-2. The principal behind the four most known accelerometer types. _____	10
Figure 2-3. the growth of the use of low-cost microcontrollers in the civil engineering sector adopted from [120] _____	18
Figure 2-4. (a) Arduino Due, and, (b) NOEMCU microcontrollers. _____	21
Figure 2-5. Raspberry Pi B+ _____	22
Figure 3-1. Developed signal and acquisition systems: (a) schematic CHEAP and (b) CHEAP on the experiment jack _____	28
Figure 3-2. Diagram of needed steps for proposed kit data acquisition. _____	29
Figure 3-3. Control systems: (a) Data acquisition system for piezoelectric accelerometers and (b) positioning of the accelerometers. _____	32
Figure 3-4. Comparing MA error of the two control systems with CHEAP _____	38
Figure 3-5. Estimated MA error for different number of sensors: one sensor (a), two sensors (b), three sensors (c), four sensors (d) _____	39
Figure 3-6. FFT data process for 0.5 Hz experiment errors for four sensors (a) and five sensors (b) _____	40
Figure 3-7. Price comparison of CHEAP with control systems _____	42
Figure 4-1. Illustration of LARA: (a) The produced product, (b) The blueprint of the designed PCB, (c) The Fritzing sketch of the system, and (d) NODE MCU microcontroller. _____	45
Figure 4-2. The required steps of real-time wireless inclination acquisition using LARA inclinometer. _____	47
Figure 4-3. HI-INC biaxial inclinometer, b) inclination streaming over X axis and c) Sampling frequency rate. _____	48
Figure 4-4. Representation of the noise ratio of a single and up to five combined inclinometers using: (a) standard deviation, and (b) noise density in frequency-domain. _____	50
Figure 4-5. Quantifying the noise progress of various inclinometer combinations in time-domain using: (a) Allan variance, and (b) Allan deviation. _____	52

XVIII

Figure 4-6. Test setup intended for comparing inclination estimation of LARA with HI-INC.	53
Figure 4-7. Estimated measured inclination difference for a different number of combined inclinometers from HI-INC estimations: One sensor (a), two sensors (b), three sensors (c), and four sensors (d).	55
Figure 4-8. Load test of a beam model: (a) test setup, (b) load test, and (c) sketch of the load test..	56
Figure 4-9. Support slope of a simply supported beam under a point load located on various spots.	58
Figure 4-10. Price comparison of LARA with traditional commercial inclinometers with a resolution of 0.003 degrees.	59
Figure 5-1. The used low-cost sensors of the project: HC-SR04 (ultrasonic sensor), DHT22 (temperature and humidity sensor for calibrating the ultrasonic sensor), TCA9548A (multiplexor), VL53L0X (ToF sensor) and VL53L1X (ToF sensor).	61
Figure 5-2. The components of the distance measuring device: a) PVC sheet for attaching the sensors and the data acquisition equipment, b) Designed 3D printed base for holding the various sensors together at a known height, c) sensor allocation, d) Wiring the system together.	64
Figure 5-3. Flowchart of the construction of the proposed measurement device	65
Figure 5-4. Scheme of the connections between the microcontrollers and the Raspberry pi.	65
Figure 5-5. The laboratory experiment equipment.	66
Figure 5-6. Excluding the outliers of HC-SR04 estimations.	68
Figure 5-7. Filtered output of distance sensors for an experiment: (a) results of VL53L0X, (b) results of VL53L1X, and (c) results of HC-SR04.	71
Figure 5-8. Combined outputs of similar sensors.	72
Figure 5-9. Comparing the worst-case sensor combination for VL53L0X with and without ambient light	73
Figure 5-10. Comparing the worst-case sensor combination for VL53L1X with and without ambient light.	74
Figure 5-11. Comparing the worst-case sensor combination for HC-SR04.	75
Figure 5-12. The normal distribution function of VL53L0X for tests with ambient light.	78

XIX

Figure 5-13. The normal distribution function of VL53L0X for tests with no excessive ambient light. _____	79
Figure 5-14. The normal distribution function of VL53L1X for tests with ambient light. _____	81
Figure 5-15. The normal distribution function of VL53L1X for tests with no excessive ambient light. _____	83
Figure 5-16. The normal distribution function of HC-SR04 for various distance measurements.	85
Figure 6-1. LARA elements: (a) the adjustments and wire connections of the sensing part, (b) the sensing and acquisition part and (c) LARA in detail. _____	90
Figure 6-2. Calibration certificate of the developed accelerometer. _____	93
Figure 6-3. Frequency domain diagrams for Z axis of: (a) MPU9250, (b) CHEAP, (c) LARA.	95
Figure 6-4. Frequency domain diagrams of LARA for: (a) Z, (b) X and (c) Y-axis. _____	96
Figure 6-5. Laboratory validation of LARA: a) mounting CHEAP and LARA to the shaking part of the jack, b) The used vibrating platform (INSTRON 8803). _____	99
Figure 6-6. FFT representation of the low-frequency signals: a) 0.1 Hz, b) 0.2 Hz, c) 0.3 Hz, and d) 0.5 Hz. _____	100
Figure 6-7. displacement report of the jack in a frequency-domain diagram. _____	102
Figure 6-8. Displacement report of the accelerometers: (a) MPU9250, (b) CHEAP and (c) LARA. _____	103
Figure 6-9. The time-domain presentation of a vibration acquisition with RMS value of one g by LARA. _____	104
Figure 6-10. The time-domain presentation of acceleration amplitude saturation of LARA _____	104
Figure 6-11. The location of the Pasarela Polvorín footbridge in Barcelona, Spain. _____	105
Figure 6-12. (a) A picture of the Footbridge (Pasarela Polvorín), (b) plan of the bridge and (c) section of the pass way bridge (all units are in mm). _____	106
Figure 6-13. Mounting the sensors to the mid span of the bridge under study: a) Mounting diagram of LARA to the bridge and b) Photo of the mounted LARA and HI-INC sensors. _____	107
Figure 6-14. Eigenfrequency analysis of a footbridge using LARA for (a) Vertical, (b) Longitudinal, and (c) Transversal directions of the footbridge. _____	108

XX

Figure 6-15. The location of the Andoain bridge in Donostia-San Sebastian, Spain. _____ 109

Figure 6-16. Andoin Bridge: a) A photo of the bridge before instrumentation, b) The dimensions of the bridge under study. _____ 110

Figure 6-17. Data acquisition part of LARA: a) Box of the data acquisition equipment of LARA, b) The installation of the box on the bridge _____ 111

Figure 6-18. Instrumentation of Andoain bridge using two LARA (sensing part only) mounted next to the PCB 607A61 accelerometers. _____ 112

Chapter 1 Introduction

1.1 Motivation

Civil structures and infrastructures can be considered the leading basis of any modern society. Typically bridges serve as symbols of a country's infrastructure. It should be noted that bridges are crucial for tying together people, goods, and transportation. For that, bridges have significant economic, political and cultural impacts on society.

It should be noted that depending on the nation and the built asset, these structures are planned for a service life of 50 to 120 years [1]. Over time, several factors and situations such as fatigue, construction defects, environmental factors and fatigue can reduce the safety, performance and serviceability of a structure [2]. In fact, the American Society of Civil Engineers (ASCE), which publishes a Report Card for America's Infrastructure every four years, provides information on the state and performance capabilities of every sort of infrastructure in the United States of America (USA). The report of ASCE infrastructures in 2021 indicates that about 617,000 bridges in the USA currently exist, out of which more than 42% are at least 50 years old. It is essential to mention that most of these bridges are designed for a service life of 50 years.

Consequently, an increasing number of bridges will need rehabilitation and monitoring as time goes by. Additionally, more than 7.5% (or 46,154) of them are considered structurally deficient and are in poor condition. It is also reported that bridge repairs across the country are estimated to cost \$125 billion [3].

The increasing need for infrastructure monitoring and rehabilitation is not exclusive to the United States; for example, in Spain, various media outlets, including "La Voz de Galicia" [4] and "El Confidencial" [5], have discussed the issues caused by the lack of maintenance in the infrastructures. In reality, the pathologies (such as those associated with a lack of structural and mechanical properties of the materials) in the structures can advance substantially faster due to a lack of or ineffective continuous maintenance and repair efforts. It is essential to highlight that these pathologies can endanger the very stability of the structures [6]. The possibility of lowering the risks connected with structural pathologies depends on the feasibility of accurately analyzing its structural performance [7]. In addition, continual maintenance and repair activities are required to ensure functional and safe conditions throughout the life cycle of civil infrastructures and buildings [8].

Visual examination or non-destructive testing are typically used to analyze the serviceability of structures. In fact, structural system identification techniques [9] are generally used to supplement the information gained from inspections of the damages. Structural system identification is a domain whose application is to evaluate the integrity and the state of a structure for determining the actual characteristics of a structure. It should be noted that structural system identification

approaches require the actual reaction of the structure assessed on-site as input data to detect and quantify structural damages. This required information is typically collected using a sensor based Structural Health Monitoring (SHM) application [10]. Nowadays, several commercial sensors are available to accurately measure the response in structural members (such as accelerations, inclinations, and crack width) and the environmental parameters (such as temperature and humidity).

The literature review of structural health monitoring applications shows the following detected gaps:

- 1- **The high price of the commercial accelerometers:** Commercial accelerometers are expensive, restricting their application to singular complex and iconic structures (such as long-span bridges) with a high budget for their SHM monitoring. However, the installation of accelerometers is not usual in conventional structures, which are those in which a more significant number of pathologies occur. No low-cost solutions are available to measure low acceleration amplitudes with high accuracy that could be compared with traditional commercial sensors.
- 2- **The high price of the commercial inclinometers:** Low-cost inclinometers found in the literature review of SHM of bridges show the following shared drawbacks: (1) Production plan: Building instructions for these inclinometers are not available. Consequently, researchers cannot use those works to create their own tailored inclinometer, (2) Accuracy: Most of the available low-cost solutions do not have comparable resolution or precision with the commercial ones. Consequently, they may not be suitable for bridge damage detection applications that need bridge inclination measurement.
- 3- **Improving the standard deviation of low-cost noncontact ranging sensors:** The resolution and accuracy of low-cost noncontact range measuring sensors are significantly lower than that of conventional commercial systems, which is one of their biggest shortcomings. Moreover, standard deviation and distribution functions for distance measuring equipment are needed to model theoretical physical models to improve structural system identification techniques. However, researchers who are knowledgeable in analytical analysis may not have access to experimental records. Consequently, they often estimate these values.
- 4- **High price and lack of versatility of commercial data acquisition systems:** The development of low-cost accelerometers is not enough for an economic SHM application. In fact, a system capable of recording the measured structural response is needed. Furthermore, long-term monitoring is also economically expensive due to the high maintenance and repair expenses associated with costly data acquisition equipment and sensors. There is a lack of consistent work, including all the following points in single inception for a low-cost data acquisition equipment (1) Access to the time through the Internet, for accurate post synchronization of the low-cost accelerometers, (2) Remote

control and data management, (3) Automatic data acquisition, and, finally, (4) Performing experimental eigenfrequency analyses on actual infrastructures.

To fill these gaps, novel low-cost accurate sensors (low-cost accelerometers and an inclinometer) and data acquisition equipment based on the Internet of Things (IoT) for SHM of bridges are developed and validated in this work. Moreover, a study aiming to improve the accuracy of low-cost noncontact ranging sensors and an analysis of their standard deviation and distribution function is presented.

It is also to be noted that funding for this research has been provided for Seyedmilad Komarizadehasl by Spanish Agencia Estatal de Investigación del Ministerio de Ciencia Innovación y Universidades grant and the Fondo Social Europeo grant (PRE2018-083238). The research is also indebted to the Spanish Ministry of Economy and Competitiveness for the funding provided through the research project BIA2017-86811-C2-1-R directed by José Turmo and BIA2017-86811-C2-2-R.

1.2 Objectives

The global objective of this work is to develop and validate low-cost reliable sensors and data acquisition equipment based on Arduino and Raspberry Pi technology for economical SHM of bridges. To reach this aim, the following partial objectives are detailed:

Objective 1: Development and laboratory validation of a novel Cost Hyper Efficient Arduino Product (CHEAP) for accurately measuring frequency and acceleration amplitude of vibrations with low frequency and acceleration amplitude range.

Objective 2: Development and laboratory validation of an IoT based Low-cost Accurate Reliable Angle-meter (LARA) for economically measuring rotations that is accurate enough to be used for weight in motion applications and damage detection of bridges using deformation measurements.

Objective 3: Improving the accuracy of low-cost noncontact distance measuring sensors based on Arduino technology and presenting their corresponding standard deviation and distribution functions.

Objective 4: Development and field validation of a reliable data acquisition device with microsecond resolution time stamp capability that can be used for post synchronization of several accelerometers.

1.3 Thesis organization

Based on the presented objectives, this thesis is organized into seven chapters. Each chapter deals with a particular topic: (1) State of the art, (2) Development of a low-cost system for the accurate measurement of structural vibrations, (3) A novel wireless low-cost inclinometer made by combining the measurements of multiple MEMS gyroscopes and accelerometers, (4) Low-cost sensors accuracy study and enhancement strategy, and, (5) Low-cost wireless structural health monitoring of bridges. It should be noted that the sequence of the presented chapters is based on the written journal articles. After writing each paper, new gaps in the literature were found, and they were satisfied or studied in the subsequent publication. It should be noted that the published date of the papers is not the same as their written order.

The summary of the introduced chapters is as follows:

In Chapter 2, first, the state of the art of structural health monitoring applications is gathered. Secondly, the standard sensors used in structural health monitoring applications are illustrated. Lately, four gaps have been detected according to the illustrated literature review.

In Chapter 3, a novel application for improving the accuracy of low-cost accelerometers based on Arduino technology is demonstrated. The accuracy of the developed sensor (CHEAP) is then compared with two commercial accelerometers (PCB 393A03 and PCB 356B18) through laboratory experiments.

In Chapter 4, a low-cost accurate inclinometer is introduced. This inclinometer is based on the fusion of five synchronized accelerometers and gyroscopes. Furthermore, this inclinometer's noise analysis is studied using time domain noise characterizing applications (such as Allan variance). Finally, the accuracy of the developed inclinometer is compared with a commercial inclinometer suitable for SHM. This comparison is performed through a series of laboratory experiments.

In Chapter 5, the accuracy improvement of three types of noncontact range measuring systems (HC-SR04, VL53L0X and VL53L1X) based on Arduino technology is studied. The improvement is made using averaging the outputs of several similar synchronized sensors. In addition, useful information about standard deviation and distribution of the studied sensors under various environmental situations are detailed.

In Chapter 6, a low-cost data acquisition equipment based on Raspberry technology is announced. This data acquisition equipment can be used with any Arduino-based system and is capable of remote control and data management. This system is used for the eigenfrequency and modal analyses of an under-operation bridge. Moreover, the acquired eigenfrequencies of the low-cost solution are compared with those of the commercial accelerometers (PCB 607A61).

Finally, in Chapter 7, a summary of the thesis plus the conclusion of the aforementioned chapters are drawn. In addition, the significant contributions of this thesis together with its future research work, are described.

1.4 Methodology

To satisfy the objectives of this thesis, the following steps are taken:

Step 1: Bibliography and state of the art review.

- 1) Literature review of SHM applications and the used commercial sensors
- 2) Literature review and carrying out Internet surfing to find eligible low-cost sensors.
- 3) Literature review of low-cost microcontrollers and single board computers.
- 4) Deep studying of possible ways of connecting several similar sensors to the same Inter-Integrated Circuit (I2C) port of a single microcontroller.
- 5) Literature review of signal processing and noise characterizing in both time and frequency domains.

Step 2: Microcontroller coding and grasping on working with low-cost sensors.

- 1) Master writing codes in the Arduino platform.
- 2) Python programming for possible ways of real-time data acquisition and visualization.
- 3) MATLAB coding for writing signal and data post-processing applications.

Step 3: Development of the solutions:

- 1) Low-cost accelerometer development based on Arduino technology (First objective).
- 2) Low-cost IoT-based Inclinometer development using NODEMCU technology (Second objective).
- 3) Building of a range measurement device composed of 75 sensors (Third objective).
- 4) Development of a low-cost versatile data acquisition equipment based on Raspberry Pi technology (Fourth objective).

Step 4: Static and Dynamic validation experiments carried out in the Laboratory of Technology of Structures & Materials "Lluís Agulló" (LATEM).

- 1) Vibration acquisition validation of the developed accelerometer on the available actuator in the LATEM (First objective).
- 2) Accuracy validation of the developed inclinometer employing several experimental tests on a beam model (Second objective).
- 3) Range measurement tests of the developed distance measuring device using the available static hydraulic jack of LATEM (Third objective).

Step 5: Analysis of bridges using the developed data acquisition system and the accelerometer (Fourth objective).

- 1) Eigenfrequency analysis of a footbridge in Barcelona
- 2) Operational modal analysis of a Bridge in Donostia-San Sebastian.

Step 6: Preparation of journal articles, the doctorate dissertation and participation in international conferences:

- 1) Publishing four journal papers as the consequence of this thesis
- 2) Collaborating with other researchers in publishing three journal papers through sharing the technology and the developed systems of this thesis.
- 3) Participation in international conferences, presenting and publishing 12 conference papers from this thesis.
- 4) Preparation and writing of the doctoral dissertation.

Chapter 2 : State of the art

In this Chapter, the first subsection details a brief literature review of traditional structural health monitoring applications. This subsection also includes a thorough literature review of traditionally used and recently developed low-cost sensors for measuring the static and dynamic structural responses. Further in this subsection, the most famous microcontrollers compatible with low-cost sensors are presented. Finally, the second subsection presents the gaps found in the given literature review and the proposed solutions of this work.

2.1 Structural health monitoring

The methods used for construction have seen a significant change throughout the years. The building business has witnessed a consistent trend of simple to complicated construction, from natural materials to composite materials for a specific structure [11]. These constructions are subjected to a variety of environments, which causes them to deteriorate and finally results in structural deficiency [12]. There are many causes of structural deterioration, including heavy traffic volume, natural disasters, and others [13]. Therefore, for maintenance applications, optimizing repair costs, and, eventually, ensuring building/infrastructure safety, monitoring and assessing the health condition of these structures is needed [14].

The structural deficiency reduces the margin of safety margin and serviceability span, ultimately endangering civilians' life[15]. Therefore, structural Health Monitoring (SHM) applications are widely used as an emergent and powerful diagnostic tool for damage detection and condition monitoring of civil structures [16].

In fact, the past failures of civil structures have increased the interest of engineers and researchers in SHM applications [17] as the central system of preventing future accidents and human death [18]. Applications for SHM systems provide assessments on the status of structures, how they operate, and how they respond structurally [19]. In addition, the SHM is broadly used for calibrating the computer-based model (also known as digital twin [20]) of the understudy structure [21]. In fact, the calibrated digital twin can then be used for system performance evaluation that helps the decision-making process during the maintenance phase [22]. In addition, it should be noted that one of the essential purposes of any SHM application is to measure the current structural conditions accurately and to detect possible structural damages [23].

SHM typically consists of four critical elements of: (1) Data acquisition [24], (2) Structural system identification [25], (3) Structural condition assessment [26], and, (4) Decision making/maintenance [27]. These key elements are illustrated in Figure 2-1. Data acquisition is reported to be the most expensive part of any SHM application due to the high price of the available commercial sensors, data acquisition equipment, installation and maintenance costs [28]. Moreover, the high price of data acquisition elements limits studying multiple nodes and long-term SHM of structures to unique structures with a relatively high structural health monitoring budget [29]. Therefore, this thesis and its corresponding literature review focus mainly on this element.

8

The data acquisition element of SHM measures the structural response (such as accelerations, rotations, strains, or deflections) over time. Some environmental parameters (such as humidity or temperature), which can cause crack opening, rotations, settlements, corrosion, and other pathologies, change over time at such a slow rate that they may be called static or quasi-static [24]. On the other hand, the nature of some structural reactions that some events, such as the wave response owing to earthquake ground motion, traffic-induced vibrations, or ambient activities, must be taken into account for the dynamic response of the structure. Figure 2-1 also shows the two branches of data acquisition applications with the measurement of a structure's structural dynamic responses on one side and the static or quasi-static responses on the other.

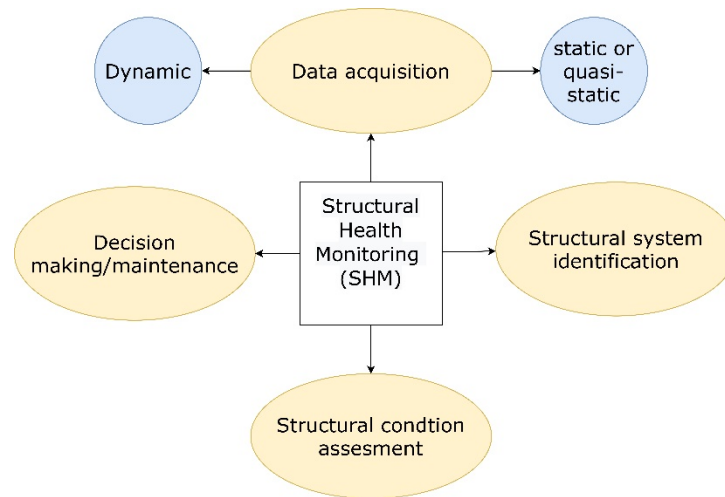


Figure 2-1. Key elements of SHM applications

Sensors are frequently utilized in SHM applications to measure static and dynamic responses. Accelerometers are reported to be often employed to track the structures' dynamic behavior. In contrast, strain gauges, inclinometers, and thermometers are the most frequently used sensors for measuring static structural responses. It should be noted that all sensor types need data acquisition equipment to save their outputs.

In the following, first, an introduction to commercial and recently developed low-cost solutions for measuring the dynamic responses of a structure under the subsection of “Accelerometers” is presented. Next, a subsection entitled “Inclinometers” details the price and characteristics of a number of commercial and inclinometers and low-cost prototypes. The third subsection, “Noncontact Distance measuring sensors” presents a brief literature review of noncontact distance measuring sensors in which both traditional range measuring systems and recently trending ones are detailed. Finally, the fourth subsection (“Low-cost microcontrollers”) illustrates a literature review on the current low-cost microcontrollers and that can be programmed to work with low-cost sensors.

2.1.1 Accelerometers

Accelerometers can calculate and pinpoint a structure's dynamic properties by measuring variations in the structural response. It is also essential to note that different SHM applications require accelerometers with specific characteristics [30][31]. In fact, the literature (see, for instance, [32]) states that the important natural frequencies of most civil constructions range between 0.2 and 100.0 Hz. For example, short-span bridges (with span lengths up to 40 m [33]) often have an eigenfrequency range between 3 and 30 Hz [34]. Moreover, medium-span and long-span bridges' eigenfrequencies vary from 0.1 to 8.0 Hz (such as [35]). Additionally, it should be emphasized that the majority of ambient vibrations in civil structures have low amplitudes [36]. In actuality, these structures' acceleration amplitudes might be as low as 0.04 g. This feature demonstrates the need for accelerometers with high sensitivity and low noise density for SHM of bridges [37].

Accelerometers are typically force-sensors that are fastened to a seismic mass. In the presence of external vibration, the mass exerts a particular force that is inversely proportional to the measured acceleration. The applied force of the seismic mass results in an electrical signal that can be converted to acceleration and saved using data acquisition equipment [38].

One of the following three major principles—piezoelectricity, piezoresistivity, or differential capacitive measurement—underpins the most popular kind of vibration sensing technology [38]. The four most popular accelerometers based on the aforementioned principals are detailed below:

- 1) Piezoelectric accelerometers can function at a wide range of frequencies (up to 12 kHz) and record dynamic changes in mechanical variables by using the piezoelectric action of certain materials [39].
- 2) Piezoresistive accelerometers are also known as strain gauge accelerometers and when mechanical loads are applied, they can measure the change in the electrical resistance of a piezoresistive element [40].
- 3) Differential capacitive accelerometers determine the displacement of the proof mass by monitoring changes in their capacitance [40].
- 4) Micro Electro Mechanical Systems (MEMS) can be manufactured from any of the mentioned acceleration measurement principles (piezoelectricity, piezoresistivity, or differential capacitive measurement). It should be noted that the majority of MEMS sensors include signal processing circuitry and can have a bandwidth of up to a few kHz [26]. MEMS accelerometers have found their way into various industrial applications because of their significant continuous technological developments. Several of these accelerometers provide more economical options than traditional Piezoelectric accelerometers [27].

Figure 2-2 presents the used principal for manufacturing the reviewed accelerometer types.

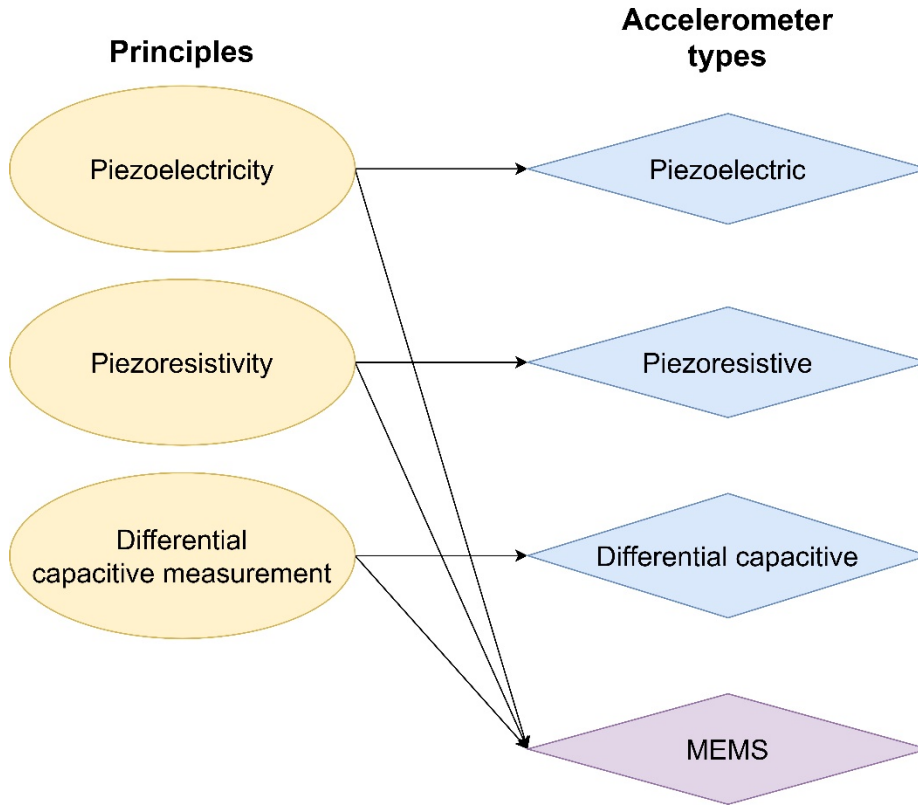


Figure 2-2. The principal behind the four most known accelerometer types.

Table 2-1 provides a summary of information on several accelerometers that are now on the market for various structural health monitoring applications. The pricing of the accelerometers has determined the order of this table. This table includes the following information sorted in columns: (1) Sensor number, (2) Sensor name: the title of the sensor and the reference to its datasheet, (3) Acceleration range: saturation capacity of the sensors, (4) Frequency range, (5) Spectral noise density: more information about spectral noise density and its calculations are presented in [41], (6) Sensor price: The prices are based on early quotes from retailers in the year 2020 and do not include the VAT. Although the prices can vary slightly and often depend on the supplier, they can be used as a good approximation, and, (7) Used application: The structure type where the sensors are used.

Table 2-1. Summary of the characteristics of the accelerometers commonly used in the literature.

No.	Name	Acceleration range (g)	Frequency range (Hz)	Spectral noise ($\mu\text{g}/\sqrt{\text{Hz}}$)	Price (€)	Used application
1	3713B112G [42]	± 2.0	[0.00, 250]	22.90	2070.0	Wind Turbine [43]
2	356B08 [44]	± 50.0	[0.50, 5000]	40.00	1610.0	Bridge Crane [45]
3	356A45 [46]	± 50.0	[0.70, 7000]	125.00	1410.0	Forward Swept Wing [47]
4	356B18 [48]	± 5.0	[0.50, 3000]	11.40	1300.0	Motorbike Speedway Stadium [49]
5	3711B1110G [50]	± 10.0	[0.00, 1000]	107.90	870.0	Railroad Bridges [51]
6	KB12VD [52]	± 0.6	[0.30, 2000]	0.06	828.0	Concrete School Building [53]
7	393B12 [54]	± 0.5	[0.15, 1000]	1.30	820.0	Historical Masonry Structures [55]
8	KS48C [52]	± 6.0	[0.25, 130]	0.60	750.0	Footway Bridge [56]
9	393A03 [57]	± 5.0	[0.50, 2000]	2.00	710.0	Brick Masonry Constituents [58]
10	352A24 [59]	± 50.0	[1.00, 8000]	80.00	540.0	Hallow Square Beams [60]
11	352C33 [61]	± 50.0	[0.50, 10000]	39.00	380.0	Bridges [62]
12	LIS344ALH [63]	± 2.0	[1.00, 500]	50.00	12.0	Steel beam [64]
13	ADXL335 [65]	± 3.6	[0.50, 550]	300.00	10.7	Bridges [66]
14	MPU9250 [67]	± 16.0	[0.24, 500]	300.00	5.8	Steel Pile and Column [68]
15	MPU6050 [69]	± 16.0	[0.24, 500]	400.00	5.4	Building Model [70]

The analysis of Table 2-1 illustrates a great range of sensor prices. For example, 3713B112G accelerometer (the most expensive accelerometer in this table with the price of 2070 €), is 385 times more expensive than MPU6050 (the cheapest accelerometer in this table with the price of 5.4 €). One of the primary barriers to the practical implementation of SHM applications is the cost of the accelerometers, which many scholars have stated (see, e.g. [28]). However, the cost of vibration acquisition applications is not limited to the price of accelerometers, as they typically need data acquisition equipment (such as real-time controller, data acquisition software, and workforce for data analysis). On average, 700 € per channel of an accelerometer needs to be invested in the data acquisition equipment [41].

Further analysis of this Table shows that sensors with lower noise density have lower acceleration range (such as 4, 7). As illustrated in Table 2-1, low-cost accelerometers typically are characterized by higher noise density and a lower frequency range. Consequently, the literature review [71][67][66][64][68][70] shows the implantation of these sensors typically in projects with strong motions and low frequencies.

To tackle the high price of commercial accelerometers, numerous researchers attempted to develop an adequate low-cost solution for SHM applications [72]. In the following, a literature review of some inexpensive accelerometers is organized.

- Grimmelsman et al. [66] developed a low-cost accelerometer using the ADXL335 circuit. They compared the performance and capabilities of their inexpensive accelerometer with those of commercial accelerometers from PCB company (PCB 393A03 and 3741E122G).
- Girolami et al. [64] proposed a system for analyzing the modal analysis of a beam modal using a number of synchronized low-cost sensors manufactured from LIS344ALH circuits.
- Ozdagli et al. [71] developed a Low-cost Efficient Wireless Intelligent Sensor (LEWIS) using MPU6050 circuit. To examine the accuracy of LEWIS, it was mounted on a shaking device and its measured outputs were compared to those of a commercial accelerometer (PCB 3711B1110G) and a Linear Variable Differential Transformer (LDVT)
- Agüero et al. [67] presented an updated model of LEWIS using MPU9250 circuit. LEWIS 2 is developed to have data storage, be battery-powered, and have better accuracy than LEWIS. The results of the laboratory experiments of LEWIS 2 on an actuator were compared with LDVT sensor.
- Meng et al. [73] represented a low-cost vibration acquisition system composed of a LSM9DS1 circuit and a Raspberry Pi 4. The outputs of this device were compared with those of a commercial accelerometer (PCB 356B18).

The essential characteristics of the reviewed accelerometers are summarized in Table 2-2. This table includes the following information sorted in columns: (1) Sensor number, (2) Sensor name: The proposed name of the developer or the name of the used chipset for developing the system, (3) Acceleration amplitude range: the saturation magnitude of the accelerometer, (4) Sampling frequency: also known as rate sample is the speed rate of the accelerometer. It should be noted that

13

the bandwidth of an accelerometer is equal to half of its sampling frequency, (5) Noise Density (ND), (6) NTP: Network Time Protocol (NTP) column refers to the capability of the system to be connected to the accurate time of the Internet or the Global Positioning System (GPS), (7) Remote access, and, (8) Used application.

Table 2-2. Some of the low-cost vibration acquisition applications of the civil engineering literature.

No.	Name	Acceleration Range (g)	Sampling Frequency (Hz)	Noise Density ($\mu\text{g}/\sqrt{\text{Hz}}$)	NTP	Remote Access	Used application
1	ADXL335	± 3 g	100	300	No	No	[66]
2	LIS344ALH	± 2 g	100	50	No	Yes	[64]
3	MPU6050 (LEWIS)	± 2 g	100	400	No	No	[71]
4	MPU9250 (LEWIS 2)	± 2 g	500	300	No	No	[67]
5	LSM9DS1	± 2 g	952	No data	Yes	Yes	[73]

The analysis of Table 2-2 illustrates that the majority of the presented solutions have almost the same sampling frequency and acceleration ranges. However, LSM9DS1 (No. 5 in Table 2-2) is the only developed system with a very high sampling frequency, which requires further studying since the sampling frequency of the developed accelerometer is equal to the sampling frequency of the used circuit (LSM9DS1). Furthermore, it should be noted a developed vibration acquisition system from a circuit requires further laboratory validation tests because depending on the used microcontroller, cable and connections quality, and the data acquisition system, the noise density, sampling frequency and accuracy may alter [74]. Furthermore, the shown noise density in Table 2-2 is not reported from the experimental tests of the researchers. In fact, this noise density is declared from the datasheets provided by the circuit producer company. Finally, it is essential to state that only the developed system of Meng et al. [73] could synchronize its internal clock with the exact time of the Internet through the NTP procedure. In addition, further analysis of Table 2-2 represents that only developed solutions No. 2 and 5 (LIS344ALH and LSM9DS1) can be reached remotely.

It should be noted that accelerometers are used for Operational Modal Analysis (OMA) techniques [75] OMA is a technique used for modal characterization of structures and when it is hard to excite the structure artificially. In fact, OMA evaluates the reaction and interplay of environmental and operational influences during structure usage [76]. In vibration testing, there are two primary OMA methods: the non-parametric technique in the frequency domain and the parametric method in the

time domain. The Frequency Domain Decomposition (FDD) approach analyzes structures under environmental excitations in the frequency domain. Because of its simplicity, this approach is commonly utilized in civil engineering applications. Because of its capacity to detect many roots, this approach is also known as Complex Mode Indicator Function (CMIF) [77]. It should be noted that to compare the mode shapes extracted from an OMA analysis of two different types of accelerometers Modal Assurance Criterion (MAC) value is typically used. MAC can also be used to compare an experimental test's mode shapes with those of an analytical model [78].

2.1.2 Inclinometers

To calculate the angular rotation of a target item about a synthetic horizon, angular sensors (inclinometers or tilt sensors) are typically used. This angular rotation may also be utilized to compute the vertical deflection of the horizontal parts as well as the drift of the vertical members [79]. The majority of inclinometers follow the principle of measurements induced by pendulum behavior due to gravity [80].

In several industries during the last few decades, inclinometer sensors have been employed extensively. In fact, in the civil engineering sector, inclinometers were initially used for geotechnical purposes [80]. Improvements in sensor accuracy over time have made it possible to use inclinometers in other areas of civil engineering, such as monitoring the structural health of bridges [79]. It should be noted that many scholars implanted inclinometers in their research for monitoring and checking various parts of bridges. An example of this implantation is the work of Glišić et al. [81], who analyzed the performance of a post-tensioned concrete bridge during its construction, post-tensioning and first-year operation stages, using inclinometers and long-gauge deformation sensors. This study evaluated the understudy bridge's health state and post-tensioning verification. It is essential to mention that reviewing the literature on civil engineering [82] also shows the significant role of inclinometers in the long-term monitoring of cable-stayed and suspended bridges [83][84][85]. It should be noted that literature shows the traditional use of inclinometers in civil engineering for analyzing the boundary condition response of the bridge abutments [86] [87]. Furthermore, it can be seen that number of researchers have also used inclinometers for calculating the deflection of the bridge deck [88]. In addition, the literature review shows the use of inclinometers for model calibration techniques. In fact, Robert-Nicoud et al. [89] used an inclinometer on the Lutrive bridge in Switzerland to validate several model calibration techniques.

Table 2-3 lists the characteristics of some commercial inclinometers and is organized by sensor cost. This table includes the following information sorted in columns: (1) Sensor name, (2) Measurement range, (3) Resolution, (4) Sampling rate, (5) Sensor price: The prices are based on early quotes in the year 2021 from retailers and do not include the VAT. Although the prices can vary slightly and often depend on the supplier, they can be used as a good approximation, and, (6) Reference: Reference to the datasheet of the introduced inclinometer.

Table 2-3. Characteristics of some of the commercially available inclinometers.

Inclinometer	Measurement Range (Degrees)	Resolution (Degrees)	Sampling rate (Hz)	Price (€)	References
ZEROTRONIC	$\pm 0.5^\circ$	$10 \times 10^{-5^\circ}$	10	3950	[90]
JDI 200	$\pm 1.0^\circ$	$10 \times 10^{-5^\circ}$	125	2250	[91]
T935	$\pm 1.0^\circ$	$3 \times 10^{-5^\circ}$	10	1696	[92]
ACA2200	$\pm 0.5^\circ$	$10 \times 10^{-5^\circ}$	20	710	[93]
HI-INC	$\pm 15.0^\circ$	$100 \times 10^{-5^\circ}$	100	650	[94]

Analysis of Table 2-3 reveals a broad price variation ranging from €650 to €950. Further study of this table shows a varying measurement range (from 0.5 to 15.0 degrees) of the presented inclinometers. It is clear that inclinometers with a smaller range have greater prices and resolution. Additionally, inclinometers with better resolution often cost more.

Several researchers developed low-cost inclinometers to tackle the high price of the current inclinometers. For example, Yan et al. [95] developed a low-cost wireless inclinometer with a resolution of 0.002° . This inclinometer was able to transmit its data streaming up to 2000 m away. Moreover, Ruzza et al. [96] presented a low-cost inclinometer with an accuracy of between ± 0.162 and $\pm 0.304^\circ$. Andò et al. [97] introduced a low-cost multi-sensor system based on Arduino technology to analyze structures' structural responses.

2.1.3 Noncontact Distance measuring sensors

It should be noted that in load testing range sensors can help pinpoint the damage and its extension as long as a specific reference point is present. The literature review shows the following latest trends in noncontact distance measuring systems developed for SHM applications.

- Park et al. [98] developed Terrestrial laser scanning (TLS) device for measuring the 3D displacement of any particular point and the static deformed shape of a structure. Unfortunately, this system has a maximum error of 10 mm. Therefore, a displacement measurement model is further developed to increase the system's accuracy. The model's accuracy and dependability were tested experimentally using a steel beam that was simply supported and underwent a concentrated load. The accuracy of this system is reported to be 1 mm and within 1.6% of those measured directly by a Linear Variable Displacement Transducers (LVDT) sensor.
- Yoon et al. [99] presented a noncontact distance measuring device using an Unmanned Aerial System (UAS) equipped with a commercial-grade video camera. The observed displacement of a railroad bridge under revenue-service train traffic was replicated using a motion simulator in a laboratory experiment to test the suggested technique. The experimental tests show a difference of 2.14 mm between the developed system and the reference value obtained by a Krypton 3D measurement system (K600) with an accuracy of 0.02 mm.
- Nasimi et al. [100] illustrated a noncontact displacement measuring system for railroad inspections within the US rail bridge inspection manuals. A camera and a laser sensor are

combined to make this system. The system's camera corrects the laser's rotation and translation during the measuring. Additionally, the dynamic movement of the structure may be recorded using this novel technology, which is impossible with just a laser or camera.

- Artese et al. [101] developed a system for eigenfrequency analysis and measurement of the acceleration amplitude of the oscillations of tall structures. This methodology is formed from the fusion of Terrestrial Laser Scanner (TLS) and a Ground-Based Real Aperture Radar (GB-RAR) applications. Using TLS and GB-RAR system fusion, the comparison of numerical and experimental analysis reveals a precise displacement measurement with a 5mm error.

It should be noted that traditional range sensors are typically categorized by their measuring methods. In the following four most famous measuring principals of noncontact range sensors are described:

- (1) Ultrasonic sensors: These sensors, also known as sonar sensors, are among the most popular devices for detecting distances. They start by sending out high-frequency ultrasonic waves to determine their distance from the target. The wave then encounters any item within the range of the ultrasonic sensor, bounces off, and reflects back toward the sensor. Finally, the sensor determines the distance using the speed of sound and the wave's transit time [102]. The color and transparency of the object have no bearing on ultrasonic measurement equipment. Additionally, they are unaffected by the brightness of their surroundings. However, they are unable to gauge a distance between objects having a complicated surface (such as a sponge). Additionally, this sensor is typically combined with humidity and thermometer sensors to increase the accuracy of ultrasonic sensors because the speed of sound is sensitive to both humidity and temperature [103].
- (2) Infrared sensors (IR): They typically calculate the angle of reflection after producing infrared light signals (triangulation principle [104]). This angle is then used to determine the distance from an object. It should be noted that these types of sensors are sensitive to the ambient light and surface color of the object [105].
- (3) Light Detection and Ranging (LiDAR) sensors: The working principal of LiDAR sensors can be introduced as a hybrid of an IR and ultrasonic sensor. The transmitter component of LiDAR emits a laser beam on the target to measure the distance to an item. Then, the target object's reflected light signal is picked up by the LiDAR's reception section. The distance of the test object is then determined by multiplying the time it takes for the laser signal to traverse a certain distance by the constant speed of light in the air [106]. Among the other techniques, this one can measure the distance of small objects with the highest accuracy (like 0.005% of their final range [107]). These sensors can cost up to 4,700 euros [108], and some of them can hurt unprotected eyes.
- (4) Time-of-flight (ToF) sensors: These sensors use the time-of-flight concept methodology to estimate distances falling under the wide LiDAR spectrum. ToF sensors detect the time between each pulse's emission and reception using brief light pulses [105].

Table 2-4 presents the characteristics of some low-cost sensors based on the introduced principles and is organized by sensor cost. This table includes the following information sorted in columns:

17

(1) Measuring principle, (2) Limitations: the limitations of this specific distance measuring principle, (3) Low-cost sensor: Model of a famous low-cost sensor based on the presented principle, (4) Sampling frequency, (5) Distance range, (6) Dimension: the dimension of the sensor, (7) Input voltage, (8) Sensor price: The prices are based on early quotes in the year 2021 from retailers and do not include the VAT, and, (9) Used application: the application in which the presented low-cost sensor was used. Although the prices can vary slightly and often depend on the supplier, they can be used as a good approximation.

Table 2-4. Specifications of different low-cost range sensors.

Measurement principle	Limitations	Low-cost sensor	Sampling frequency (Hz)	Distance Range (cm)	Dimension (mm)	Input voltage	Price (€)	Used application
LiDAR	Dangerous to eyes, expensive	Lite v3 [109]	500	5-4000	48.0*40.0*20.0	5.0	109.0	Drones [110]
IR	Low frequency and sensitivity to ambient light and surface color	GP2Y0A21YK0F [111]	26	10-80	29.5*13.0*13.5	5.0	7.8	Air Levitation [112]
ToF	sensitive to Surface color and ambient light	VL5310x [113]	500	3-200	13.0*18.0*2.0	3.3	5.4	Rail gap measurement [114]
Ultrasonic	Complex objects, low frequency, sensitive to temperature variation	HC-SR04 [115]	40	2-400	45.0*20.0*1.5	5.0	2.5	Robotics [116]

Table 2-4 analysis reveals that the HC-SR04, while being less expensive, outperforms the GP2Y0A21YK0F sensor in terms of reading range and data sampling speed. Additionally, the only sensor in Table 2-4 whose calculations are unaffected by ambient light is HC-SR04. However, the distance measurement from objects with an area range of less than 0.5 square meters or a complicated surface is acknowledged in this sensor's datasheet as inaccurate [115]. Further study of this table shows that Lite V3 sensor, which is the most expensive sensor in this table, has the widest measurement range. Even though this gadget employs laser class 1 technology, it is strongly suggested to avoid gazing directly at the laser beam, according to its datasheet [109]. It can also be deduced that the introduced ToF sensor has the same sampling frequency as the LiDAR one

18

with an affordable price tag. Moreover, the beam lights produced by this type of sensor are indicated as safe for bare human eyes. This makes working with this type of sensor easier and safer.

It is also important to mention that standard deviation and distribution functions for measuring equipment such as those presented in Table 2-4 are needed when modeling theoretical physical models in order to further improve structural system identification techniques. However, as researchers who are knowledgeable in the analytical analysis may not have access to experimental records [6][117]. Subsequently, these values are often approximated [118].

2.1.4 Low-cost microcontrollers

Nowadays, demands for low-cost monitoring are continuing to rise. In the study of Mobaraki et al. [119], a thorough literature review on using inexpensive sensor applications for building monitoring is detailed. The increasing implantation of low-cost sensors in civil engineering is demonstrated in Figure 2-3. The data was taken between the years 2011 and 2021 from the SCOPUS database.

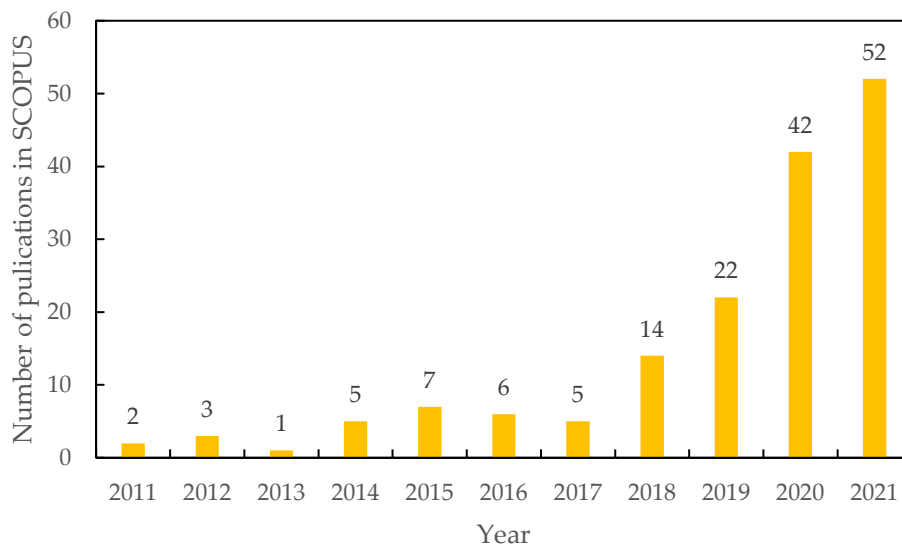


Figure 2-3. the growth of the use of low-cost microcontrollers in the civil engineering sector adopted from [120]

Figure 2-3 demonstrates that from 2011 to 2017, the number of publications related to the use of inexpensive sensors for structural monitoring was negligible (18.2%), and more than 81% of the articles found had been published within the previous four years.

It should be noted that low-cost sensors are typically controlled, programmed and set up using low-cost microcontrollers. Low-cost microcontrollers come in wide varieties, with Arduino being one of the most well-liked ones on the market [121].

Further in this subsection, the literature review of Arduino microcontrollers and Raspberry Pi as the most famous single board computer available on the market are presented.

2.1.4.1 Arduino

Arduino is a low-cost microcontroller capable of connecting with many different types of analog and digital sensors.

It has a friendly interface, active developer, and user community. Moreover, its open-source hardware and software allow its users to customize their systems.

It is essential to point out that normally Arduino microcontrollers can interact with third-party sensors or other microcontrollers through several communication means. Some of the shared and most used communication means of low-cost microcontrollers such as Arduino are: Digital pins: Which can be set up to work as either inputs or outputs, Analog pins: These pins' primary purpose is to read analog sensor data and return 10-bit integers with a range of 0 to 1023. Additionally, they can be used and worked as digital pins as well, Integrated Circuit Bus (I2C): These ports are generally used for serial data exchange between integrated circuits and the microcontroller. They can also be used for connecting multiple microcontrollers as well. In this scenario, one microcontroller will serve as the Master while the others work as slaves. (The term Master and Slave are known terminologies of this type of communication), Serial Peripheral Interface (SPI): These pins are typically used for synchronous serial data protocol for communication of the microcontroller with one or more peripheral devices [122][123].

Moreover, the Arduino platform and devices are supported by a vibrant development and the user community is the significant benefit of utilizing this kind of microcontroller. To solve problems, this group communicates constantly. Arduino products also offer a flexible design, a user-friendly interface, and are simple to understand. Finally, Arduino's open-source hardware and software let users modify their developed systems [71]. It should be noted that many low-cost valuable sensors in monitoring applications can interact directly with an Arduino microcontroller (accelerometers 12 to 15 from Table 2-1 can be connected to an Arduino) [124].

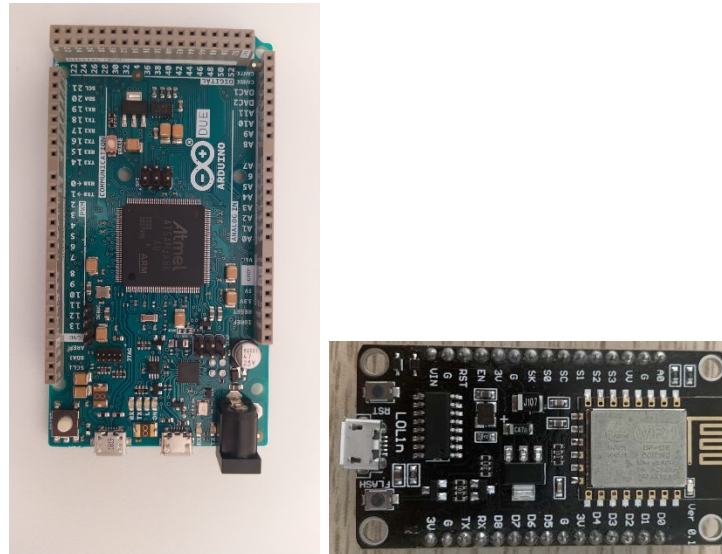
Many scholars used Arduino microcontrollers for developing low-cost structural monitoring systems. For example, Mei et al. [125] developed an unmanned ground vehicle based on an Arduino microcontroller for evaluating the pavement distress. Nasimi et al. [126] illustrated an acoustic monitoring for SHM of bridges based on Arduino technology. This system is built to assist bridge inspectors to find surface deterioration using nondestructive tests. Angelini et al. [127] created a portable Electrochemical impedance spectroscopy (EIS) instrument based on an Arduino to research the efficacy of coatings in protecting metallic historical artifacts.

Table 2-5 summarizes the characteristics of some of the Arduino products. The information gathered in this table is based on the presented data on the Arduino website [128].

Table 2-5. Characteristics of the Arduino products

Arduino product	Flash Memory	SRAM	Clock Speed	Microcontroller processor
Arduino Uno	32 KB	2.0 KB	16 MHz	ATmega328P
Arduino Nano	32 KB	2.0 KB	16 MHz	ATmega328
Arduino Leopard	32 KB	2.5 KB	16 MHz	ATmega32U4
Arduino Micro	32 KB	2.5 KB	16 MHz	ATmega32U4
Arduino Nano Every	48 KB	6KB	20MHz	ATMega4809
Arduino Nano 33 BLE	1 MB	256KB	64MHz	nRF52840
Arduino Due	512 KB	96 KB	84 MHz	AT91SAM3X8E
Arduino Mega	256 KB	8 KB	16 MHz	ATmega2560

The analysis of Table 2-5 shows a variety of choices of Arduino products. It should be noted that each system may be useful for a specific use. Among the presented microcontrollers, Arduino Due seems to have the highest clock speed, making it very interesting for further development of low-cost solutions with the need for high sampling frequency [74]. Figure 2-4.a shows an Arduino Due microcontroller.



(a)

(b)

Figure 2-4. (a) Arduino Due, and, (b) NOEMCU microcontrollers.

It should be noted that other microcontrollers are imitating the functionality of Arduino products. NODEMCU is one of the most famous types of microcontrollers based on Internet of the Thing (IoT) technology and can be programmed using the Arduino platform. NODEMCU is shown in Figure 2-4.b. The performance of this system can be compared with Arduino Due. However, its value is one-tenth of the price of the Arduino Due. NODEMCU runs on the ESP8266 chipset, a low-cost Wi-Fi microchip with the Internet protocol suite (TCP/IP) capability [129]. The low price and versatility of NODEMCU make its use very interesting in IoT systems and further development of low-cost sensors [130].

2.1.4.2 Raspberry Pi

Raspberry Pi is a single board small size Linux-based computer with many capabilities. In fact, due to the high demand for Raspberry Pi in different industry sectors, there is a shortage of this type of single-board computer nowadays. Raspberry Pi systems have the possibility of communicating, programming and controlling the third-party microcontrollers (such as Arduino) that are connected to them. This way, the operator can access the microcontroller codes for modifying or upgrading purposes.

Additionally, Raspberry Pi products run on Linux operating system and have preinstalled Python programming language. In fact, Python helps turn this low-cost computer board into low-cost data acquisition equipment. Using libraries of Python, the streamed data of sensors can be saved with microsecond resolution time stamps. These time stamps can be further used for studying and measuring the sampling frequency of the attached system to the Raspberry Pi.

There are several developed monitoring systems that use Raspberry Pi products for SHM purposes. For example, Özcebe et al. [131] studied the acquired data of 15 Raspberry Pi based low-cost

22

vibration acquisition systems whose signals were captured during multiple seismic events. Caballero-Russi et al. [132] validated a recently developed wireless sensor network based on a Raspberry Pi microprocessor to monitor the dynamic structural responses for estimating the modal parameters of civil structures. Jeong et al. [133] designed a wireless smart sensor-based automated real-time serviceability assessment system to monitor cable-stayed bridges. This system is based on a Raspberry Pi processor.

Table 2-5 summarizes the characteristics of several available Raspberry Pi products. The detailed characteristics of each presented product are based on the shown data on the Raspberry Pi website [134].

Table 2-6. Characteristics of several Raspberry Pi products.

Model	WLAN	LAN	RAM	CPU power
Pi Zero	No	No	512MB	1GHz
Pi Zero W	Yes	No	512MB	1GHz
Pi 1 Model A+	No	No	512MB	700MHz
Pi 1 Model B+	No	Yes	512MB	700MHz
Pi 2 B	No	Yes	900MB	1GHz
Pi 3 A+	Yes	No	512MB	1.4GHz
Pi 3 B	Yes	Yes	1GB	1.2GHz
Pi 3 B+	Yes	Yes	1GB	1.4GHz
Pi 4	Yes	Yes	2, 4, 6 or 8 GB	1.5GHz

Analysis of Table 2-5 shows a variety of choices for Raspberry Pi products. For using Raspberry Pi as a data logger or data acquisition equipment, systems with a RAM capacity of at least 1 GB are suggested [41]. Figure 2-5 shows a Raspberry Pi 3 B+, one of the most used low-cost processors due to having a HDMI outlet, affordable price and sufficient RAM for data acquisition [119] purposes.



Figure 2-5. Raspberry Pi B+

2.2 The gaps detected and proposed solutions.

Based on the aforementioned state of the art, this thesis detects four gaps and elaborates a solution for each.

- 1) Gap: Development and laboratory validation of low-cost accurate accelerometer suitable for SHM

It is stated by many scholars (see, e.g. [28]) that the cost of the accelerometers is one of the main limitations for the practical application of SHM analyses. These high prices usually lead to high maintenance and repair costs which reduce the applicability of the sensors for long-term monitoring. To tackle this matter, many researchers tried to develop low-cost accelerometers. To apply SHM applications to structures with a low budget for their health monitoring and long-term monitoring of infrastructures, low-cost, reliable and accurate accelerometers are needed. However, most of the solutions, such as those presented in Table 2-2, do not have comparable noise density, frequency range and accuracy with those of the commercial accelerometers shown in Table 2-1.

Solution: Development and laboratory validation of a low-cost system for the accurate measurement of structural vibrations.

Chapter 3 presents a Cost Hyper-Efficient Arduino Product (CHEAP) to fill this gap. CHEAP comprises five low-cost synchronized MEMS accelerometers that an Arduino Due controls. The main novelty of this development is noise level reduction in the vibration acquisition by combining the measurements of five synchronized accelerometers. To validate this theory, a laboratory-based experiment is designed. First, the developed sensor is located on an actuator together with two commercial seismic accelerometers (PCB 393A03 and 356B18). Dynamic motions with modest range amplitudes and frequencies between 0.5 and 10Hz were evaluated in this experiment. Then, the analyzed results of CHEAP and the commercial sensors were compared with each other.

- 2) Gap: Development and laboratory validation of low-cost inclinometers with precision suitable for SHM application.

The presented literature review shows that the currently developed low-cost inclinometers based on the microcontroller technology reveal no precise, inexpensive inclinometers based on Arduino or NodeMCU technology that could be utilized in SHM of bridges because of the unique characteristics of this type of monitoring [80]. In fact, scholars (such as [135]) indicate that the minimum accuracy of tilt measurement of the developed solutions for measuring the deformation of a bridge should be at least 0.05 degrees. It can be seen in the literature review of bridge damage diagnosis using inclinometers that a passing loaded truck induces a deformation of an order of magnitude of 0.2 degrees on the mid-span of a simply supported bridge with a span length of 20 m.

It can be deduced that the commercial inclinometers with high accuracy and an acceptable resolution are too expensive for SHM monitoring of the majority of the bridges and the currently developed low-cost inclinometers do not have an adequate accuracy for their integration in SHM applications.

Solution: Development and laboratory validation of a novel wireless low-cost inclinometer made from combining the measurements of multiple mems gyroscopes and accelerometers

To fill this gap, Chapter 4, for the first time in the literature, presents a Low-cost Adaptable Reliable Angle-meter (LARA) solution that is suitable for SHM of bridges. LARA is a wireless inclinometer powered by NodeMCU microcontroller with an accuracy of inclination measurement of 0.003 degrees. Furthermore, this Chapter studies the complementary and Kalman filter for the fusion of the measurements of accelerometers and gyroscopes of a microcontroller-based inclinometer. Moreover, a custom-designed Printed Circuit Board (PCB) containing five aligned gyroscopes and accelerometers is designed and manufactured to build an accurate inclinometer with low noise density. Finally, the Allan variance and deviation of LARA are further studied to illustrate the noise characteristics of the produced inclinometer.

- 3) Gap: There is a gap in the literature with the study of the accuracy improvement and reducing the negative impacts of personal or environmental noises of low-cost noncontact distance measuring devices. Moreover, various low-cost sensors' standard deviation and distribution functions are typically unavailable. It should be noted that those who work on developing structural system identification methods need these values for modeling measurement data. In fact, knowledgeable researchers in the analytical analysis of modeling theoretical physical models for further improvement of structural system identification methods, in the absence of access to actual measurement data, assume values for standard deviation and distribution functions.

Solution: Study of the accuracy of low-cost sensors and enhancement strategies.

Chapter 5 aims to investigate the improvement accuracy ratio of low-cost noncontact range sensors and mitigation of the ambient noises using similar sensor combinations. In addition, it is investigated whether when several comparable sensors are coupled together to measure the same parameter, the overall accuracy will be better than the estimate of a single sensor.

This Chapter employs 75 different distance sensors installed on a firm foundation with 3D printed bases to test the similar sensor combination theory. Only two microcontrollers (An Arduino Mega and an Arduino Uno) have been coupled to control 25 of each type of sensors (HC-SR04, VL53L0X, and VL53L1X). The serial communication gates of the microcontrollers' transmission and receiving ports (RX and TX ports) have been used to link the microcontrollers. A Raspberry Pi was attached to one of the microcontrollers to perform the data acquisition process. Furthermore, these low-cost range sensors' standard deviation and distribution functions for various environmental conditions are presented.

- 4) Gap: Performing low-cost vibration acquisition systems comparable to commercial solutions.

Most of the data acquisition equipment in the market is restricted by the technology of the companies that developed them and cannot be customized or connected easily with solutions developed by other companies. This characteristic might result in the need to apply technologies from different companies to monitor the structures' main structural and environmental parameters.

There is a gap in the civil engineering literature with the development of a low-cost versatile data acquisition system with a steady sampling frequency with an accurate timestamp with microsecond resolution is missing. Further study of the presented literature review reveals a lack of consistent work, including all the following points: (1) Data acquisition system with access to the accurate time of the Internet for post synchronization of different nodes. (2) Remote control, (3) A system capable of scheduling for a synchronized data acquisition initiation, and, finally, (4) Performing experimental eigenfrequency and modal analyses on an operational structure.

Solution: Development, laboratory and field validation of a low-cost wireless structural health monitoring prototype for bridges.

Chapter 6 aims to upgrade CHEAP to tackle all the detected drawbacks. To do so, this Chapter develops a system containing an accelerometer and data acquisition equipment. The system's name is chosen Low-cost Adaptable Reliable Accelerometer (LARA). Compared with CHEAP, LARA has the following significant upgrades: (1) Higher sampling frequency: by efficiently rewriting all the library codes of CHEAP, LARA achieved almost four times higher sampling frequency (333Hz) than CHEAP, (2) Data acquisition equipment: this system has its own attached data acquisition equipment which is built from a Raspberry Pi and can save the acquired data on its SD card and later upload it to a cloud drive, (3) Triaxial accelerometer: Unlike CHEAP, LARA is a triaxial accelerometer, (4) Noise Density (ND): Through laboratory experiments the actual noise density of LARA and CHEAP are presented, (5) Internet timestamp for post synchronization: By activating the Network Time Protocol (NTP) of LARA, it has access to the accurate time of the Internet. Furthermore, using python scripts and libraries, LARA can perform scheduled data acquisition. Subsequently, various LARAs located on different nodes of a structure can start a data acquisition procedure simultaneously, (6) Modal analysis: in this Chapter, a short-span footbridge situated in Barcelona, Spain, was instrumented and the analyzed eigenvalues by a certified vibration sensing device were compared with those of LARA. Moreover, a bridge in Donostia-San Sebastian, Spain was instrumented using LARA and commercial sensors (PCB 607A61) and the mode shapes generated from OMA analysis of the acquired vibrations of LARA are compared with those of PCB 607A61 accelerometers, and (7) remote access: the system can be reached, controlled or reprogrammed remotely.

Chapter 3 : Development and laboratory validation of a Low-Cost System for the Accurate Measurement of Structural Vibrations

3.1 Introduction

Nowadays, engineers are widely using accelerometers to record the vibration of structures for structural verification purposes. The main obstacle for using these data acquisition systems is their high cost, which limits its use to unique structures with a relatively high structural health monitoring budget. In this Chapter, a Cost Hyper-Efficient Arduino Product (CHEAP) has been developed to measure accurately structural accelerations. CHEAP is a system that is composed of five low-cost accelerometers that are connected to an Arduino microcontroller as their data acquisition system. Test results show that CHEAP not only has a significantly lower price (14 times cheaper in the worst-case scenario) compared with other systems used for comparison but also shows better accuracy on low frequencies for low acceleration amplitudes. Moreover, the final output results of Fast Fourier Transformation (FFT) assessments showed a better observable resolution for CHEAP than the studied control systems.

This Chapter is organized as follows: Firstly, in Subsection 2, CHEAP is fully explained and presented. Then, two piezoelectric sensors as the control systems are introduced together with their needed equipment. Finally, in Subsection 3, the laboratory test carried out in the Laboratory of Technology of Structures & Materials "Lluís Agulló" (LATEM) to validate the proposed methodology and the developed accelerometer is presented the obtained results are detailed.

3.2 Signal acquisition and processing system

In this section, the characteristics of CHEAP and control accelerometers are introduced. Moreover, the needed equipment for each sensor is reviewed together with their setting up protocol.

3.3 A Cost Hyper-Efficient Arduino Product (CHEAP)

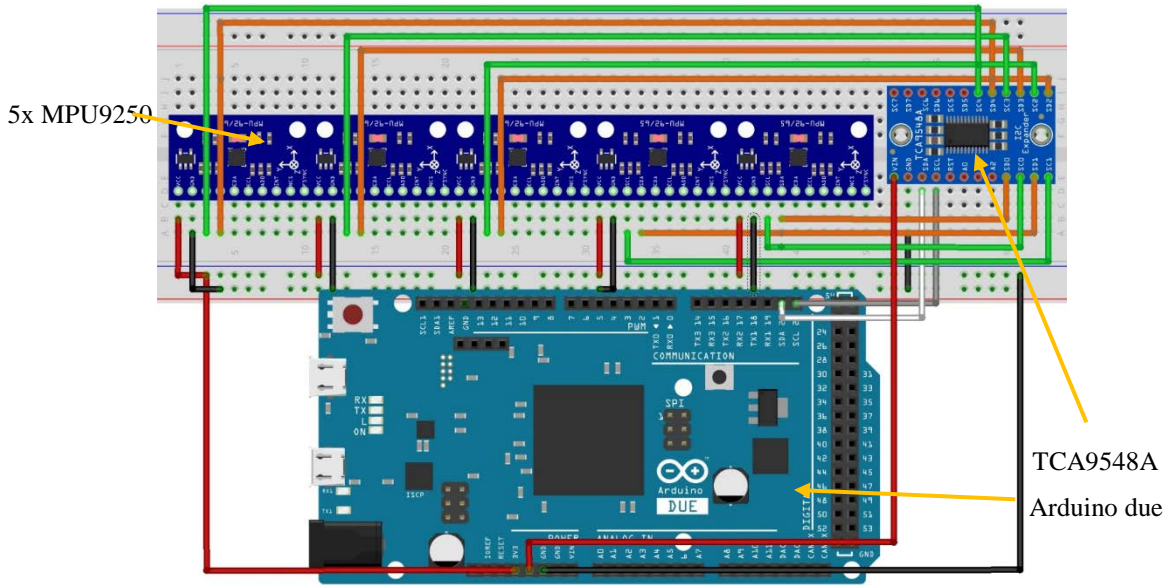
In this section, a low-cost system is proposed to accurately measure accelerations. The main novelty, which is never done before in the literature, is that instead of using the results of a single sensor, this approach averages the results of five similar low-cost MEMS accelerometers. This combination results in amending the noises, improving the resolution, and lowering the sensitivity of low-cost accelerometers. The experiences finally selected this number of combined sensors learned from the analyzed structures in the frame of the present research.

CHEAP is composed of the following elements:

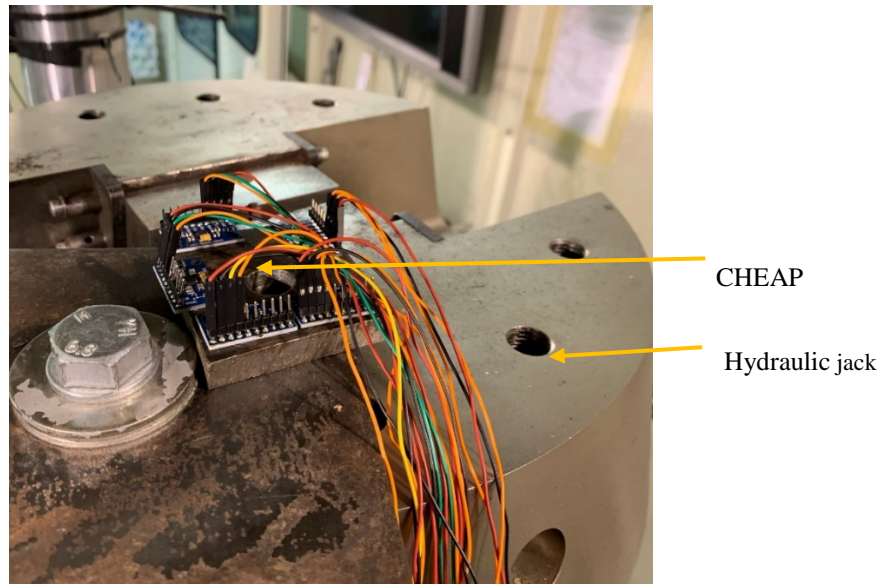
- **Microcontroller:** for this project, Arduino Due has been selected among many others provided because, firstly, it can provide a reasonable amount of memory to upload

complicated codes. Secondly, it has a faster clock speed (84MHz) of communication compared with other alternatives. In Figure 3-2.a, a sketch of this microcontroller created with the software Fritzing [136] is provided.

- MPU9250 accelerometers: the reason why MPU9250 was chosen for CHEAP is the fact that this one is the newest among those that were presented in Table 2-1, has a reasonable price, uses less energy compared with MPU6050 with less noise density and has a better range of frequency in comparison with LIS344ALH and ADXL 335, especially on low-frequency signals. The developed accelerometer needs five aligned synchronized MPU9250 sensors.
- Multiplexor: MPU9250 sensor uses the inter-integrated circuit (I2C) protocol for communicating with the Arduino [137]. I2C allows multiple “slave” digital integrated circuits (Sensors) to communicate with one or more “master” chips (Arduino). Each one of the sensors is introduced into the Arduino with a different address. On this application, five similar addressed MPU9250 have been used. Figure 3-2.b shows the attachment of the low-cost accelerometers (MPU9250) on a stiff steel plate producing the sensing part of the CHEAP. The Arduino needs a different address for each connected component to its I2C port to interact and control the sensor. A multiplexer (TCA9548A) was used to change the address of similar sensors. The multiplexer has eight bi-directional switches that are controlled by the I2C bus. For introducing each sensor in the Arduino platform, only the address of this multiplexer and the occupied channel by the sensor on the multiplexer is required [138].
- Sensor alignment: Since CHEAP consists of five sensors, they have to be placed on a rigid plate. This plate should be from a material that would not absorb or dissipate the vibrations (such as steel or aluminum). The MPU9250 sensors have their Z-axis perpendicular to their surface. Since this Chapter presents a uniaxial sensor, all MPU9250 sensors must be glued to this plate with only their Z-axis paralleled with each other.
- Ground connection: Connecting the system to the ground: the GND pin of Arduino Due must be connected to earth ground [139]. It was noticed that in the absence of this connection, the system initiation could face problems and rebooting the system would be required.



(a)



(b)

Figure 3-1. Developed signal and acquisition systems: (a) schematic CHEAP and (b) CHEAP on the experiment jack

After the hardware setting up was finished, a code was written on the Arduino platform, which gets the acceleration from all five of the accelerometers (MPU9250) simultaneously. Experiences show that Arduino Due can print information with a frequency of 250 data per second (250 Hz) for one MPU9250. With more sensors connected to the Arduino, more data has to be printed by the microcontroller with the consequent speed reduction. In fact, the frequency decreases to 85 Hz when five of these MPU9250 sensors are connected. The data printing is a highly time-consuming

operation, ergo the frequency of the overall kit decreases dramatically when more results have to be printed. The five sensors in CHEAP are not synchronized. The Arduino executes codes one line at a time. It means that when the code is executed, the Arduino connects with the first sensor and gets its measurement, and then, with the second one, and so on. This takes time. In the current CHEAP, the lag between each sensor-print is about 2.2 milliseconds. This lag is not hampering the FFT application, as this does not work with the exact time of data capture. However, if the timeline has to be improved, CHEAP measurement time output can be modified deducing 4.4 milliseconds (half the total lag between the first and last measurement).

Once recorded by Arduino, the data was saved into a PC using Python. This programming language was chosen because of its: (1) Connectivity: The library Serial enables a direct communication between Python and the Arduino serial-port, and (2) Resolution: by using the date-time library, the exact capture time of data became possible with a resolution of one microsecond. To do so, Python saved the printed data from the Arduino serial port along with their capture-time on a text file. Finally, the acceleration from all five of the MPU9250 accelerometers was averaged and reported as the final output of CHEAP.

A few essential points need to be indicated about the CHEAP project are as follows: (1) Dependency: The python program needs to be run from a computer physically attached to the Arduino. In other words, the data acquisition equipment the present system needs is a computer. It is also important to mention that the used data acquisition equipment for commercial accelerometers (PCB 393A03 and 356B18) is also dependent on an attached computer. In a nutshell, both compared systems are not wireless, (2) Automation: Even though python can be scheduled for the experiments described in this Chapter it was activated manually. Since programming the jack for each experiment was time consuming, the beginning and finishing of the data collection for the commercial accelerometers as well as for the CHEAP were done manually, (3) Serial-port: The acquired data of both commercial accelerometers and CHEAP are transferred to the attached computer during the data acquisition, and (4) Internet of Things (IoT): By running the written acquisition python code of CHEAP from a shared folder with OneDrive, the saved information was uploaded to cloud storage when the test was finished automatically. This way, the acquired data from every test is accessible.

Figure 3-3 illustrates the required steps of the proposed metering system. This process is as follows: (1) Uploading the written code to the memory of the Arduino microcontroller from the Arduino platform. (2) Connecting all the sensors and the multiplexor to the Arduino. (3) Connecting the Arduino USB port to the computer activates the sensors, and(4) Acquiring data by executing the code written in Python by the computer.

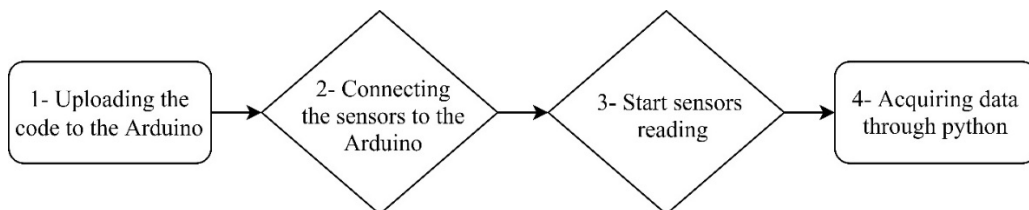


Figure 3-2. Diagram of needed steps for proposed kit data acquisition.

In a nutshell, CHEAP is an accelerometer with a low noise density and high resolution which is constructed from five low-cost accelerometers (MPU9250 sensor) with high noise density and consequently low resolution. Using a multiplexor, CHEAP receives data from all five accelerometers at the same time. At every time stamp, Arduino due receives the acquired data of all sensors. In the following, Arduino due averages the received data of five sensors and prints a single output which contains the inherent noises of the five MPU9250 sensors and the understudy signals.

CHEAP was developed for uniaxial data acquisition purposes, but MPU9250 has the possibility of recording data from all directions (Table 2-1). In other words, CHEAP is a potential triaxial accelerometer that has been programmed to be uniaxial. Unlike the usual uniaxial sensors, which only can acquire data only from one axis, CHEAP can be programmed to receive uniaxial data from any of the three directions. By programming three sets of CHEAP, one in the X direction, one in the Y direction, and one in the Z direction, a triaxial dynamic data acquisition system can be built.

It is also important to point out that the current accelerometer requires a voltage-current of 3.3 up to 5 Volt that consumes 200 mA per hour. Moreover, the currently developed accelerometer is not evaluated on an actual structure. However, for applying CHEAP for testing an actual structure, further developments are needed. CHEAP it is not waterproof or humidity-proof. For making this accelerometer waterproof, an appropriate box must be designed. Furthermore, CHEAP needs to be screwed or glued [140] properly [141] to the structure for accurate data acquisition.

3.4 Control systems description

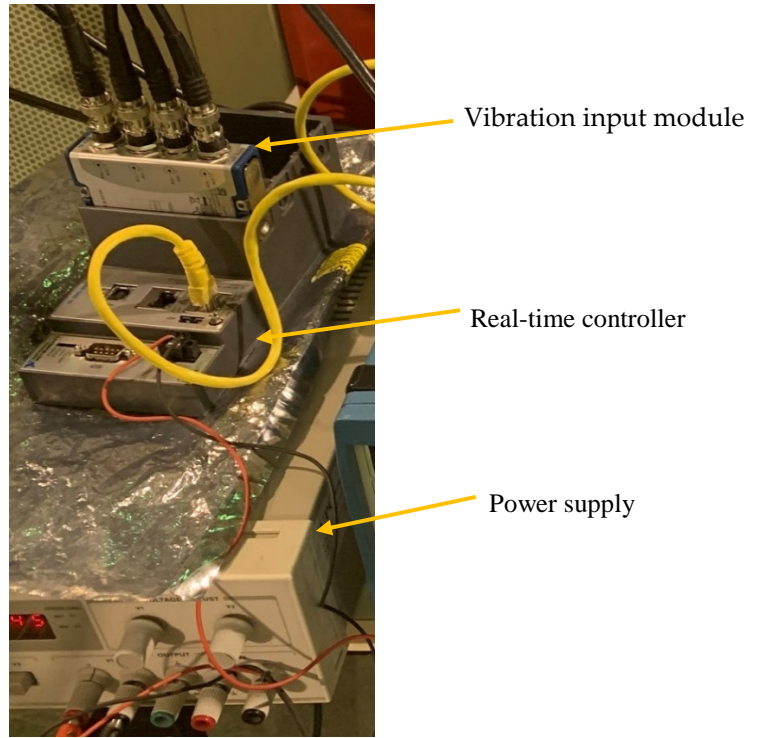
In this section, the main characteristics of the signal acquisition and processing system of two famous piezoelectric sensors are detailed. The acquisition equipment is presented as follows: (1) cRIO-9064: Embedded real-time sound and vibration input module controller that provides up to 12 channels [142], and (2) NI9234, four-channel dynamic signal acquisition module that incorporates integrated electronic piezoelectric signal conditioner for accelerometers [143]. The needed power for the real-time controller was supplied through a constant current power supply. The signal conditioner, together with this power-supply, assured the constant current excitation to the sensors required for proper operation [58]. The program used for data acquisition was able to record the acceleration time-history from the two connected accelerometers simultaneously [58]. The bestowed program was created using NI LabVIEW 2016 [144].

Two individual piezoelectric accelerometers (393A03, 356B18) were connected to the introduced acquisition equipment for reporting separated readings. The sensor 393A03 was chosen for its low noise density. Consequently, it is used as a comparison benchmark for CHEAP. This sensor is a uniaxial piezoelectric accelerometer with a sensitivity of 1000 mV/g with a proof mass of 210 grams [57]. On the other hand, the sensor 356B18 is a triaxial piezoelectric accelerometer that has the same sensitivity and a frequency range as low as 393A03 with a proof mass of 25 grams [48].

31

Although the 356B18 has a higher noise density compared with 393A03, it was used as the second reference point for CHEAP. This second reference point was used because it was thought that CHEAP may not be able to provide data as accurate as 393A03. Although 393A03 has a noise density of $2 \mu\text{g}/\sqrt{\text{Hz}}$, the accelerometers which are used to make CHEAP have each a noise density of $300 \mu\text{g}/\sqrt{\text{Hz}}$. The rest of the characteristics of both sensors are listed in Table 2-1 (sensors 4 and 9).

Acquisition system of the two studied accelerometers can be seen in Figure 3-1. a. As illustrated in this figure, both accelerometers were connected to the real-time controller equipped with the vibration input module. Finally, the real-time controller was connected to a computer using a LAN wire. The used accelerometers and their positioning in the laboratory tests are illustrated in Figure 3-1.b.



(a)



(b)

Figure 3-3. Control systems: (a) Data acquisition system for piezoelectric accelerometers and (b) positioning of the accelerometers.

3.5 Laboratory test and results

This section illustrates the resolution and accuracy of CHEAP in laboratory conditions. Firstly, the laboratory test performed is described. Then, the results obtained from the carried-out experiments are presented and discussed.

3.5.1 Laboratory test

In this section, the equipment and test setup for producing the input acceleration time-waves are presented. In these tests, the acceleration recorded by the CHEAP was compared with those obtained by the control systems. These tests were carried out on the servo-hydraulic fatigue testing machine (INSTRON 8803 [145]), shown in Figure 3-2.b, located at the Structural Laboratory Lluís Agulló of Technical University of Catalonia (Spain). This jack was programmed using WaveMatrix2 Dynamic Software [146].

To launch the acceleration time-wave signals, this device was programmed to vertically move its lower jaw with various frequencies but with the same movement of +/- 0.1 millimeters from its equilibrium location. The input acceleration amplitudes for each frequency test was calculated by getting two time differential of Eq.3-1.

$$y = d * \sin(2 * \pi * f * t + \varphi), \quad (3-1)$$

where y represents the position of the lower jack plate based on the time t , d represents the maximum allowed Jack displacement (0.1 mm), f is the set frequency, and φ is the phase constant. By getting the second-order derivative of Equation (1), the accelerations presented in Eq.3-2 can be obtained.

$$a = \frac{d^2 * y}{dt^2} = \ddot{y} = -d * (2 * \pi * f)^2 * \sin(2 * \pi * f * t + \varphi) \quad (3-2)$$

Altogether 11 experiments were launched. In Table 3-1, the set frequencies of performed tests, input amplitude during each part of the test, and the number of performed cycles are presented. In this Table, IF is the Input Frequency, and IA is the Input Acceleration Amplitude. IF and IA are expected to be recorded by the accelerometers. In this Table, the number of cycles was chosen to ensure that each experiment had the same data length for post-processing evaluations.

Table 3-1. Characteristics of introduced Waves.

IF (Hz)	IA (milli-g)	Number of cycles
0.5	0.1006	200
1.0	0.4024	400
2.0	1.6097	800
3.0	3.6219	1200
4.0	6.4389	1600
5.0	10.0610	2000
6.0	14.4874	2400
7.0	19.7191	2800
8.0	25.7550	3200
9.0	32.5970	3600
10.0	42.9300	4000

It is essential to mention that a real structure typically faces a sum of the waves introduced in Table 3-1. However, using FFT evaluation helps engineers to extract all the summed waves from a mixed signal and illustrate them individually. In fact, the commercial accelerometers are certified and calibrated on shaking tables and not on actual structures. The shaking table, which typically is uniaxial, induces vibrations within known acceleration amplitudes and frequencies. Furthermore, the results of the studied accelerometers are then compared with the known induced vibrations by the shaking table. The aforementioned information has been conducted through studying, communicating and meeting with commercial companies. Such companies sell calibrated and certified accelerometers by testing their products on a uniaxial shaking table. Then, by changing the frequency and acceleration amplitude they validate the reliability of their products. Moreover, they recalibrate or certify custom made accelerometers such as CHEAP. In the future projects, CHEAP will be calibrated and certified in one commercial company to make a professional data-sheet for it. In the current work for avoiding high expenses of sensor certifications, the introduced experiments of this work (Table 3-1) have been designed for frequency and acceleration accuracy tests.

The setting up of the sensors had to be done carefully in order to avoid any unwanted noise. Figure 3-1 and Figure 3-2 illustrate the set up for the test for both sensors (control and CHEAP). There are many ways of mounting the sensors; each one has its advantages and disadvantages, as reported in [140]. Since the surface flatness plays a vital role, special consideration was given to the mating surface. If needed, machining processes (such as lapping, spot-facing, grinding, milling, or

turning) can provide an acceptably flat mounting surface [141]. In this work, for a proper attachment of the sensors, a steel plate was bolted to the jack firmly, and the sensors were glued to this plate to avoid independent vibrations.

The sampling frequency of the CHEAP kit was fixed on 85Hz due to the speed capacity of Arduino. The sampling frequency for the two control systems was fixed to the same frequency for comparison purposes.

In this Chapter, after getting the saved signals from the accelerometers, they have been fed to the FFT assessment method.

While the control systems are feeding FFT with the data of each independent sensor, CHEAP uses averaged results of the five sensors to feed the FFT evaluation. The FFT process highlights the most captured signal as the main one and dials down the emphasis of the less frequent data. With this evaluation, the primary signal from the averaged data of five sensors gets more robust.

3.5.2 Results and discussions

In this section, firstly, the frequencies and amplitudes obtained by the different sensors (CHEAP, 393A03, 356B18) are compared. Secondly, the Marginal benefits of increasing the number of sensors in CHEAP are studied. Finally, the price comparison of the different measuring systems is presented.

3.5.2.1 Accuracy and resolution of CHEAP

By comparing the final results of the CHEAP with those of the control systems acquired is studied in this section. Furthermore, the errors of their reported data from the input frequencies and acceleration amplitudes are reported in this section. Finally, the better functionality of CHEAP compared with the control sensors is shown.

After feeding the measured data from the accelerometers to the FFT application, frequencies and amplitudes of the experiment were calculated. In Table 3-2, frequencies extracted from each of the acquisition systems are presented together with their errors from the IF (Input Frequency). In this Table, MF is the Measured Frequency obtained by the sensors.

Table 3-2. Frequency extracted from the acquired accelerometers together with their error.

IF (Hz)	393A03		356B18		CHEAP	
	MF (Hz)	Error (%)	MF (Hz)	Error (%)	MF (Hz)	Error (%)
0.5000	-	-	-	-	0.5012	0.2420%
1.0000	-	-	-	-	0.9993	0.0690%
2.0000	2.0003	0.0150%	2.0003	0.0150%	2.0002	0.0100%
3.0000	3.0005	0.0167%	3.0005	0.0167%	2.9996	0.0133%
4.0000	3.9997	0.0075%	3.9997	0.0075%	3.9996	0.0100%
5.0000	4.9998	0.0040%	4.9998	0.0040%	5.0007	0.0140%
6.0000	6.0002	0.0117%	6.0002	0.0117%	5.9997	0.0050%
7.0000	7.0004	0.0057%	7.0004	0.0057%	6.9994	0.0086%
8.0000	8.0006	0.0075%	8.0006	0.0075%	7.9991	0.0112%
9.0000	8.9998	0.0022%	8.9998	0.0022%	9.0004	0.0044%
10.0000	9.9996	0.0040%	9.9996	0.0040%	10.0004	0.0040%

Table 3-2 shows that all the accelerometers are working correctly on frequencies equal and higher than 2 Hz and are reporting precisely the input frequencies (IF). CHEAP (unlike the control systems) works well even for low range frequencies. In fact, while the control sensors were unable to allocate signals lower than 2 Hz, CHEAP was able to capture them. Although the data-sheet of the control systems (Table 2-1, sensor 4 and 9) illustrates that these sensors should be able to read frequencies from 0.5 Hz to 3000 Hz, the obtained results showed that they were not able to read accurately frequencies lower than 2 Hz with low acceleration amplitudes. The results of all applications are pretty close from 2Hz to 10 Hz (less than 0.014 % of error from the reference frequency).

In Table 3-3, amplitudes extracted from the accelerometers for the Z-axis, together with their errors from the IA (Input Acceleration), are presented. In this Table, MA refers to the Measured Acceleration amplitudes by the sensors.

Table 3-3. Amplitudes extracted from the accelerometers together with their error.

IA (input wave) (Milli- g)	393A03		356B18		CHEAP	
	MA (Milli- g)	Error (%)	MA (Milli- g)	Error (%)	MA (Milli-g)	Error (%)
0.1006	-	-	-	-	0.1022	1.5530%
0.4024	-	-	-	-	0.3966	1.4538%
1.6097	1.7319	7.5900%	1.7561	9.0934%	1.5977	0.7468%
3.6219	3.4947	3.5113%	3.7569	3.7281%	3.6638	1.1576%
6.4389	6.3189	1.8635%	6.3507	1.3696%	6.3536	1.3245%
10.0608	9.9082	1.5164%	10.2988	2.3660%	10.0016	0.5880%
14.4918	14.5964	0.7517%	14.4106	0.5308%	14.5063	0.1298%
19.7191	19.8035	0.4281%	20.1582	2.2268%	19.3468	1.8880%
25.7555	25.4122	1.3331%	25.9151	0.6195%	25.5072	0.9642%
32.5969	33.1459	1.6843%	33.4779	2.7028%	33.5534	2.9345%
40.2430	40.0529	0.4725%	40.5612	0.7906%	41.1806	2.3298%

The analysis of Table 3-3 shows that for those accelerations whose value was lower than 25.5, Mili-g, CHEAP worked better than the 356B18. For the accelerations whose amplitude was lower than 14.5 Milli-g, CHEAP worked better than the 393A03. These data clearly show that CHEAP was able to compete with the two control systems. This Table also illustrates how the performance of CHEAP is especially interesting for small amplitudes.

In Figure 3-4, the MA error of the control systems and CHEAP is shown. The horizontal axis represents the frequency (Hz) of the experiment, and the vertical axis shows the error in percentage.

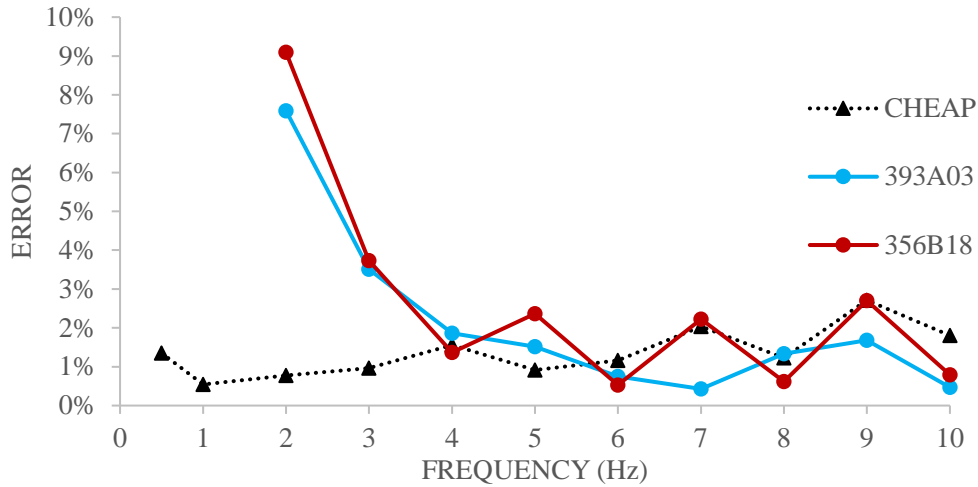


Figure 3-4. Comparing MA error of the two control systems with CHEAP

Analysis of Figure 3-4 shows that on lower amplitudes, CHEAP (compared with the two control systems) worked steadier and more accurately until 6 Hz. This figure also illustrates that the control systems only began to provide better accuracy on frequencies higher than 6 Hz. Moreover, in higher amplitudes, the errors of the different applications were quite close. The maximum experienced errors from the input acceleration amplitude on the highest experienced amplitude for CHEAP, 393A03 and 356B18 were as low as 0.47%, 0.79%, and 2.33%, respectively.

3.5.2.2 Effect of the number of sensors

In this section, the beneficial effects of adding an increasing number of averaged sensors are studied in detail.

In Figure 3-5, estimated errors obtained for a different number of sensors in CHEAP are compared. The Max and the Min in each graph represent the enveloped error for all the possible sensor selections from the five available accelerometers (CHEAP represents the proposed kit with five sensors). The results of the increasing number of sensors are presented in Figure 3-5.a (one sensor), 3-5.b (two sensors), 3-5.c (three sensors), 3-5.d (four sensors). In all these figures, the horizontal axis presents the frequency of the experiment, and the vertical one illustrates the MA error in percentage. The MA for 0.5 Hz is not presented in Figure 3-5.a and 3-5.b because the system resolution for acquiring low acceleration amplitudes was insufficient.

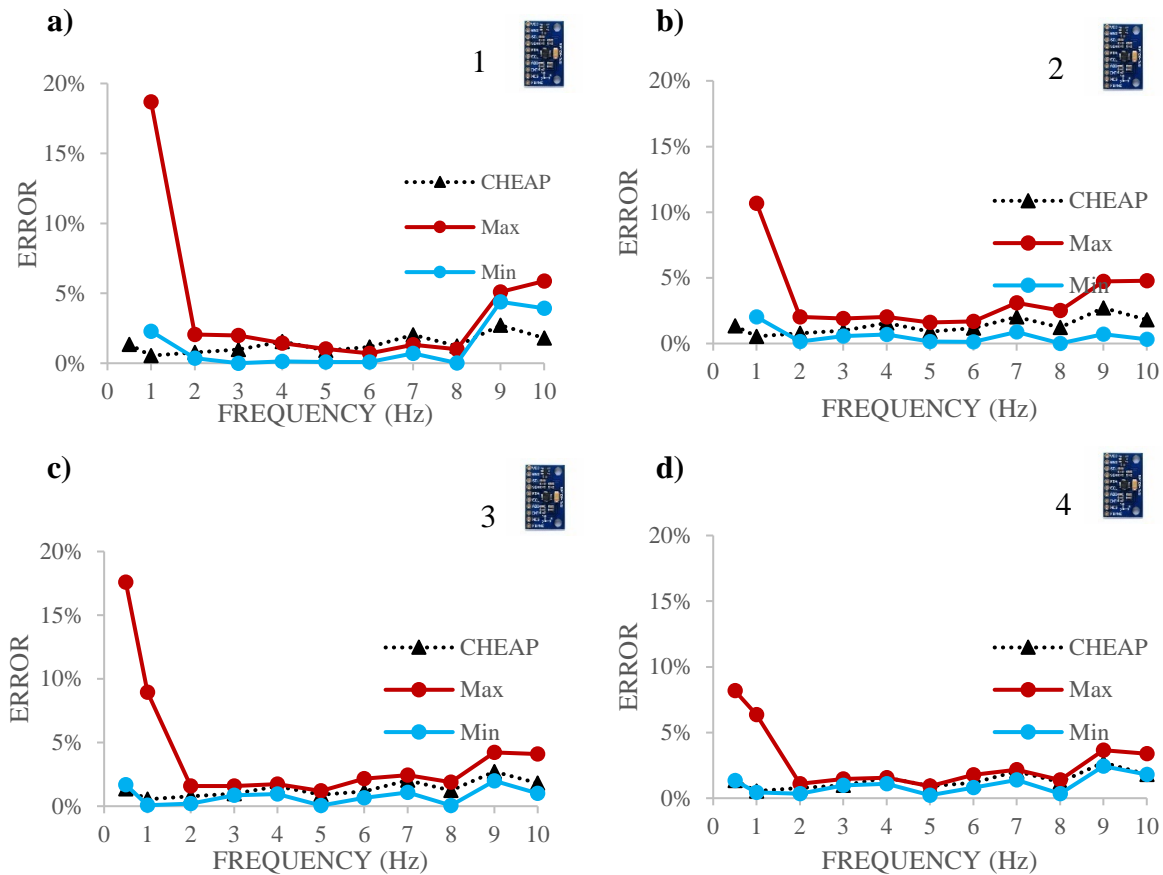


Figure 3-5. Estimated MA error for different number of sensors: one sensor (a), two sensors (b), three sensors (c), four sensors (d)

The analysis of Figure 3-5 shows that, as expected, the error depends to a greater extent on the number of sensors and the analyzed frequency. The experienced error for one, two, three, four and five (CHEAP) were at the worst-case scenario 18.67%, 20.12%, 17.58%, 8.17%, and 1.55% respectively. Therefore, it can be concluded that lower errors are obtained when the number of accelerometers is increased, especially on the tests with lower acceleration amplitude (less than 0.4 milli-g). Results in Figure 3-5 also show that the part of the experiment which had the lowest frequency (0.5 Hz) could be considered as the most important one for the following reasons. Firstly, the highest experienced error appears there. Secondly, the lowest acceleration amplitude (0.1022 milli-g) is in this part of the experiment. In a nutshell, locating this low-level acceleration amplitude (MA) from the FFT evaluation was an opportunity to compare the resolution and accuracy of CHEAP with a different number of sensors.

For a single MPU9250 accelerometer, the resolution for this part of the experiment was not enough. The resolution of the kit with a single accelerometer appeared to be at least 0.19 Milli-g. The amplitude of the needed signal was less than this resolution. As a result, finding and reporting this signal from the FFT output was not possible. The resolution for the kit of sensors with two MPU9250 accelerometers was not entirely clear either. This resolution was at least 0.13 milli-g, which is still 0.03 milli-g higher than the value of the captured signal. The resolution for the kit of

40

sensors with three MPU9250 was about 0.10 milli-g. As a result, finding the amplitude of this part of the experiment was still impossible.

Results of the FFT application for the lowest tested frequency (0.5 Hz) for a different number of sensors is presented in Figure 3-6.a (four sensors), Figure 3-6.b (five sensors).

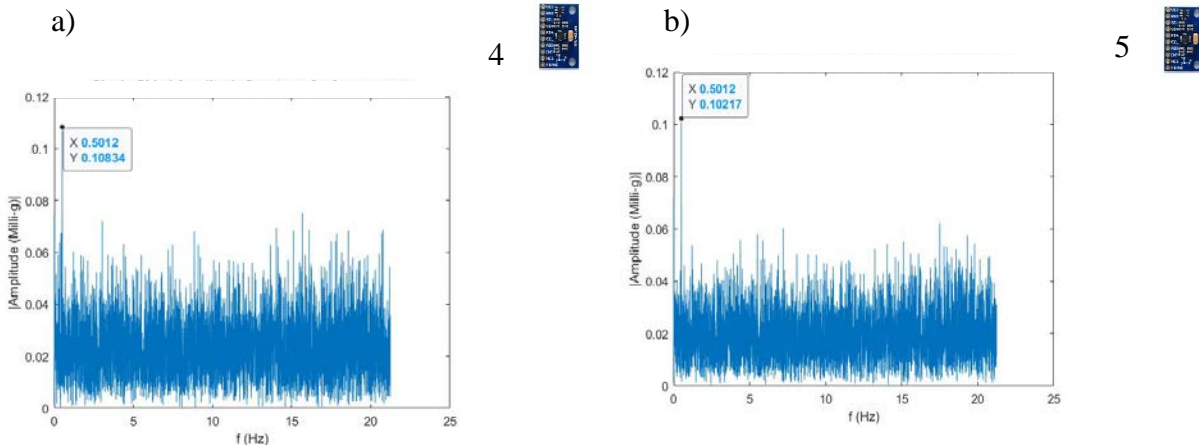


Figure 3-6. FFT data process for 0.5 Hz experiment errors for four sensors (a) and five sensors (b)

For reporting the resolution of each system from the FFT diagram, the amplitudes of acquired signals were investigated. It is known in this figure that the MA should have a frequency of 0.5 Hz. As a result, any other wave can be considered as an unwanted signal, and the highest amplitude among these unwanted signals is the resolution of this system. Table 3-3 reports the IA for the signal with a frequency of 0.5 Hz as 0.1006 Milli-g. The analysis of Figure 3-6.a illustrates that with four MPU9250 accelerometers, the resolution of the system is slightly less than 0.08 Milli-g. This resolution enabled locating the needed signal from the FFT output diagram possible. This figure reports the MA of the signal as 0.10384 Milli-g, which has a 3.22% error from the IA. On the other hand, the analysis of Figure 3-6.b shows that the kit of sensors with five MPU9250 (CHEAP) provides a resolution of around 0.06 Milli-g. In addition, it was deduced that CHEAP had an error of 1.55% from the IA.

A kit of sensors with five MPU9250 (CHEAP) has a sampling frequency of 85Hz and a resolution of 0.06 Milli-g. In addition, CHEAP provided exceptionally accurate outputs for accelerations less than 14.5 milli-g. Moreover, CHEAP worked properly where the commercial sensors were unable to provide any data whatsoever. As it was already discussed, the two studied control systems were not able to provide MA of the needed signal for the experiment with 0.5 Hz frequency. This was due to the low resolution of the control accelerometers. From the FFT outputs for the experiment with 0.5 Hz frequency, it was seen that 393A03 and 356B18 have a resolution of about 0.5 and 1.6 milli-g, respectively.

3.5.2.3 Price comparison

The overall price comparison of the used sensors and their equipment has been presented in this section.

In Table 3-4, the price of the equipment of each of the studied acquisition applications is presented. This Table includes the following information organized in columns: (1) System: the application which uses the illustrated accelerometer, (2) Price of the used accelerometers: the accelerometer of CHEAP was composed of five MPU9250 with a unitary cost of 5.76 €, a 3.22 € multiplexor (TCA9548A) and a 4.03 € breadboard, (3) Price of the microcontroller, (4) Price of the cable: the cable for all of the systems were three meters. CHEAP is using normal cables, whereas cables required by the two control systems are special noiseless cables, (5) Price of the real-time controller, (6) Price of the vibration input module, (7) Dimension of the sensing part, (8) Weight of the sensing part. It can be deducted that CHEAP is not much bigger or heavier than the control accelerometers. It must be noted that although the software used for the control systems was 3549 € CHEAP used the Arduino platform and Python, both free. It should be noted that the indicated prices in this table are based on the declaration of the realtors in 2021.

Table 3-4. Price comparison of the three systems

System	Cost of the Accelerometer (€)	Cost of the Microcontroller (€)	Cost of the Cable (€)	Cost Real-time controller (€)	Cost Vibration input module (€)	Dimension of the sensing part (mm)	Weight of the sensing part (gr)
393A03	710	-	75	2010	2050	28*28*56	210
356B18	1300	-	210	2010	2050	20*26*20	25
CHEAP	36.1	38.017	10	-	-	50*50*10	357

From the analysis of Table 3-4, it can be seen that the price of an acquisition system with a single 393A03 is 57 times higher than CHEAP. Nevertheless, the introduced equipment for the control systems has the capacity for more sensors. In order to make a fair price comparison between the control systems and CHEAP, the full capacity of the equipment should be taken into account. Real-time control provides 12 channels, and the vibration module has four channels. For a uniaxial control system on full capacity: 12 393A03 accelerometers, 12 sets of single channeled cables, one real-time controller, three vibration input modules are needed. The overall price is about 17580 € (VAT excluded). For a triaxial control system on full capacity: four 356B18 accelerometers, four sets of three channeled cables, one real-time controller, three vibration input modules are needed. The overall price is about 14200 € (VAT excluded). As it was mentioned before, three sets of CHEAP can be programmed to make a triaxial sensor. As a result of this potentiality, 12 sets of CHEAP can either be used as 12 uniaxial accelerometers or four triaxial accelerometers with a proximate price of 1008.84 (VAT excluded).

In Figure 3-7, a comparison of the total price of the different measuring devices, when each acquisition system has 12 channels, is presented. This comparison does not take into account the price of the control system software nor the needed power supply for the control sensors. It should

be noted that comparing an academically developed device with a commercial alternative is not fair.

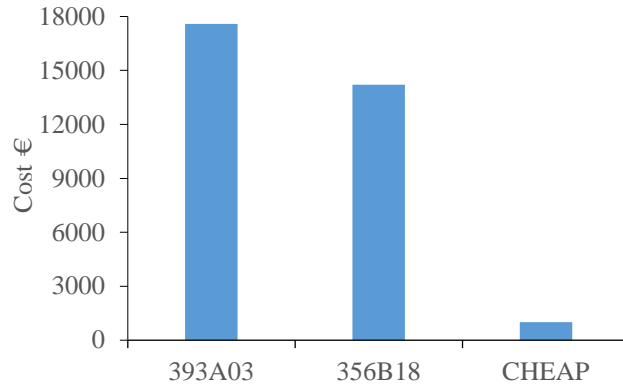


Figure 3-7. Price comparison of CHEAP with control systems

As shown in Figure 3-7, the total price of an acquisition system with 12 channels of CHEAP is about 17 times lower than the control acquisition system with all the 12 uniaxial (393A03) accelerometers and 14 times lower than the same system occupied with four triaxial (356B18) accelerometers. In addition, the needed equipment for running the CHEAP is fewer than the control systems, which would make setting up the CHEAP easier and faster than the control systems.

There are a few developed SHM applications in the literature that use low-cost solutions for vibration acquisition that stand out. Using the CHEAP methodology in either of them can make the SHM system cheaper and will be addressed in future works. For example, P. Barsocchi et al. [147] proposes a united structural simulation and monitoring application for health assessment of a historical building. It is mentioned that the wireless SHM system has an acceleration amplitude range of 0.1 up to 1000 milli-g with a sampling frequency of 100 Hz. P. Barsocchi et al. [148] presents a monitoring system connected to a wireless network with automated continuous data evaluation in real-time. This Chapter presents informative data on the long-term monitoring of a heritage building. This application has an automatic modal identification procedure that allows long-term monitoring of the effects of the temperature and wind on the eigen frequencies of the under-study structure. The vibration acquisition has been made by a custom-made uniaxial accelerometer with a sensitivity of 1.35 V/G, noise output of $7 \mu\text{g}/\sqrt{\text{Hz}}$ and acceleration amplitude range of $\pm 2\text{g}$. (3) M. Bacco et al. [149] illustrates the implementation of a remote SHM application that uses an Unmanned Aerial Vehicle (UAV) for collecting environmental and mechanical acquired data of several sensors. The used vibration acquisition system of this project uses the same chipset (Colibrays Safran model VS1002) as in [148] It is essential to mention that this methodology can make structural inspection faster, easier and safer. P. Barsocchi et al. [150] also present a remote long-term structural monitoring system. This system uses the LIS344 (Number 12 in Table 2-1) circuit. For solving the low resolution of the used accelerometer, a signal-processing procedure was performed, which limited the outputs of the vibration acquisition to a

frequency range between 0 and 5 Hz. CHEAP uses several fused sensors for noise enhancement and has a frequency range of 85 Hz. Moreover, the presented results of CHEAP in this Chapter are carried out without using any data post-processing or applying low-pass or high-pass filters.

Chapter 4 : A Novel Wireless Low-Cost Inclinometer Made from Combining the Measurements of Multiple MEMS Gyroscopes and Accelerometers

4.1 Introduction

Structural damage detection using inclinometers is getting wide attention from researchers [151]. However, the high price of inclinometers limits this system to unique structures with a relatively high Structural Health Monitoring (SHM) budget. This Work presents a novel low-cost inclinometer, Low-cost Adaptable Reliable Angle-meter (LARA), that combines five gyroscopes and five accelerometers to measure the inclination. LARA incorporates an Internet of Things (IoT) based microcontroller technology enabling wireless data streaming and free commercial software for data acquisition. This Work investigates the accuracy, resolution, Allan variance and standard deviation of LARA produced with a different number of combined circuits, including an accelerometer and a gyroscope. To validate the accuracy and resolution of the developed device, its results are compared with those obtained by numerical slope calculations and a commercial inclinometer (HI-INC) in laboratory conditions.

The results of a load test experiment on a simple beam model show the high accuracy of LARA (0.003 degrees). The affordability and high accuracy of LARA makes it applicable for structural damage detection of bridges using inclinometers.

This Chapter is organized into four Subsections. In the second Subsection, first, the proposed low-cost solution (LARA) is presented. Then, the commercial inclinometer used as a reference value in the Chapter (HI-INC) is introduced. In the third Subsection, resolution experiments analyzing the beneficial effect of a similar sensor combination are illustrated. Finally, the fourth Subsection is dedicated to laboratory experiments verifying the accuracy and resolution of the LARA, plus the results and discussions.

4.2 Control system and the proposed inclinometer

In this section, first, the proposed inclinometer of this work is presented. In addition, the needed equipment and the setting up protocol of the control system and the proposed inclinometer are reviewed. Then, the main characteristics of a control system for measuring inclination are drawn.

4.2.1 Low-cost Adaptable Reliable Angle-meter (LARA) system

In this section, the hardware architecture of the proposed inclinometer is presented. Then, the software part of this system is explained and shown.

4.2.1.1 Hardware Architecture of LARA

This Chapter proposes multiple combinations of gyroscopes and accelerometers for producing a more accurate inclinometer. To this end, five chipsets of MPU9250 are engineered together on a

45

single PCB and synchronized using a multiplexor (TCA9548A). To avoid the problems of a manual fabrication (such as nonalignment of the circuits, time-consuming process of aligning, soldering and sensor quality control and size), the PCB of LARA was designed and produced to satisfy the delicacy of current project measurements. In addition, the required components of LARA are soldered to the PCB using machine assembly. Figure 4-2.a and Figure 4-2.b show the produced sensor and its blueprint.

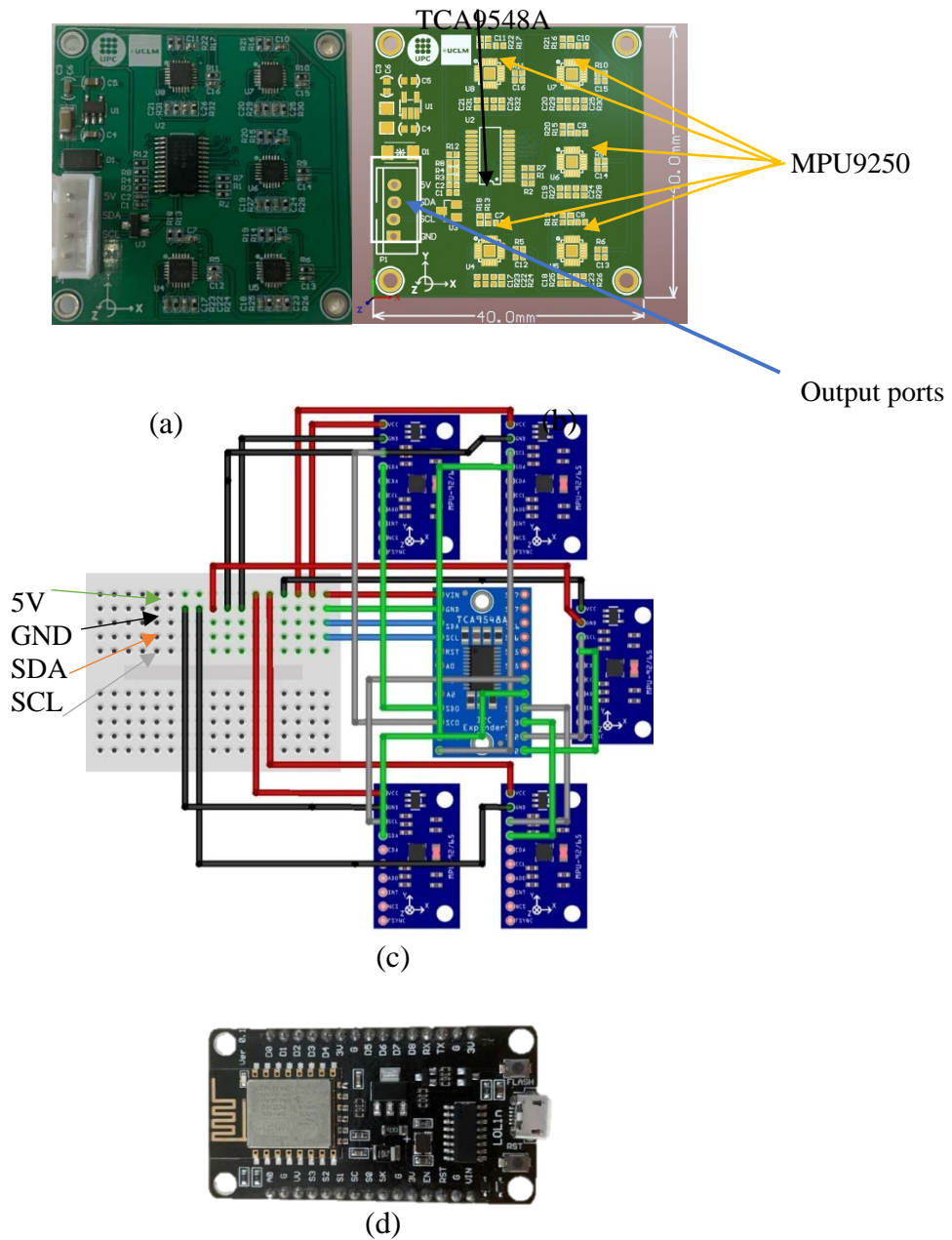


Figure 4-1. Illustration of LARA: (a) The produced product, (b) The blueprint of the designed PCB, (c) The Fritzing sketch of the system, and (d) NODE MCU microcontroller.

It should be noted that LARA can be assembled by hand using available commercial MPU9250 circuits and a TCA9548A multiplexor. Figure 4-2.c shows the Fritzing [136] sketch of the system. The cost of a LARA made by connecting five MPU9250 and TCA9548A and a bulk company-produced PCB with assembled components is around 37 and 51 € respectively.

As shown in Figure 4-2.a and b, LARA has four output ports. These wires should be connected to a microcontroller to power up the sensors, acquire the sampled data, and convert the gyroscope and the accelerometer to tilt and pitch inclination. The used microcontroller of this Chapter is NodeMCU and shown in Figure 4-2.d. This low-cost open-source Internet of Things (IoT) platform runs on the ESP8266 chipset. ESP8266 is a low-cost WiFi microchip with the Internet protocol suite (also known as TCP/IP) capability [129].

4.2.1.2 Software Architecture of LARA

In this section, the used software for this project is presented in the following:

- Arduino platform: NodeMCU is first programmed using the Arduino platform. This program first estimates the angle in real-time from each of the individual MPU9250 chipsets. Then, the formulas for calculating the rotation using a triaxial accelerometer for X and Y axes are presented in Eq.4-1 and Eq.4-2, respectively.

$$angle_{accX} = \tan^{-1} \left(\frac{accY}{\sqrt{accZ^2 + accX^2}} \right) \times \left(\frac{360}{2\pi} \right) \quad (4-1)$$

$$angle_{accY} = \tan^{-1} \left(\frac{accX}{\sqrt{accZ^2 + accY^2}} \right) \times \left(\frac{360}{2\pi} \right) \quad (4-2)$$

where, $angle_{accX}$ and $angle_{accY}$ are the calculated angles from the acquired data of a MPU9250 accelerometer around the X-axis and Y-axis, respectively. The $accX$, $accY$ and $accZ$ represent the obtained acceleration data of X, Y and Z axes. Then, using a complementary filter, the calculated angle from the accelerometers and the acquired data of the gyroscopes are combined. Eq.4-3 and Eq.4-4 present the used complementary equation for the fusion of the gyroscope and the accelerometer results for measuring the rotation around X and Y axes, respectively.

$$\bullet \quad angleX = (0.96 \times (angleX_0 + gyroX \times time)) + 0.04 \times angle_{accX} \quad (4-3)$$

$$\bullet \quad angleY = (0.96 \times (angleY_0 + gyroY \times time)) + 0.04 \times angle_{accY} \quad (4-4)$$

where, $angleX$ and $angleY$ are the final calculated rotations around X and Y-axes, respectively. The $angleX_0$ and $angleY_0$ are the estimated angle of the system from the previous measurement. In the initiation of the data acquisition, it should be noted that this value equals zero. After that, it represents the rotation progress. The $GyroX$ and $GyroY$ represent the measured angular speed of the gyroscope for X and Y axes, respectively. The $time$ presents the interval time between two measurements. Further analysis of these equations shows that the angle calculated from the accelerometer is multiplied by a smaller coefficient than that of the gyroscope [152]. This low coefficient factor of $angle_{acc}$ is for

mitigating the impact of environmental vibrations (also known as cross-talk of vibration) and can vary between 0.02 and 0.05 [153].

These equations are repeated for every MPU9250 chipsets of LARA. Then, the inclination values of the five chipsets are averaged separately for X and Y axes. It is to be known that this code makes the implemented accelerometers and gyroscopes of LARA to sample data and estimate the angles in a synchronized way. Finally, using the already introduced Service Set Identifier (SSID) and the router's password in the Arduino code, the averaged results of X and Y axes are transmitted to a made-up server client by the built-in ESP8266 chipset. LARA prints a server address and a port number at this stage on the serial port of the Arduino. This information should be noted and LARA can be detached from the programming computer. After this, the sensor can be disconnected from the PC and plugged into any available USB power break.

- Virtual serial port: After connecting LARA to a USB power source, the data sampling function initiates automatically. This chipset's TCP/IP capability helps this sensor provide its outputs on a local server. A computer connected to the same SSID as LARA can stream the sampled data by introducing the noted server address and port number of LARA. In order to acquire the sampled data and have a real-time graphical representation of the LARA inclination, a virtual serial port application is used [HW [154]]. This free software needs the server address and the port number of LARA and creates a virtual serial port communication connection between LARA and a windows-based computer. By selecting the provided virtual port of the HW software on the Arduino platform, LARA's sampled data can be streamed or graphed just when the sensor is connected to the computer. A computer can indeed be connected physically to several sensors, but with HW virtual serial port, up to 99 devices can be wirelessly attached to a single computer.
- Data acquisition: Unlike the Arduino platform, free commercial software like SerialPlot [155] can represent the sampled data in real-time in a graphical interface and save the data with the date and timestamp of data acquisition. The presented flowchart in Figure 4-3 shows the steps of real-time inclination acquisition using LARA.

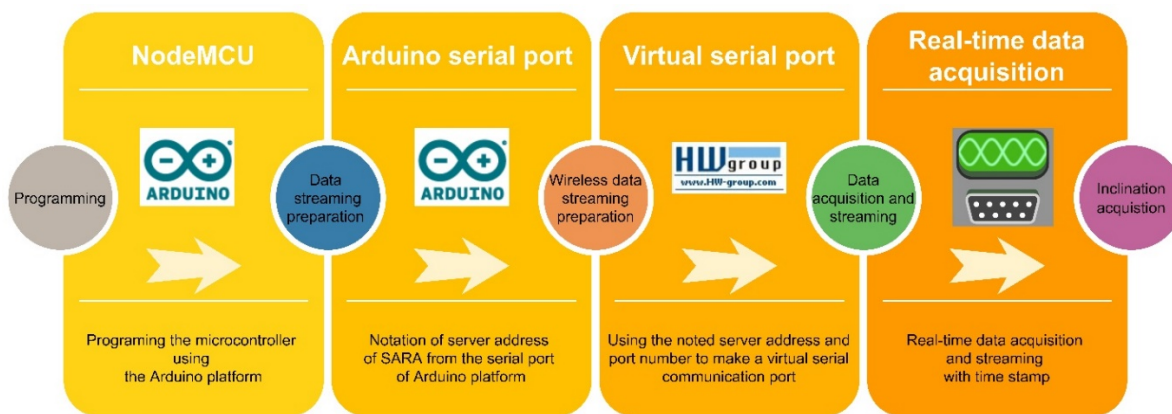


Figure 4-2. The required steps of real-time wireless inclination acquisition using LARA inclinometer.

4.2.2 Control system description

In the current study BeanDevice® Wilo HI-INC (Figure 4-1.a), an Ultra-Low-Power (ULP) biaxial WIFI inclinometer, was used as the high-accuracy controlling system. This device contains a built-in data logger that can store up to 5 million data logs with a maximum wireless range of 200 meters. Regarding angle measurements, it combines a high-performance inclinometer sensor and a 24-bit delta-sigma analog-to-digital converter, making it possible to have a high-level accuracy of $\pm 0.003^\circ$ for $\pm 15^\circ$ and a resolution of 0.001° . In addition, the body of the HI-INC inclinometer is composed of a lightweight aluminum casing with waterproof capability [156]. The program used for data acquisition is a commercial solution promoted by the BeanDevice company and costs 350 € By taking in the price of this inclinometer from Table 2-3 and the needed commercial software for data acquisition. In other words, the whole solution costs around 1000 € It should be noted that these prices are based on the purchase of the Bean air company's commercial solution in 2021.

The data acquisition program of BeanDevice company acquires and in real-time illustrates the X and Y axis' inclinations (Figure 4-1.b). Finally, it should be noted that the settings of data acquisition (such as sampling frequency) can be modified from the main menu of the commercial program (Figure 4-1.c).

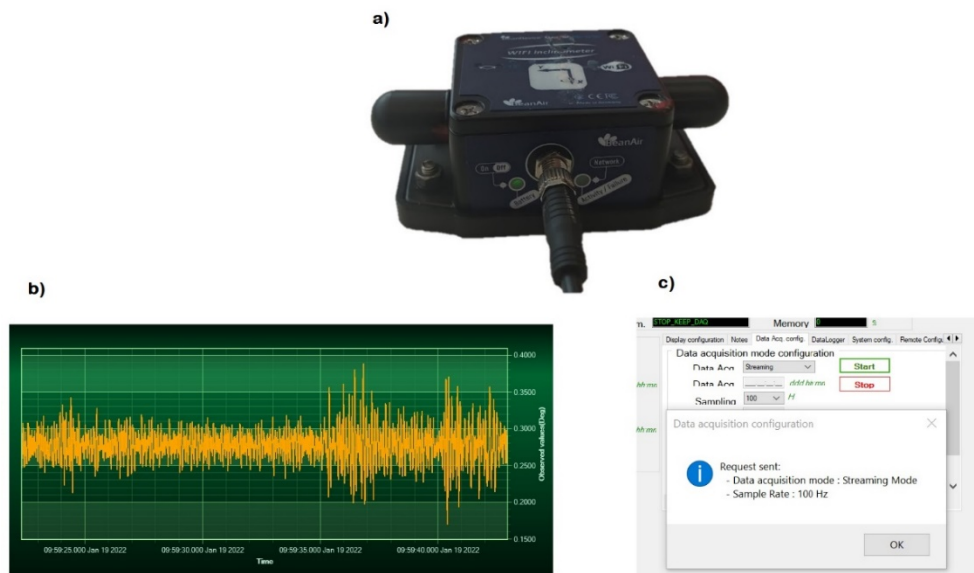


Figure 4-3. HI-INC biaxial inclinometer, b) inclination streaming over X axis and c) Sampling frequency rate.

It should be noted that the inclinometer HI-INC has been recently used as a wear on gadget for frequency analysis of a walking pedestrian for assessment of lightweight glass slabs (see e.g. [157]).

4.3 Statistical representation of combining dynamic-sensor theory

This section first studies the effect of sensor combination on the noise density, standard deviation and resolution of angle measurements. Then, the Allan variance and its importance in evaluating the noise density of inclinometers in the literature are explained. Finally, the Allan variances of several combined sensors are presented.

4.3.1 Noise reduction of Inclinometers

This section explains an experiment that leads to combining up to five similar circuits (MPU9250) for reducing the overall dynamic (harmonic) noises. During this experiment, the inclinometers were placed in a quiet environment, far away from crowds and with reduced induced ambient vibrations. The aim of this experiment is to measure and evaluate the pure noise ratio of different combined inclinometers.

It was noticed that the average value of outputs of several aligned synchronized inclinometers has lower noise density than the those of a single one. The standard deviation of up to five combined inclinometers is presented in Figure 4-4.a.

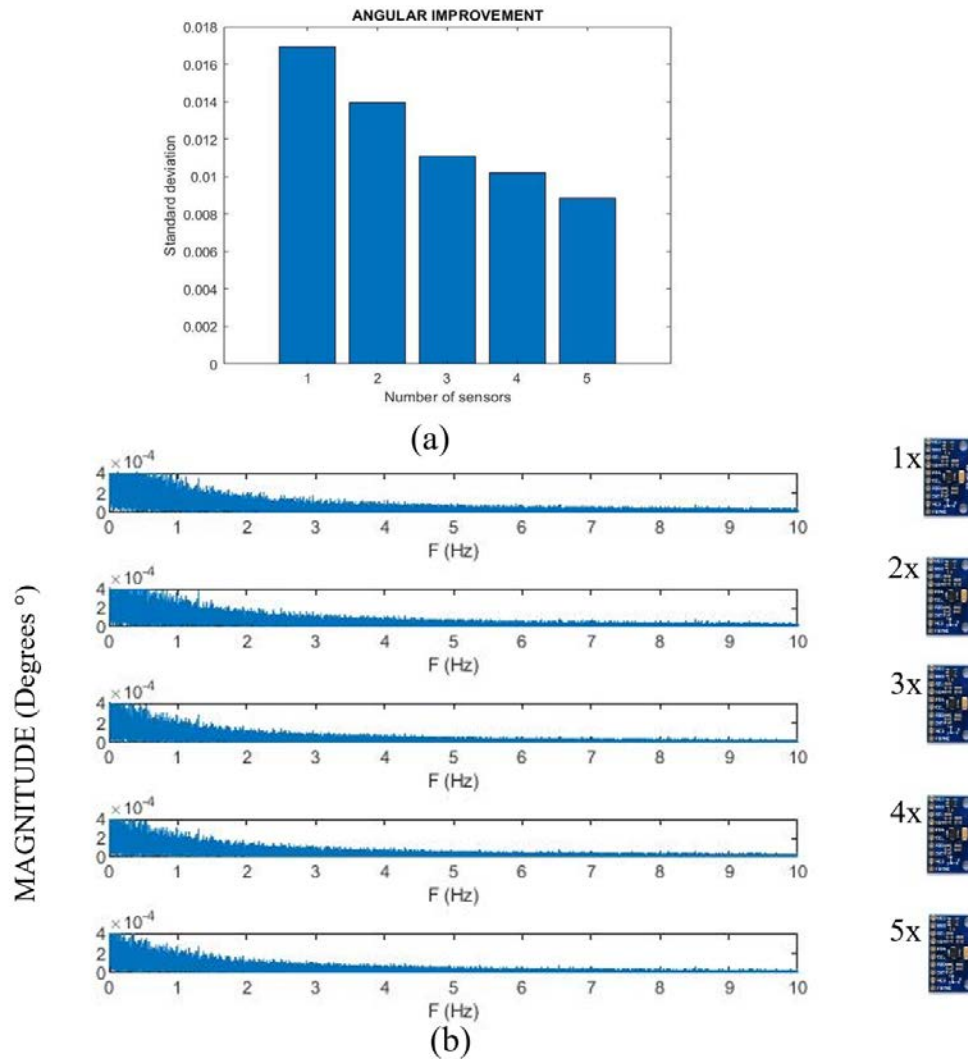


Figure 4-4. Representation of the noise ratio of a single and up to five combined inclinometers using: (a) standard deviation, and (b) noise density in frequency-domain.

The analysis of Figure 4-4.a shows that the higher the number of sensors considered the lower the noise density of their averaged measurements that the more combined inclinometers have a lower noise density. The reason behind the beneficial behavior of combined inclinometers is within the inherent dynamic noises of the produced accelerometers and gyroscopes chipsets. Figure 4-4.b shows the frequency domain illustration of the performed experiment. Data transformation from the time domain to frequency domain is done using Fast Fourier transformation (FFT). The analysis of Figure 4-4.b shows that the magnitude of the dynamic noises of the averaged values of a set of sensors made from combined inclinometers is lower than that of a single one. It can be seen that on 1 Hz the measured noises for a single inclinometer and five combined inclinometers are 3.9×10^{-4} and 2.6×10^{-4} degrees, respectively.

These results led to investigating the beneficial impact of dynamic sensor combinations. Analyzing the individual outputs, the five used MPU9250 sensors showed that every single sensor has unique dynamic noises.

Furthermore, a single output that includes the averaged inherent noises of all individual inclinometers plus the understudy signal (the rested situation or sets of dynamic movements) is obtained by averaging the outputs of several inclinometers. Since the understudy signals are not dependent on the characteristics of the inclinometers, they have not affected throw-out the FFT process. The FFT highlights the most repeated signals (the understudy ones) and undervalues those that are repeated less, such as the inherent individual noises of the sensors. By improving the noise density, the inclinations that in the first place were smaller than the noise density of the sensor can now be detected due to the improved noise level.

4.3.2 Study of Allan variance

Allan variance is typically used to characterize and analyze those noises that drift throughout time in time-domain series [158]. In fact, Allan variance quantifies the measurement variance of a sensor across different timescales. On the contrary to frequency-domain noise evaluation methods such as spectral Noise Density (ND), Allan variance is a time-domain evaluating tool of different noise sources (such as Quantization, angle random-walk, bias instability, rate random-walk, and rate ramp) [159]. Allan variance shows the progress of a noisy sensor signal over time which can be very useful to identify the progressive random walk of a gyroscope instead of ND that quantifies the noise density of an accelerometer [158]. Allan deviation is more commonly used as the square root of Allan variance [160]. The available acquired inclination acquisition data for measuring the standard deviation of the previous subsection was used for the Allan variance and deviation calculations. Figure 4-5.a and Figure 4-5.b shows the log-log plot of Allan variance and Allan deviation of a single and up to five synchronized inclinometers, respectively.

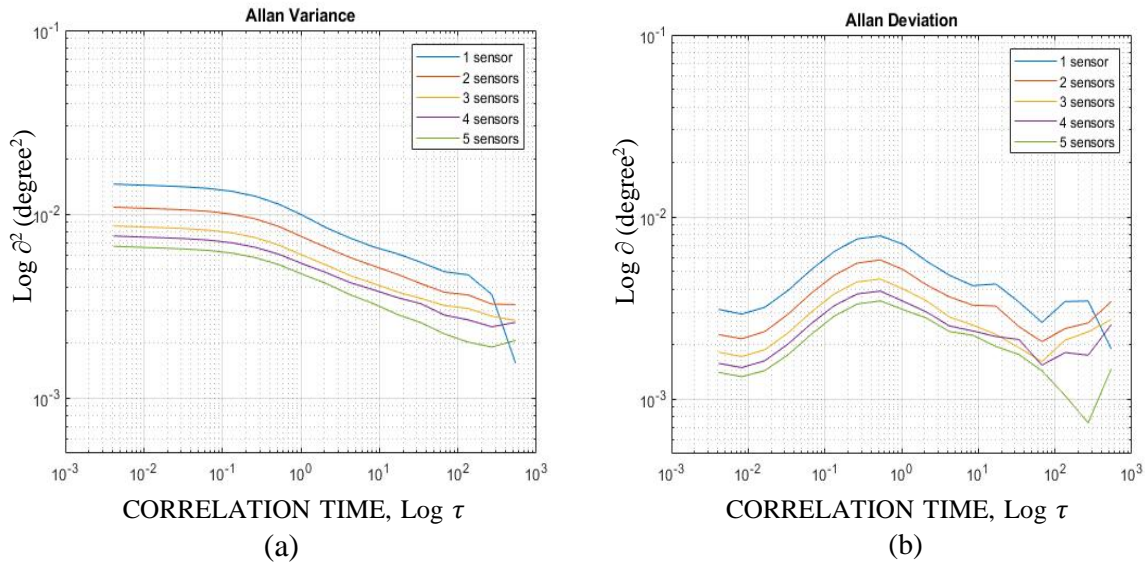


Figure 4-5. Quantifying the noise progress of various inclinometer combinations in time-domain using: (a) Allan variance, and (b) Allan deviation.

Analysis of Figure 4-5.a shows that the higher number of combined inclinometers, the lower progressive the noise is. For example, the first calculated value of Allan variance (Figure 4-5.a) of a single inclinometer and five combined ones are 0.0145 and 0.0067, respectively. The beneficial effect of additional synchronized sensors can also be seen in the Allan variation presented in Figure 4-5.b. It is indicated in the literature [161] that various noise types (such as White noise, Flicker noise and Random) can be detected from the log Allan deviation plot. Detection of different noise types from a gyroscope output is presented in [162].

This Figure showed that sensor combination decreases noise magnitude in both time-domain and frequency-domain.

4.4 Laboratory experiments

In this section, LARA's measurement accuracy is evaluated by comparing its results with the estimations of a HI-INC inclinometer in four tests in the LATEM. Then, the combinatory analysis presents the accuracy improvement of inclination measurement of up to five combined inclinometers. Finally, the accuracy and resolution of HI-INC and LARA are validated by performing four load tests on a simply supported aluminum beam.

4.4.1 Accuracy evaluation

In this section, the experimental tests targeted at verifying the accuracy of LARA are shown. In order to make sure that LARA and the commercial inclinometers measure the same inclination, LARA was glued on top of the HI-INC clinometer. Then, the HI-INC was connected to the rigid metallic plate using its magnetic plate. After that, the metallic plate was connected to a rotational device (Figure 4-6). By rolling the small gear of this rotational device, the connected stiff plate

rotates. Then, induced rotations were measured by the LARA and HI-INC. Finally, the outputs of LARA for the tests were compared with those estimated by the HI-INC inclinometer.

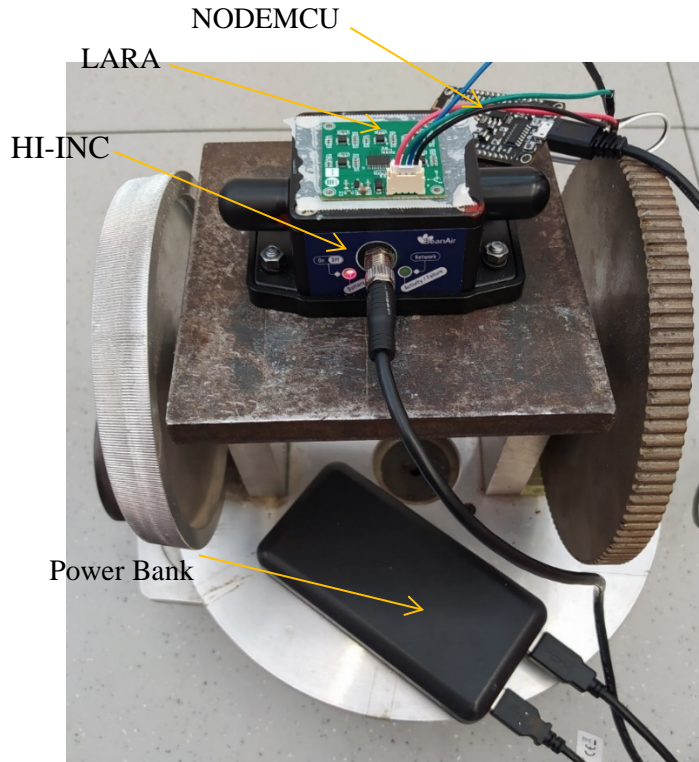


Figure 4-6. Test setup intended for comparing inclination estimation of LARA with HI-INC.

Table 4-1 presents the results of the carried out experimental tests. This table takes in the following information collected in columns: (1) No.: Four tests are carried out for evaluating the accuracy of LARA in different inclinations, (2) HI-INC: the estimated inclination by HI-INC inclinometer, (3) LARA: the measured inclination of LARA, and (4) Difference: the absolute difference of LARA and HI-INC measurements.

Table 4-1. Accuracy comparison of LARA with HI-INC.

No.	HI-INC (Degrees)	LARA (Degrees)	Difference (Degrees)
1	0.9996	0.9615	0.0382
2	1.9770	1.9267	0.0503
3	3.0180	2.9618	0.0563
4	4.0254	3.9583	0.0671

The analysis of Table 4-1 shows that the difference in LARA measurement from the HI-INC is related to the induced inclination. In fact, it was seen that for more than five degrees of change,

54

the difference of LARA from HI-INC was higher than 0.1 degrees. For that reason, their data are not included in Table 4-1. Therefore, it can be concluded that the accurate measuring range of LARA is up to four degrees. This range is accurate enough for the target application of bridge monitoring as in this kind of structures increments of rotation higher than 0.5 degrees are not expected [135][163].

4.4.2 Combinatory analysis

In order to study the difference of the measured values from the reference sensor for different inclinometer combinations, a combinatory analysis was performed. This evaluation illustrates the maximum and minimum envelope difference from the commercial inclinometer for all the possible sensor selections from the five available inclinometers. The maximum and minimum values of the increasing number of inclinometers are shown in Figure 4-7, 7.a (one sensor), 7.b (two sensors), 7.c (three sensors), and 7.d (four sensors). It is to be noted that in all these figures LARA shows the estimation calculated by combining the results of five inclinometers together.

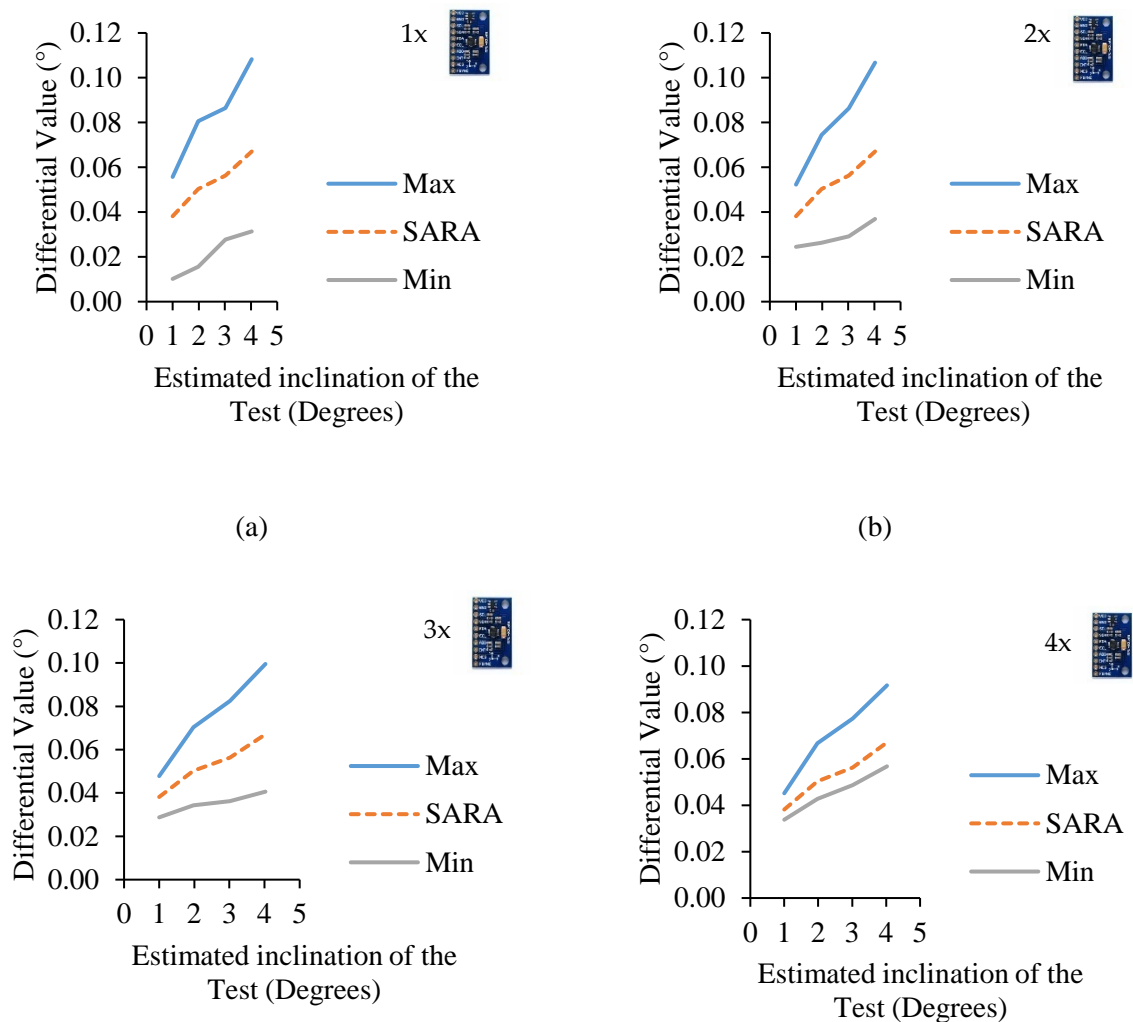


Figure 4-7. Estimated measured inclination difference for a different number of combined inclinometers from HI-INC estimations: One sensor (a), two sensors (b), three sensors (c), and four sensors (d).

The analysis of Figure 4-7 shows that the accuracy of the whole system is directly influenced by the number of combined inclinometers. For example, the minimum accuracy of a single inclinometer (Max difference from HI-INC) is 0.0557 degrees for an induced inclination of 0.9996. However, for the same experiment, LARA showed a measurement difference of 0.0381 from HI-INC. As expected, the higher the number of sensors, the better the accuracy of the modular system. It is essential to note that the minimum difference from HI-INC estimations reported in Figure 4-7.a does not correspond to the measurement of a single sensor for all four experiments. It can also be seen that the distance between minimum and the maximum differential from HI-INC values is decreasing with a higher number of combined sensors. In fact, having a lower range of possible errors can help making the final product more reliable. This reliability is very important when an

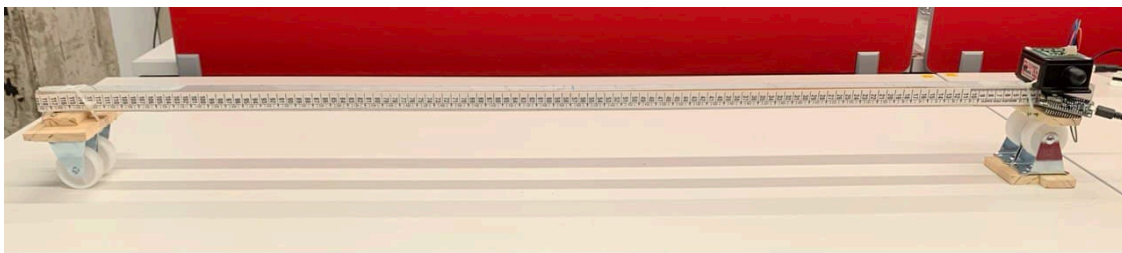
56

inclinometer has a high sampling frequency. This way, optimizing filters (such as different Kalman filter formulations [164]), which could alter the primary signal and slow down the acquisition speed, are no longer necessary.

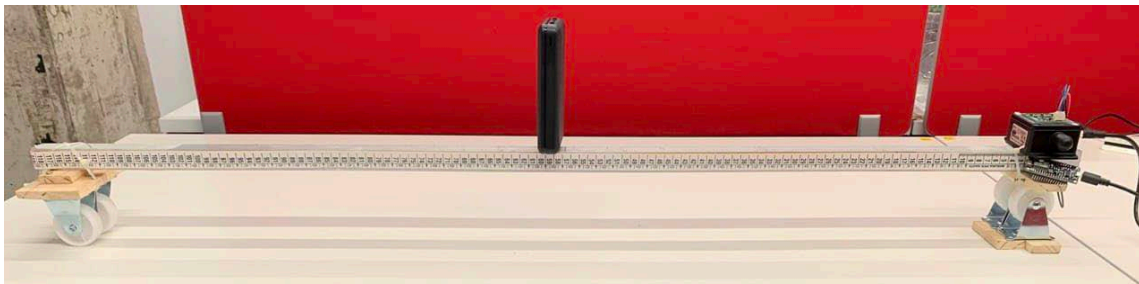
4.4.3 LARA resolution and accuracy verification

In order to present the resolution and accuracy of LARA more clearly, a load test is performed on a small-scale beam with a length of 1.24m. This section compares the slope estimation of two sensors (LARA and H-INC) located on the support of a simply supported aluminum beam model under a point load of 467 gr (4.58 kN) with hand calculation of slope at the beam edges. It should be mentioned that, for this test, LARA was again mounted on the top of the HI-INC.

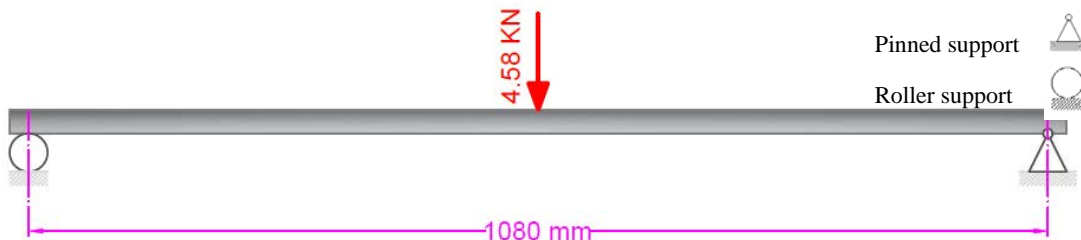
This test is carried out using a U-shaped aluminum profile with section dimensions of $25 \times 25 \times 3 \times 3$ mm in the laboratory of UPC university. The effective length of the beam model, which is the distance between the null axis of its support, is fixed as 1080 mm.



(a)



(b)



(c)

Figure 4-8. Load test of a beam model: (a) test setup, (b) load test, and (c) sketch of the load test..

The test aim was to read the maximum slope of the beam model deck under a known applied load on the mid-span. The maximum slope at the supports can be calculated by Equation 4-5. Therefore, LARA and HI-INC were attached to achieve this objective on top of the beam model support. First, LARA and HI-INC worked for a while without any loads (Figure 4-8.a) and their estimations were acquired. Next, the point load was set on the mid-span of the beam model (Figure 4-8.b and Figure 4-8.c) and then another data acquisition process was carried out to measure the slope of the beam by LARA and HI-INC. It is essential to mention that this test was repeated three times. This is done to study the human errors and possible mistakes or issues that can happen during an experiment.

The used formula for calculating the slope of a simply supported beam with a load located on its midspan by hand is presented in Eq.4-5 [165].

$$\Delta\theta_1 = \frac{P \times L^2}{16 \times E \times I} \quad (4-5)$$

In Eq.4-5, where, $\Delta\theta_1$ (Radians) is the maximum slope at the supports, P is the value of the applied load at the mid-span, L is the effective beam length, E (69637.05 MPa) is the beam elasticity module, and I (12853.08 mm⁴) is the beam moment of inertia. $\Delta\theta$ is then calculated as 0.000373 radians. This value corresponds to 0.021372 degrees on inclination. The comparison of the estimated values of LARA and HI-INC with those of the hand calculations is presented in Table 4-2. It should be noted that this test was repeated three times (Table 4-2) to check the accuracy of the developed inclinometer.

Table 4-2. Comparing the inclination estimation of LARA and HI-INC

Number of the experiments	Hand calculation slope (degrees)	LARA Difference (degrees)	LARA (degrees)	HI-INC difference (degrees)	HI-INC (degrees)
1	0.021372	0.001613	0.022985	0.002447	0.018925
2	0.021372	0.002316	0.023688	0.000853	0.020519
3	0.021372	0.001362	0.022734	0.005196	0.016176

The analysis of Table 4-2 shows that the accuracy of LARA based on these experiments is less than 0.002 degrees. Further study of Table 4-2 illustrates that the accuracy of HI-INC is around 0.005 degrees. In fact, this is very close to accuracy value detailed in its datasheet ($\pm 0.003^\circ$ for $\pm 15^\circ$ version) [166]. This value validates the accountability of the performed experiment. Therefore, having accuracy in the range of 0.05 degrees makes LARA applicable for the SHM of bridges.

Another experimental test was carried out on this beam model (Figure 4-8.a) using a heavier weight (21.942 N). In this experiment, instead of putting the weight only on the midspan, the weight was set on various beam locations. Then, the support slope was measured using HI-INC and LARA. Finally, the sensors' measurements are compared with the hand calculations [165]. Figure 4-9 presents the slope measurement comparison of HI-INC and LARA with the hand calculation

values. It is vital to mention that this experiment is carried out on the same beam model presented in Figure 4-8.a. As showed in this figure, the inclinometer is mounted on a pinned support.

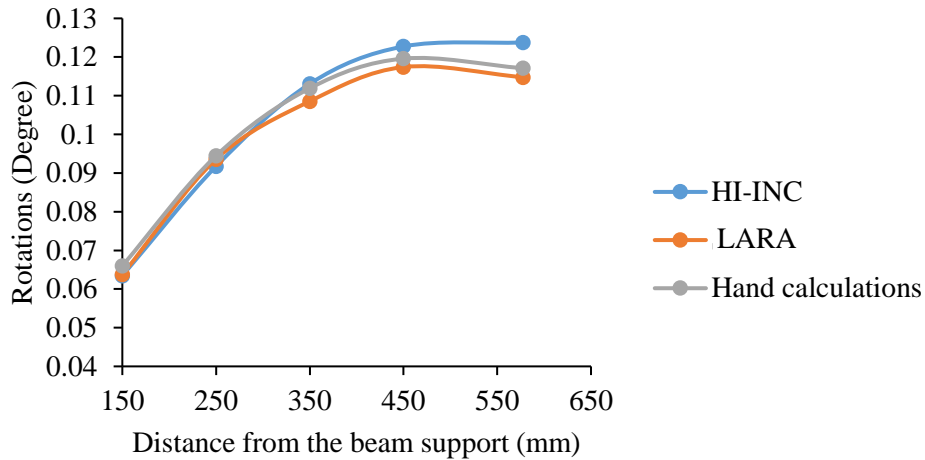


Figure 4-9. Support slope of a simply supported beam under a point load located on various spots.

Analysis of Figure 4-9 shows that LARA has a maximum measured difference of 0.003 degrees from the hand calculation slope. In addition, it can be seen that LARA has a closer trend to the hand calculation values compared to those of HI-INC.

It should be noted that LARA can be used in static load tests aiming to identify the location of structural damages which had altered the influence line of a bridge [135].

It is interesting to compare LARA's final price (54.95 €) with those presented in Table 2-3. It should be noted that comparing an academically developed device with a commercial alternative is not fair. However, the most critical contribution of current work is developing a low-cost, accurate device and for that, this comparison is needed. It can be seen from Table 2-3 that HI-INC, ZCT-CX09 and DNS have a resolution of 0.003 degrees. Therefore, LARA can be compared with them. Figure 4-10 presents the price comparison of these inclinometers.

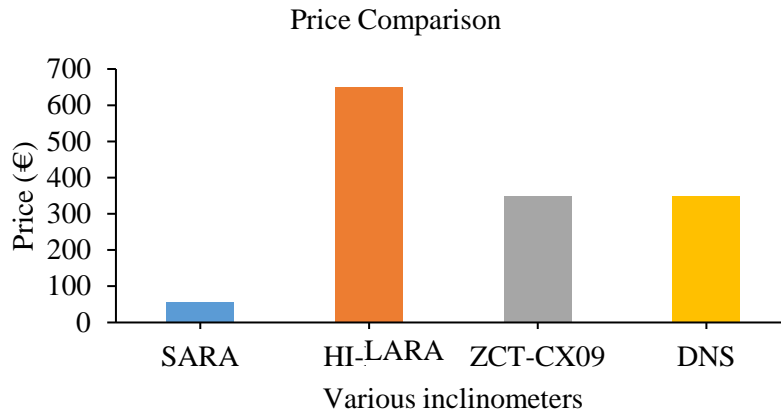


Figure 4-10. Price comparison of LARA with traditional commercial inclinometers with a resolution of 0.003 degrees.

Analysis of Figure 4-10 shows a significant difference between the price of LARA and inclinometers with the same resolution. LARA is 12, 6 and 6 times cheaper than HI-INC, ZTC-CX09 and DNS inclinometers, respectively.

Chapter 5 : Low-Cost Sensors Accuracy Study and Enhancement Strategy

5.1 Introduction

Today, low-cost sensors in various civil engineering sectors are gaining the attention of researchers due to their reduced production cost and their applicability to multiple nodes. Low-cost sensors also have the advantage of easily connecting to low-cost microcontrollers such as Arduino. A low-cost, reliable acquisition system based on Arduino technology can further reduce the price of data acquisition and monitoring, which can make long-term monitoring possible. This Chapter introduces a wireless Internet-based low-cost data acquisition system consisting of Raspberry Pi and several Arduinos as signal conditioners. This study investigates the beneficial impact of similar sensor combinations aiming to improve the overall accuracy of several sensors with an unknown accuracy range. The Chapter then describes an experiment that gives valuable information about the standard deviation, distribution functions, and error levels of various individual low-cost sensors under different environmental circumstances. Unfortunately, these data are usually missing and sometimes assumed in numerical studies targeting the development of structural system identification methods. A measuring device consisting of 75 contactless ranging sensors connected to two microcontrollers (Arduinos) was designed to study the similar sensor combination theory and present the standard deviation and distribution functions. The 75 sensors include: 25 units of HC-SR04 (analog), 25 units of VL53L0X, and 25 units of VL53L1X (digital).

This Chapter is organized as follows: first, Subsection 2 presents the methodology for making a distance measurement device, including 25 of each type of sensors (VL53L0X, VL53L1X, and HC-SR04). Subsection 3 describes the characteristics of the performed laboratory experiments and validates the benefits of combining sensors. Finally, Subsection 4 discusses the results of the performed experiments.

5.2 Material and Method

This section describes the characteristics of the sensors used in the experiment to validate the accuracy improvement of the similar sensor by coupling several together. A device containing 25 VL53L0X, 25 VL53L1X, and 25 HC-SR04 sensors was constructed to investigate the beneficial effects of averaging the results of multiple distance sensors.

The first subsection of this section introduces the low-cost distance sensors used as a measuring device. The second subsection describes the relations and connections between the microcontrollers, Raspberry Pi, and the sensors. Finally, the third subsection explains the relationship of the sensors to a single solid foundation.

61

5.2.1 Low-cost distance sensor

HC-SR04 is a low-cost distance sensor based on the sonar concept methodology with a distance measuring range of 20 to 4,000 millimeters and a resolution of 3 millimeters. The Arduino interacts with this sensor by digital pin, which is connected to the transmitter and the receiver. For the initiation, the Arduino sends a voltage pulse to the pin, which changes the digital pin from a low to high situation for a moment. This change sends a signal wave through the ultrasonic transmitter. As soon as the signal is sent, the pin status returns to low. When the transmitted signal bounces off of the targeted object toward the sensor's ultrasonic receiver, the receiver sends a voltage pulse to the digital pin, making it high again. The Arduino estimates the location of the targeted object by multiplying the interval time of the elevated pin by the speed of the sound. Since sound speed depends on ambient temperature and humidity, this data should also be estimated in every ultrasonic distance estimation. When the environmental temperature increases, the kinetic energy of air molecules and the sound velocity increase as well. Sound velocity also has a direct relation to humidity.

To estimate the sound velocity, the temperature and humidity were measured by DHT22. The sound speed is calculated from Eq.5-1 [167].

$$\text{Sound-velocity} = 331.4 + (0.606 * \text{temperature}) + (0.0124 * \text{humidity}) \quad (5-1)$$

Where Sound-velocity and temperature are measured in m/s and degrees Celsius, respectively. Humidity is given in relative terms (%) and shows the ratio of water vapor in the air at a given temperature. Figure 5-1 shows the ultrasonic, temperature, and humidity sensors.

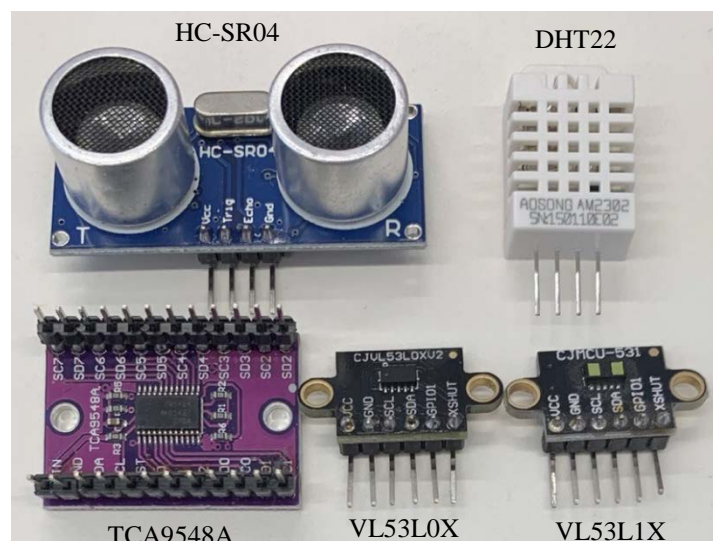


Figure 5-1. The used low-cost sensors of the project: HC-SR04 (ultrasonic sensor), DHT22 (temperature and humidity sensor for calibrating the ultrasonic sensor), TCA9548A (multiplexor), VL53L0X (ToF sensor) and VL53L1X (ToF sensor).

Two of the most widely recognized ToF sensors (VL53L0X and VL53L1X) have been used in this project. These sensors have a distance measuring range of 2 and 4 meters, respectively, with a 1 mm resolution. VL53L0X and VL53L1X communicate with the Arduino through an I2C communication port. This communication port consists of a Serial Clock Line (SCL) and a Serial Data Line (SDA) pin, which can be connected to various digital sensors (those which have SCL and SDA pins) simultaneously as long as the connected sensors have a different address. There are two different connection ways to connect a number of ToF sensors to a microcontroller: (1) by default address changing [168] or (2) through a multiplexor. Default address changing with VL53L0X and VL53L1X circuits involves using a few lines of code to change their default address to other addresses [29], [169] (TCA9548a). A multiplexor connects the sensors with the same address to Arduino. Up to 64 similar sensors can be introduced to the Arduino [170]. Although the first methodology seems more accessible and cheaper, it is not as reliable or stable as the second method. Moreover, if a ToF sensor in the first method gets damaged, burned, disconnected, or stops working for any reason stops working, the whole system stops working until the problem is solved or the burned sensor is replaced. To improve reliability, this research connected the I2C sensors to the microcontrollers through a multiplexor.

5.2.2 Microcontroller section and data acquisition

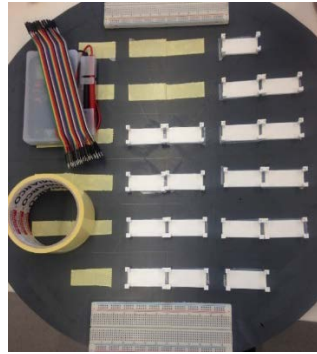
This subsection studies the correct connection of the distance sensors to microcontrollers for data sampling and data acquisition, the number of microcontrollers needed, and microcontroller communication. Data acquisition posed a few challenges, which are detailed here along with their corresponding solutions: (1) Electricity shortage: by using a single Arduino Uno with 75 sensors, the input voltage for the ultrasonic was lower than 3.5 V, which resulted in no measurement estimation from HC-SR04. An Arduino Mega connected to a spread power source was used to fix this issue. The sensors were distributed among these two Arduinos. (2) Single output: the serial communication of Arduino Uno was connected to the Arduino Mega to save data from only one Arduino and have the sensors measuring simultaneously. During the distance measurement, these Arduinos were in touch with each other. First, both Arduinos checked their connected sensors. Second, the Arduino Uno printed a character that ordered the Arduino Mega to activate its connected distance sensors. Third, the Arduino Mega received the character and confirmed the Arduino Uno by sending a different character. At this moment, both microcontrollers have already forced their connected sensors to measure the distance of the targeted object. The Arduino Uno then prints the values of its sensors in its serial communication and waits for another character from the Arduino mega. When the Arduino Mega is finished with its measurements, it triggers a short delay (making sure that Arduino Uno is finished with its printing and is waiting for Arduino Mega), it sends the character. Shortly after printing this character, the Arduino Mega sends all of its measurements to the Arduino Uno. Finally, by receiving the Arduino Mega character, Arduino Uno starts printing the outputs of the Arduino Mega with a space from its printing. This way, the information is only received from the Arduino Uno. (3) Data acquisition: Raspberry Pi is connected to the master Arduino (Arduino Uno) for saving all the measurements. The Raspberry Pi provides power for the Arduino Uno and acquires its output through a written python code. (4)

63

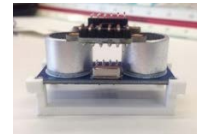
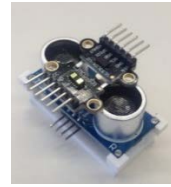
Supply: the Raspberry pi requires input power with 5V and 2.5A. Standard adaptors for mobile charging or power-banks only provide 5V and 2.1A. Consequently, the Raspberry Pi showed a low-power error that affected the connected Arduino Uno. However, the Arduino Mega can connect to any habitual power bank or micro-USB mobile charger.

5.2.3 Construction of the measurement device

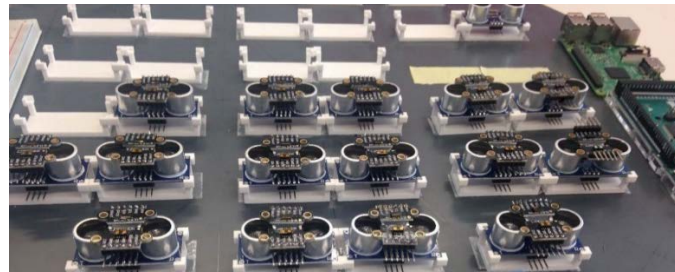
A few steps were taken to make sure that all sensors measured the same distance from the object under study. (1) Sensor base: a PVC plate (Figure 5-2.a) provided a solid, uniform, and smooth base for the sensors. (2) Sensor connection to the PVC plate: 3D printed clamps were designed to connect the sensors to the plate (Figure 5-2.b). These 3D printed clamps were developed to hold the HC-SR04, VL53L0X, and VL53L0X at a known height. These clamps were glued to the PVC plate (Figure 5.a) and then the sensors were glued to the 3D printed clamps (Figure 5-2.c). At this position, the measuring part of the ultrasonic sensors (the top of the HC-SR04 sensors) was located at a 25mm height from the PVC plate. The thickness of the ToF sensors was fixed to 2mm. These heights were taken into account by implementing these values to the Arduino code. (3) Wiring: the sensors were wired as shown in Figure 5-2.d. The 25 ultrasonic sensors were connected to the digital ports of the microcontrollers, and the 50 sets of ToF sensors were connected to I2C ports of the microcontrollers using multiplexors (Figure 5-4). (4) The Raspberry Pi was connected to the Arduino Uno for wireless control and saving measurements. Then, the Arduino Uno was connected to the Arduino Mega using two jumper wires (Figure 5-4). Finally, the Arduino Mega and Raspberry Pi were connected to an external power source. Figure 5-5 shows the developed distance measuring device in the laboratory. As seen, the device is located on a fixed platform experiment testbed. The mobile part of the actuator is the upper jaw of the jack (Figure 5-5).



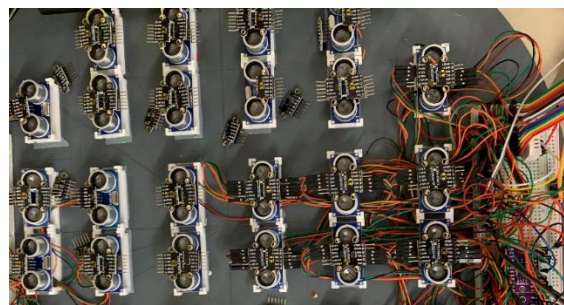
a) PVC plate and assignment of the 3D printed clamps



b) Placement of sensors on the tailored 3D printed clamps



c) Placement of the sensors for making the non-contact multisensory device



d) Connection of the sensors to the Arduino Mega and Uno using wires

Figure 5-2. The components of the distance measuring device: a) PVC sheet for attaching the sensors and the data acquisition equipment, b) Designed 3D printed base for holding the various sensors together at a known height, c) sensor allocation, d) Wiring the system together.

In addition, the flowchart of the construction of measurement device is presented in Figure 5-3.

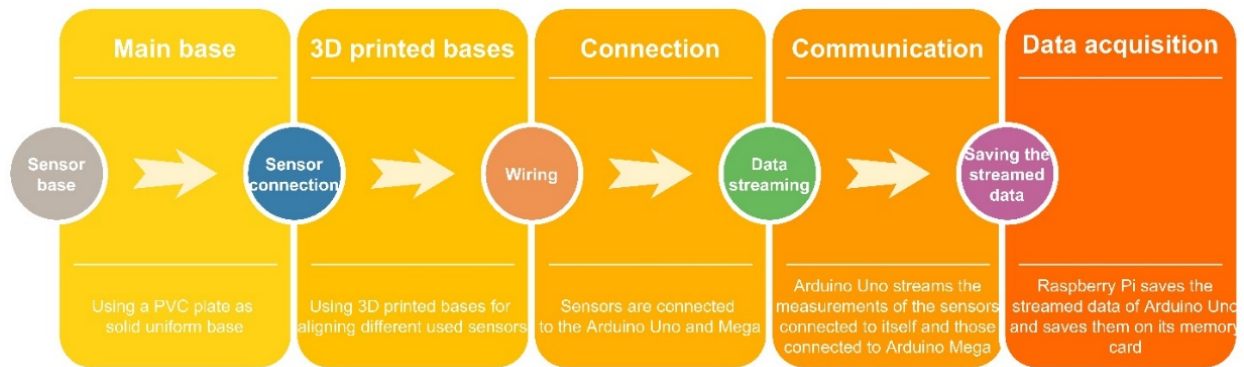


Figure 5-3. Flowchart of the construction of the proposed measurement device

In Figure 5-4 shows all of the assets required to make the multisensor distance measuring device. Figure 5-4 also displays the serial connection of Arduino Uno and Mega, as drawn by Fritzing software [136]. Pins 0 (RX) and 1 (TX) on the Arduino Uno are connected to pins 1 (TX) and 0 (RX) on the Arduino Mega, respectively. RX and TX pins stand for Receiving and Transmitting pins of the Arduino serial communication.

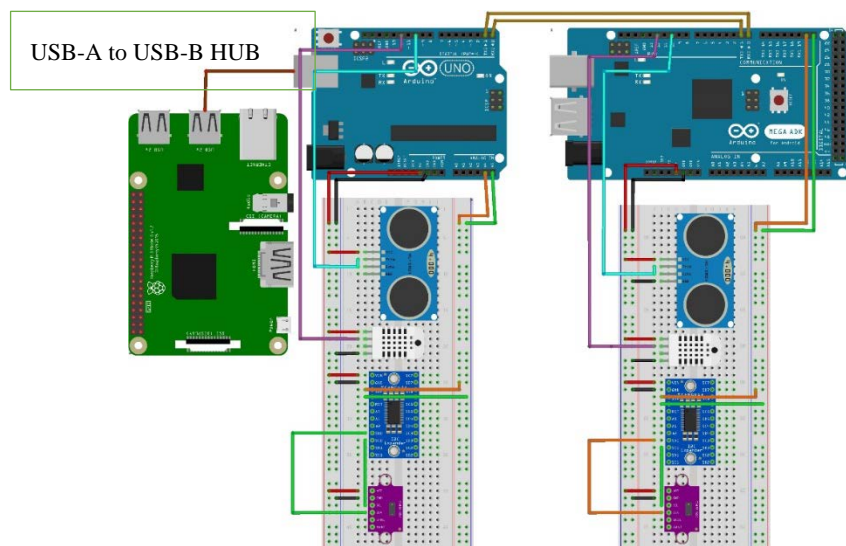


Figure 5-4. Scheme of the connections between the microcontrollers and the Raspberry pi.

Since this Chapter targets static sensors, the sensors are not synchronized with microsecond resolution. Even though the ToF sensors have a very high sampling frequency, the ultrasonic sensors need some time to measure data. For that, some delay functions have been used in the Arduino code of the tailored device. This system measures distance once every 10 seconds. In the absence of ultrasonic sensors, ToF sensors could have been synchronized with microsecond resolutions, just like the recently published article by the same authors [29].

5.3 Laboratory Validation

In this section describes the validation experiments of the multisensor distance measuring device. An experiment at the Structural Laboratory Lluís Agulló of Universitat Politècnica de Catalunya, Barcelona Tech (Spain) assessed the impact of sensor combination and provided a fair comparison between the introduced ToF and ultrasonic sensors. The jack seen in Figure 5-5 was used to measure the distance of an object from the distance measuring device. The distance between the machine's upper and lower jaw can be altered. This jack has been selected for this laboratory experiment for three key reasons, as described below. (1) Dimension of target object: the area of its movable part (the upper jaw) is slightly above 0.5 square meters. This makes the distance between the two jaws measurable by the HC-SR04 sensors [115]. (2) Movability: since the upper jaw of this jack moves, different distances can be measured by the tailored distance measuring device. The distances were calculated by a steel measurement pattern. (3) Ambient light: a projector light has been placed on the side of this jack to produce an extremely bright situation for simulating day and night in the laboratory. To show the capability of the proposed device under a noisy environment commonly found in the industry, the experiments were carried out during the active hours of the laboratory. In addition, the projector shown in Figure 5-5 was used for additional environmental noises.

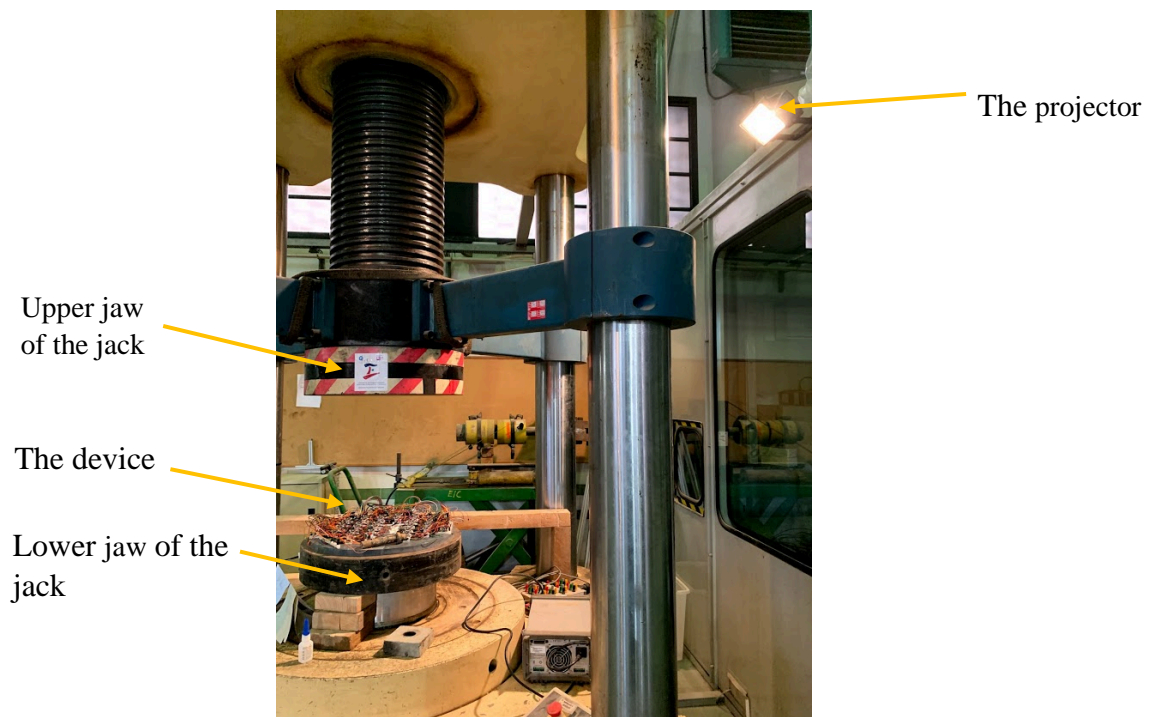


Figure 5-5. The laboratory experiment equipment.

Ten static tests were carried out on this jack. In every test, the upper jaw of the jack was fixed with a measured distance from the lower jaw by a steel measurement pattern. Every test had a duration

67

of 15 minutes. Additionally, the distance of the lower jaw from the tip of the sensors was measured for data post-processing. The lower jaw of the jack is located precisely 60mm lower than the tip of all sensors mounted on the device.

Each of these ten experiments was performed once with the projector off and once with the projector on. This ambient light simulates the presence and the absence of the sun. In outdoor measurements, there are moments when the sun may be shining directly on the distance measuring sensors. This work examines the sunlight effect through this laboratory experiment, which this work refers to as experiments with excessive ambient light. The experiments without ambient light were acquired while the projector in Figure 5-4 was off. However, the laboratory has a permanent lighting system that could not be turned off during working hours. Table 5-1 shows a summary of the experimental tests.

Table 5-1. Characteristics of the performed tests.

Test Number	Steel measurement pattern (mm)
1	290
2	340
3	440
4	540
5	640
6	740
7	834
8	940
9	1040
10	1140

All the tests listed in Table 5-1 were conducted twice (once with the projector on and once with the projector off). Steel measurement pattern was used to secure the measurements. The numbers refer to the tip of the measuring device's sensors to the jack's upper jaw.

5.4 Result and discussion

This section describes the experimental results. The first subsection discusses the detected errors of the sensors and proposes a code for data post-processing. This subsection also presents the average results of all similar sensors. The second subsection shows the beneficial effect of coupling similar sensors by comparing the results of a random sensor with the fused results of 25 similar sensors. Finally, the third subsection presents the increasing accuracy of devices with a higher number of similar coupled sensors. This investigation has been done by comparing combinations of connected similar sensors with the benchmark measurements. The results show that all other varieties of the selected sensors will have higher accuracy than the values presented in this work.

5.4.1 Error recognition

Some ultrasonic and ToF sensors reported an error during certain tests and their data were excluded from the post-process data. These errors can be categorized into two types:

- Ultrasonic errors: since the further inspection of the measuring device showed no faulty connections and no problem with the uploaded code, it was concluded that the flow of the electricity is causing issues in random sensors during some of the experiments. The ToF sensors draw more current from the device when they estimate the distance of an object which is located further away. Drawing more current from a multisensor device within a constant 400 mA current output (200mA each Arduino [122]) resulted in a voltage drop. As already mentioned, the HC-SR04 could not work with a current lower than 3.6 V. The sensors indicated an error by either printing "0" or printing a value smaller than the actual distance. Unlike ToF sensors, ultrasonic sensors are low-frequency sensors with steady outputs. By plotting the results of ultrasonic sensors and studying them, these outliers are approximately 10% smaller than the estimated value. These values have been considered faulty values as well and have been excluded from the outputs. Figure 5-6 shows an example of this error.

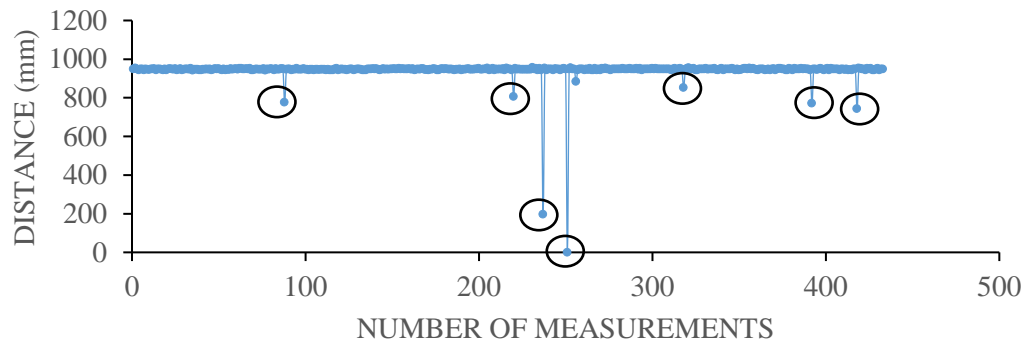


Figure 5-6.Excluding the outliers of HC-SR04 estimations.

- ToF sensors: these sensors are sensitive to ambient light. Whenever a robust environmental light beam was focused on a sensor, the sensor was printing an error coded as "8190" instead of the measured distance. Also, this type of sensor will print a coded value of "65535" if it is either burned, has a faulty connection, or the input power is not enough.

To address the issues above, a code was used to exclude the faulty readings. This code first extracts the acquired HC-SR04, VL53L0X, and VL53L1X sensor data from the Raspberry Pi output in three different matrixes. In each matrix, the columns specify a given sensor and each row is a measurement cycle. Second, the code excludes the rows in which at least one of its values is faulty. Incorrect values are the coded errors mentioned above, including: 0, 8190, and 65535.

Table 5-2 displays the average (Mean) result of all similar sensors with their standard deviation (STDEV) for each experiment in with excessive ambient light (such as VL53L1X Light) and without it (such as VL53L1X). The first column lists the distance of the sensors from the targeted object, as measured by a steel measurement pattern. The column average then represents the average results of 25 distance sensors for 80 measurement cycles. The STDEV column represents

the standard deviation of the same distance sensors on average for 80 data acquisition cycles in each experiment. The columns with no information show the incapability of distance measurement by the sensor type.

Table 5-2. The normalized values of similar sensors.

Steel Measurement Pattern (mm)	HC-SR04		VL53L1X		VL53L1X Light		VL53L0X		VL53L0X Light	
	Mean (mm)	STDEV V	Mean (mm)	STDEV	Mean (mm)	STDEV	Mean (mm)	STDEV	Mean (mm)	STDEV
290.0	302.2	0.9	301.7	5.1	303.5	6.0	319.1	7.3	319.5	8.3
340.0	348.4	1.1	347.7	5.8	350.5	7.3	367.2	8.8	368.0	10.3
440.0	448.1	1.3	448.2	7.8	452.8	11.4	471.5	13.2	475.7	18.7
540.0	547.8	1.4	550.8	10.0	557.7	13.8	575.0	18.1		
640.0	646.9	1.5	651.4	13.2	660.8	21.4	679.7	24.4		
740.0	746.1	1.9	755.9	15.4	772.7	30.9				
834.0	838.4	2.0	853.3	19.2	876.6	40.5				
940.0	945.6	2.2	980.3	22.7	1009.4	52.1				
1040.0	1047.7	2.7	1096.5	26.5	1126.0	60.3				
1140.0	1147.7	3.0	1214.1	30.5	1244.2	71.6				
1170.0	1176.7	3.1	1241.3	30.0	1270.4	75.1				

Table 5-2 shows that ultrasonic sensors can measure higher distances more accurately. Moreover, ToF sensors decrease in accuracy as its distance from the target object increases. Further analysis of Table 5-2 shows that the standard deviation of all sensors in all situations rises with the increment of the object distance. Ambient light results in lower accuracy for ToF sensors and produces a more significant standard deviation. ToF sensors are also more sensitive to ambient light at larger distances. Table 5-2 also shows that even though VL53L0X measured distances up to 68 centimeters in the absence of the projector light, it only measured distances up to 48 centimeters when the projector light was on. VL53L0X sensors were also affected by ambient light. Subsequently, the VL53L0X can be introduced as the least effective distance sensor in this experiment due to its short distance range. This higher data fluctuation resulted in a significant standard deviation ratio and incorrect calibration. HC-SR04 and VL53L1x report very similar results on short distances, which demonstrates their accurate company calibration. For distances greater than 450mm, the difference between the results of the ultrasonic sensor and VL53L1X is more than 3 millimeters. Another interesting result from the analysis of this table is the effect of

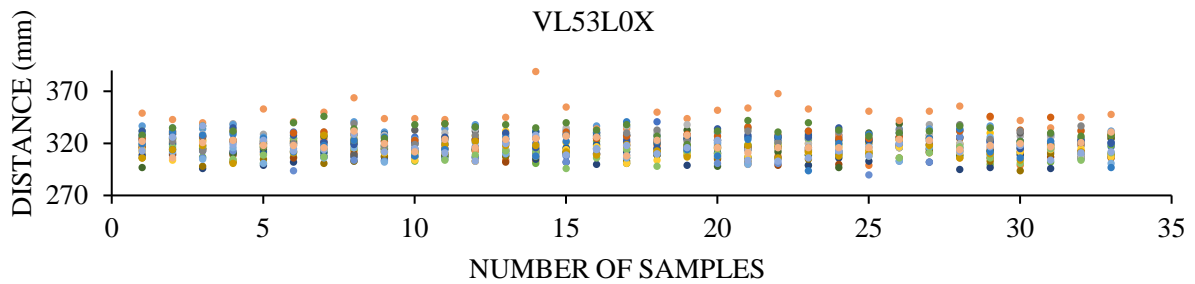
70

the projector light on VL53L1X. This sensor measured a higher distance from the estimations of the HC-SR04 and the steel measurement pattern measurements when the projector was on.

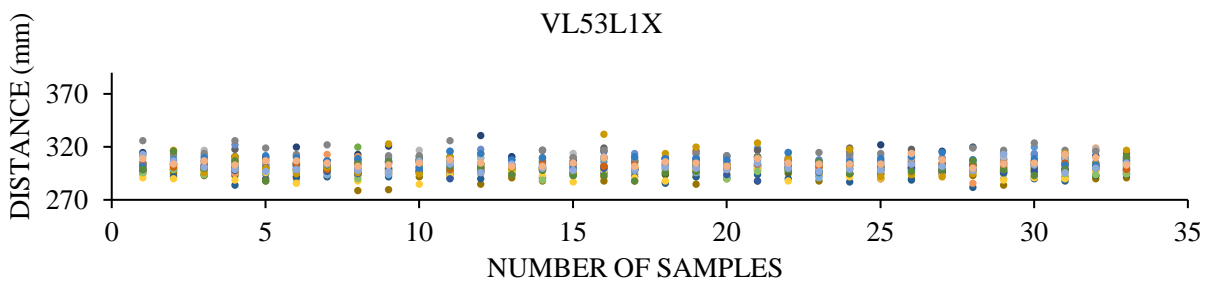
Errors of faulty sensors can easily affect the overall performance of data acquisition. Consequently, errors should be removed in post-processing evaluations. If a sensor shows dissonance among other ones, the data output of the faulty sensor or sensors should be deleted and the sensor replaced. During long-term monitoring, when the health status of a sensor that is a part of the sensor combination is suspicious, the data of that sensor can be excluded. The overall accuracy and resolution decreases by removing a sensor from the sensor combination, but the system still works at a lower resolution until the faulty part is replaced. If a traditional single sensor is used for the same purpose, however, its health status is unlikely to be evaluated because there is no other sensor to compare to its results. In such cases, no data can be acquired until the traditional sensor is identified and replaced.

5.4.2 Beneficial effect of combining similar sensors

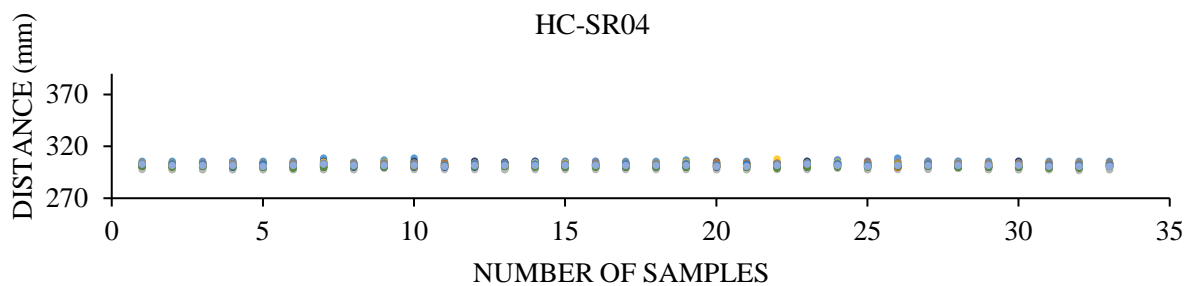
This subsection investigates the benefit of coupling all the sensors of a similar type. Figure 5-7.a, Figure 5-7.b, and Figure 5-7.c illustrate the filtered results for a single experiment for 25 sets of VL53L0X, 25 sets of VL53L1X, and 25 sets of HC-SR04 in the absence of excessive ambient light with the targeted object exactly 29 centimeters away, respectively. In these figures, the vertical axes represent the distance of the jack's upper jaw from the device, as measured by the sensors. The horizontal axes indicate the number of measurement cycles. In every Figure, 25 different colors were used to show the measurements of the 25 sensors of each type.



(a)



(b)



(c)

Figure 5-7. Filtered output of distance sensors for an experiment: (a) results of VL53L0X, (b) results of VL53L1X, and (c) results of HC-SR04.

Analysis of Figure 5-7 shows the fluctuation of acquired data by various distance measuring technologies. VL53L0X has higher data fluctuation and sensitivity to the environmental situation than the other sensor types. VL53L1X shows more stable results. For example, although data acquisition by VL53L0X shows 90mm of data fluctuation, VL53L1X shows less than 40mm.

72

Figure 5-7 also shows that HC-SR04 has the most stable data report among the selected distance measuring sensors. In fact, HC-SR04 has less than 6mm of data fluctuation. The standard deviation of a single VL53L0X, VL53L1X, and HC-SR04 sensor from Figure 5-7 was on average about 7.3, 5.1, and 0.9, respectively.

The results of all 25 sensors for each cycle have been averaged to illustrate the benefit of the sensor combination. Figure 5-8 illustrates the results of this development. The orange line refers to the measurement carried out by a steel measurement pattern.

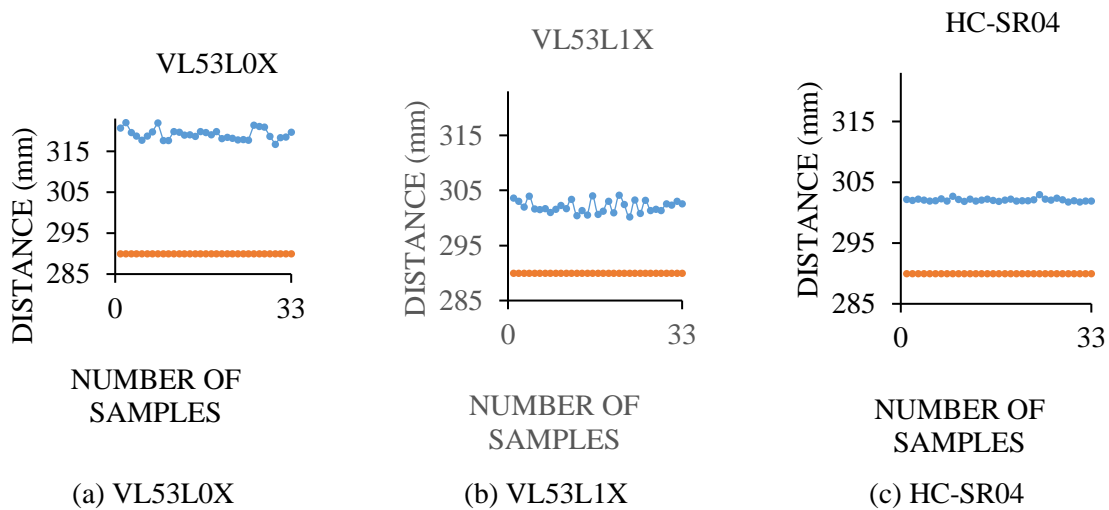


Figure 5-8. Combined outputs of similar sensors.

Analysis of Figure 5-8 shows the benefit of using the averaged results of 25 sensors for measuring a distance instead of using the results of a single sensor. The fluctuation of VL53L0X data decreased to 7mm, which is 12 times less fluctuation. The fluctuation of VL53L1X and HC-SR04 was reduced to approximately 4mm and 1mm, respectively. The standard deviation of 25 combined VL53L0X, 25 combined VL53L1X, and 25 combined HC-SR04 sensors is 1.3, 1.1, and 0.2, respectively. The combining sensors significantly improve noise-canceling and graph smoothing, as well. Each sensor has inherent noises different from the other similar sensors. By averaging the results of multiple sensors, these noises are either getting smaller or canceled altogether. The randomness of these noises has been investigated through a few experimental tests. Further analysis of Table 5-2 and Figure 5-8, shows the potential bias associated with the incorrect or lack of calibration of individual sensors. In fact, the offset of the VL53L0X sensor from the steel measurement pattern measurements is about two centimeters. Additional calibration of this sensor is needed for sensitive measurements.

5.4.3 Effect of coupled similar sensors

This subsection investigates the beneficial impacts of adding an increasing number of fused sensors in detail.

73

Errors measurements were calculated by a steel measurement pattern to compare all sensors (see Table 5-2). A combinatory program written in Matlab was used to find the least effective sensor combination for each experiment. This code first opens all the documents related to filtered outputs of similar sensors for all the experiments. Second, the code generates various sensor combination probabilities for the 25 sensors. Since the server computer used for this experiment could not calculate more than eight fused sensor combinations, this study's most effective fused sensor combination is eight. Even though 25 similar sensors have been mounted on the distance sensing device in this work, only up to eight sensors have been used for the combinatory analysis. Experimental tests show no significant improvement as of eight combined sensors. Figure 5-9, Figure 5-10, and Figure 5-11 shows the maximum possible error for every sensor combination for different experiments with different distances.

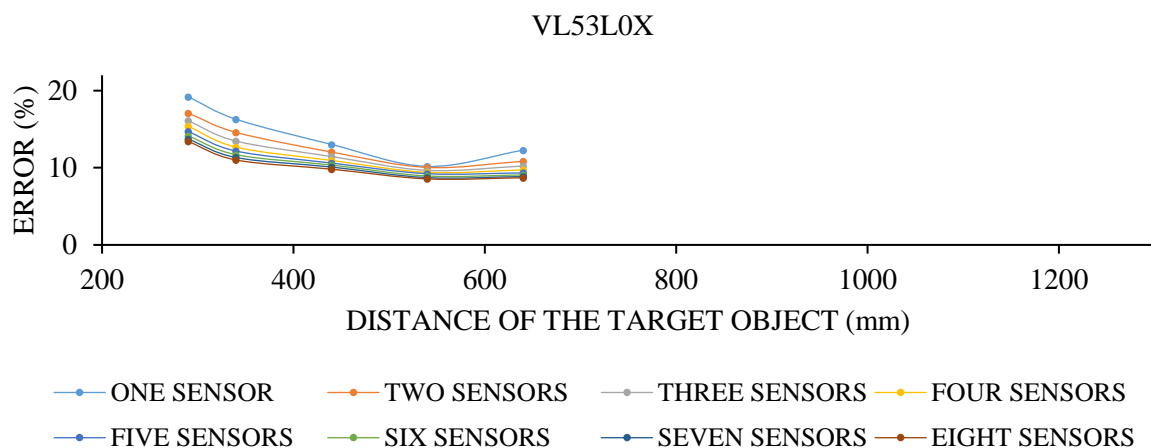
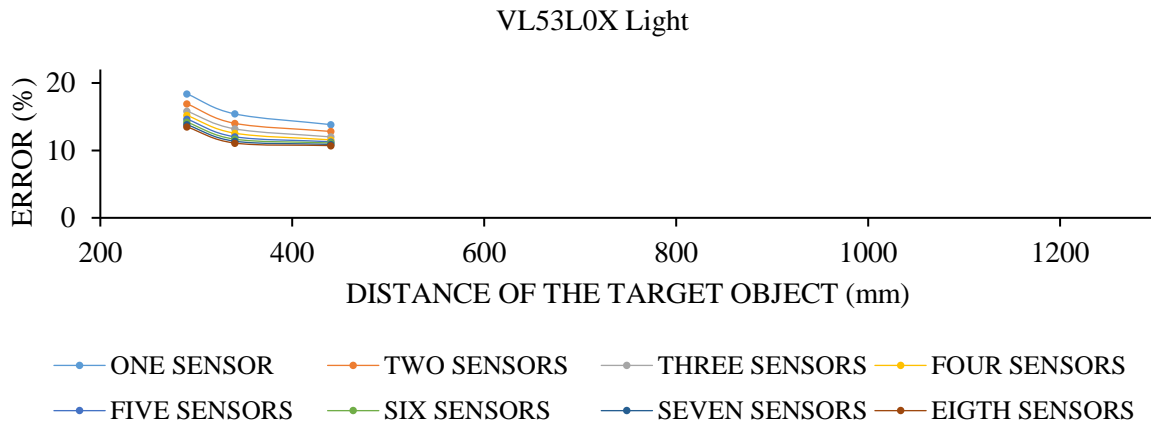
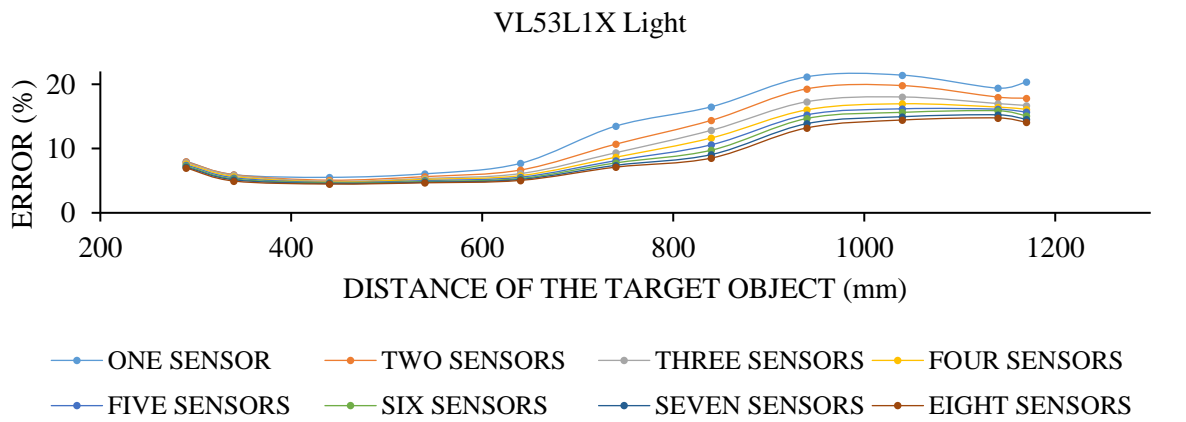
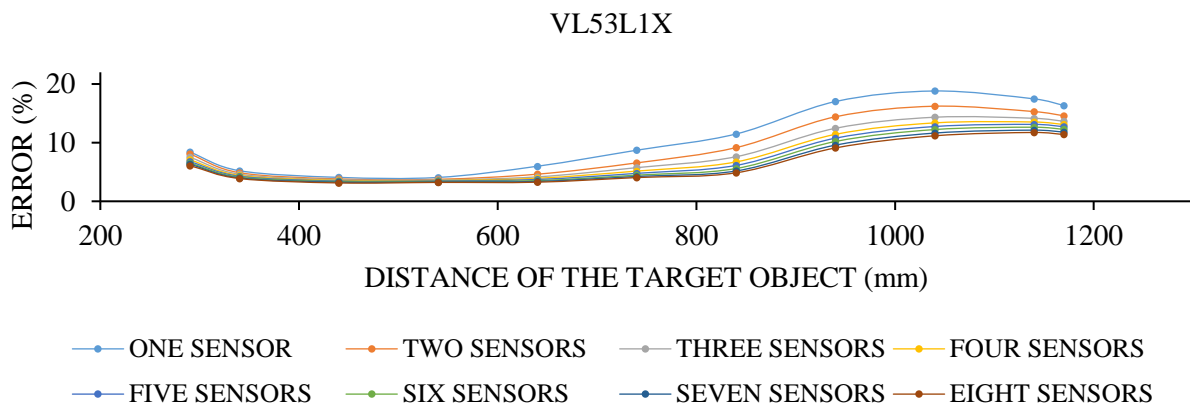


Figure 5-9. Comparing the worst-case sensor combination for VL53L0X with and without ambient light

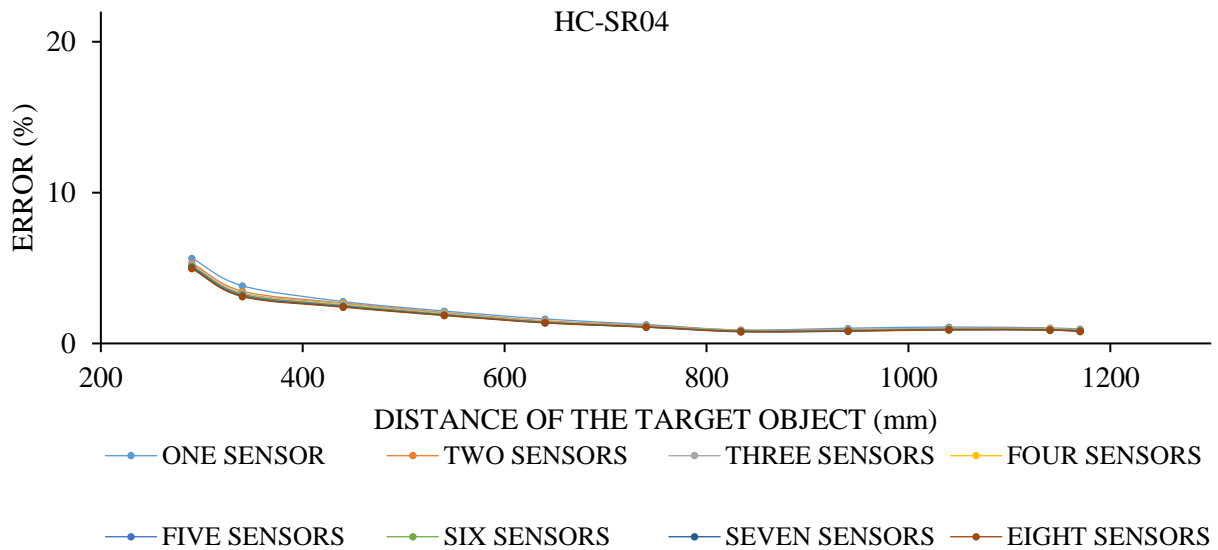


(a)



(b)

Figure 5-10. Comparing the worst-case sensor combination for VL53L1X with and without ambient light.



(e)

Figure 5-11. Comparing the worst-case sensor combination for HC-SR04.

Analyses of Figure 5-9.a and Figure 5-9.b reveal the limited distance range of VL53L0X for experiments with and without ambient light. Despite the high errors associated with this type of sensor when used alone, the error decreases with and without ambient light when multiple sensors are fused together. Even though the results of a single sensor in the worst-case scenario was 19% in the absence of ambient light, the exact measurement with eight fused sensors showed only 13% error, which confirms the benefit of combining sensors. This sensor is more accurate for intermediate ranges but does not work very well for very close or very far distances. Its lowest error appears when measuring a distance of 54 centimeters regardless of the number of fused sensors or the ambient light situation. The most significant effect of the sensor combination is seen with three VL53L0X sensors coupled together.

Figure 5-10.a and Figure 5-10.b detail the outputs of VL53L1X for experiments with and without ambient light. This sensor offers a broader range and more minor errors than VL53L0X. Like VL53L0X, this sensor works better for intermediate distances. These figures show how combining sensors reduces the overall estimation errors for both experiments with and without the ambient light. Figure 5-10.b shows that the worst-case estimation error scenario for a single sensor is 9%.

In contrast, the worst-case combination of 8 fused sensors has an estimation error of 4% in the same experiment. This sensor, like the VL53L0X, estimates distance in an intermediate range. However, the medium range of VL53L1X is more significant and is between 34cm and 64cm.

The combinatory analysis of Figure 5-10.a shows that, while the error of a single VL53L1X in the worst-case scenario is between 5% and 22%, when coupling eight sensors, the error range in the worst-case combination of the chosen sensors is between 4% and 15% when the projector was on.

76

The highest and lowest error for a single sensor in the absence of high ambient light was between 4% and 18%, and by combining eight sensors, that range became 3% to 12%. The error continues to lower more with a higher number of combined sensors. The most significant effect of sensor coupling for VL53L1X is observed with at least four averaged sensors.

Figure 5-11 shows the high accuracy and low data fluctuation of the HC-SR04 sensor, although combining sensors increases the accuracy and describes the estimation error. Analysis of Figure 5-11 shows that the effect of sensor combination is not as evident for HC-SR04 sensors when compared to ToF sensors. However, carefully studying the performance of HC-SR04 sensors shows their improving accuracy with distance increment. The most significant impact of the sensor combination is observed in the experiment when the target object is at a distance of 29 centimeters. In that experiment, the error of a single sensor in the worst-case scenario improves from 6.7% to 5.9%, with eight ultrasonic sensors fused in selecting the worst-case combination.

Further analysis of these Figures shows that the sensor combination improves the estimation accuracy of VL53L0X and VL53L1X sensors more than the HC-SR04. ToF sensors (such as VL53L0X and VL53L1X) are known to experience more noises than ultrasonic (such as HC-SR04) sensors. Consequently, the data acquisition of ToF sensors is usually post-processed for noise reduction and signal improvement [171]. Averaging the results of a number of similar sensors helps reducing individual noises or imperfections of the used sensors. Since ToF sensors are influenced by more environmental parameters (color, material, distance and lighting), their combination shows a more significant accuracy improvement than ultrasonic sensors that are only affected by fewer environmental parameters (such as temperature).

The higher benefits occur when at least two sensors are combined. In such cases, the overall error for the worst-case scenario is 6.33%. Even though the error from combining eight VL53L1X for all experiments in the absence of ambient light was between 3% and 12%, a single HC-SR04 reports errors between 1% and 7%, which is very low. Here, the precision of a single ultrasonic sensor for the distance measurement of semi-controlled laboratory experiments is higher than eight fused VL53L1X sensors. The price of a single VL53L1X is about five times more than a single HC-SR04. As a result, the low cost of HC-SR04 makes it the best candidate for sensor combination applications.

This work presents a way of improving the accuracy of low-cost sensors without post-processing or manipulating the outputs. In the current form, a device made from only ultrasonic sensor combinations can be used in different locations of a dam to measure the approximate water level or drones. The device is not currently tailored to be used in the industry. This device contains 75 sensors (analog and digital) with a radius of 250mm, which is used to research and analyze the impact of combining similar sensors. The results of this Chapter can be used further in making tailored devices with an acceptable range of accuracy for a known ambient situation. For example, in a dark place with a measuring range of 540mm, two combined VL53L1X have up to 3.7% error. The size of a device made from these two sensors would be 26x18x2mm. The price and size of any sensor combination can be calculated from the data available in Table 2-4.

It is essential to mention that combining commercial circuits will oversize the final product. To reduce this enlargement, the Printed Circuit Board (PCB) of the sensor can be redesigned for specific measuring purposes. Therefore, the proposed device of this Chapter with the current resolution is suitable for remote liquid level detection where the size of the object under-study (water level) is large enough for the oversized device made from sensor combination. In civil engineering, this level detection is commonly used for imposed load calculation of dams [172], safety and water level open and closed canals [172] and bridges [173].

5.4.4 Statistical evaluation

This subsection presents the distribution function of the sensors for every test. It is essential for every researcher who works on structural system identification methods to model measurement data in their research. As indicated by many scholars (such as [6][117]), these standard deviation functions are usually assumed without being measured. This section can further enrich the current literature with actual data by proving the standard deviation functions of various non-contact distance sensors in different ambient situations. These functions can help advance structural system identification applications and noise-canceling functions without learning the required electronic engineering skills for setting up low-cost distance sensors.

In order to show an overall distribution of each type of sensor for each performed laboratory experiment, the normal distribution function for averaged results for each kind of sensor has been calculated in Excel. The normal distribution check of the estimated data is then calculated through with SPSS software using the Shapiro-Wilk P-value and Kurtosis Z-value methods. Many scholars indicate that a distribution is normal as long as the Z-value is +/- 1.96 and the P-value is higher than 0.05.

Figure 5-12, Figure 5-13, Figure 5-14, Figure 5-15, and Figure 5-16 show the normal distribution function for VL53L0X, VL53L1X, and HC-SR04 sensors for all of the experiments presented in this study. The horizontal axis of all graphs are the averaged estimated data of all sensors in millimeters, and the vertical axis is the normal distribution function. It should be noted that title of the presented figures shows the actual range that the sensors were supposed to measure. Table 5-3, Table 5-4, Table 5-5, Table 5-6, and, Table 5-7 investigate the normal distribution of the estimation.

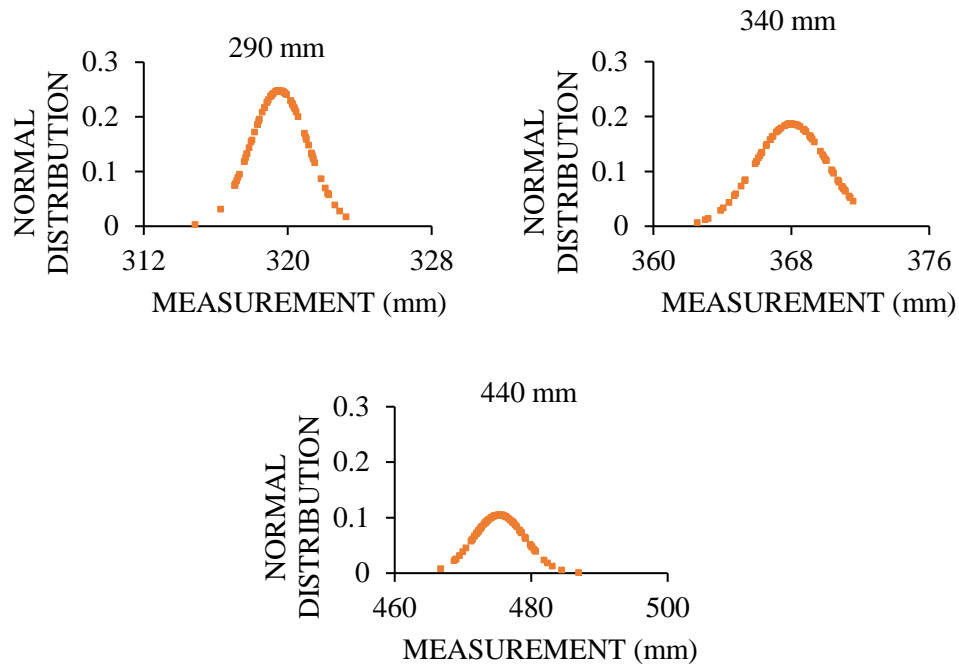


Figure 5-12. The normal distribution function of VL53L0X for tests with ambient light.

Table 5-3. Statistical analysis of VL53L0X for tests with ambient light.

Steel measurement pattern	Mean	Variance	Standard Deviation	Shapiro-Wilk P-value	Kurtosis Z-value
290	320	2.61	1.61	0.75	0.18
340	368	4.61	2.15	0.05	-0.43
440	475	14.54	3.81	0.43	0.59

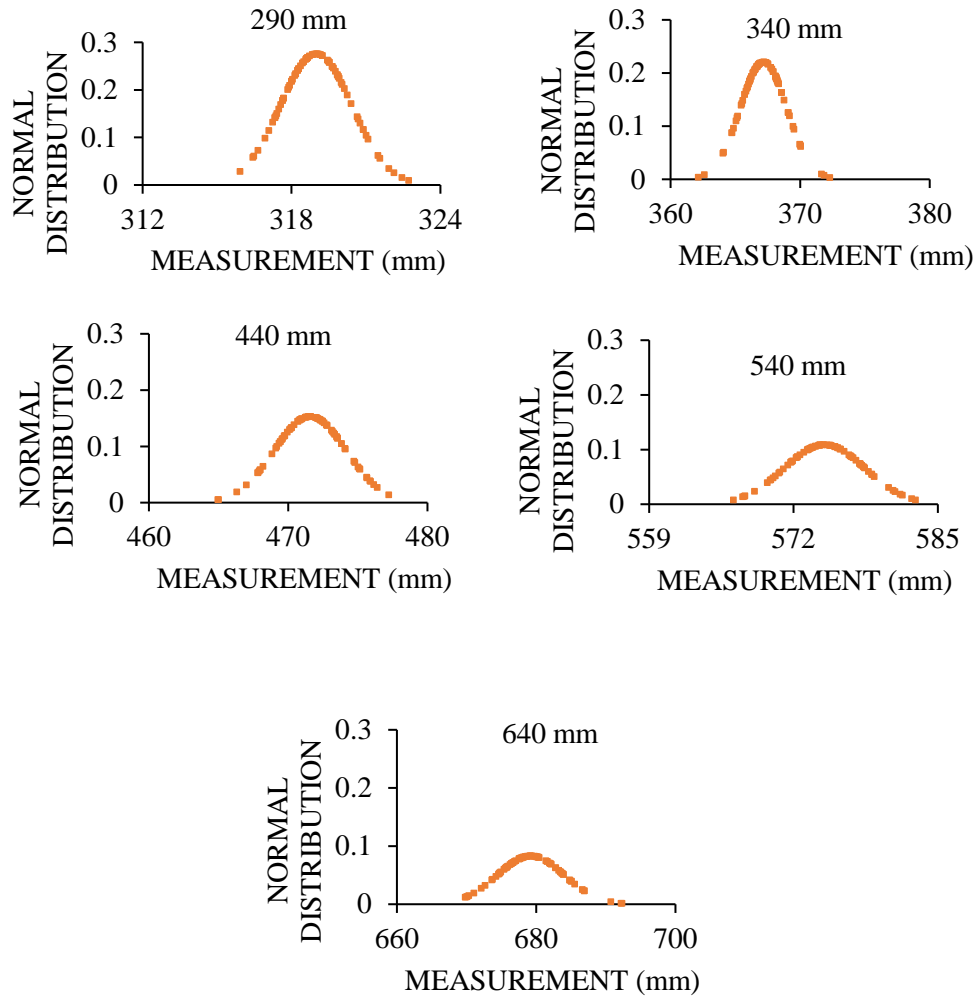
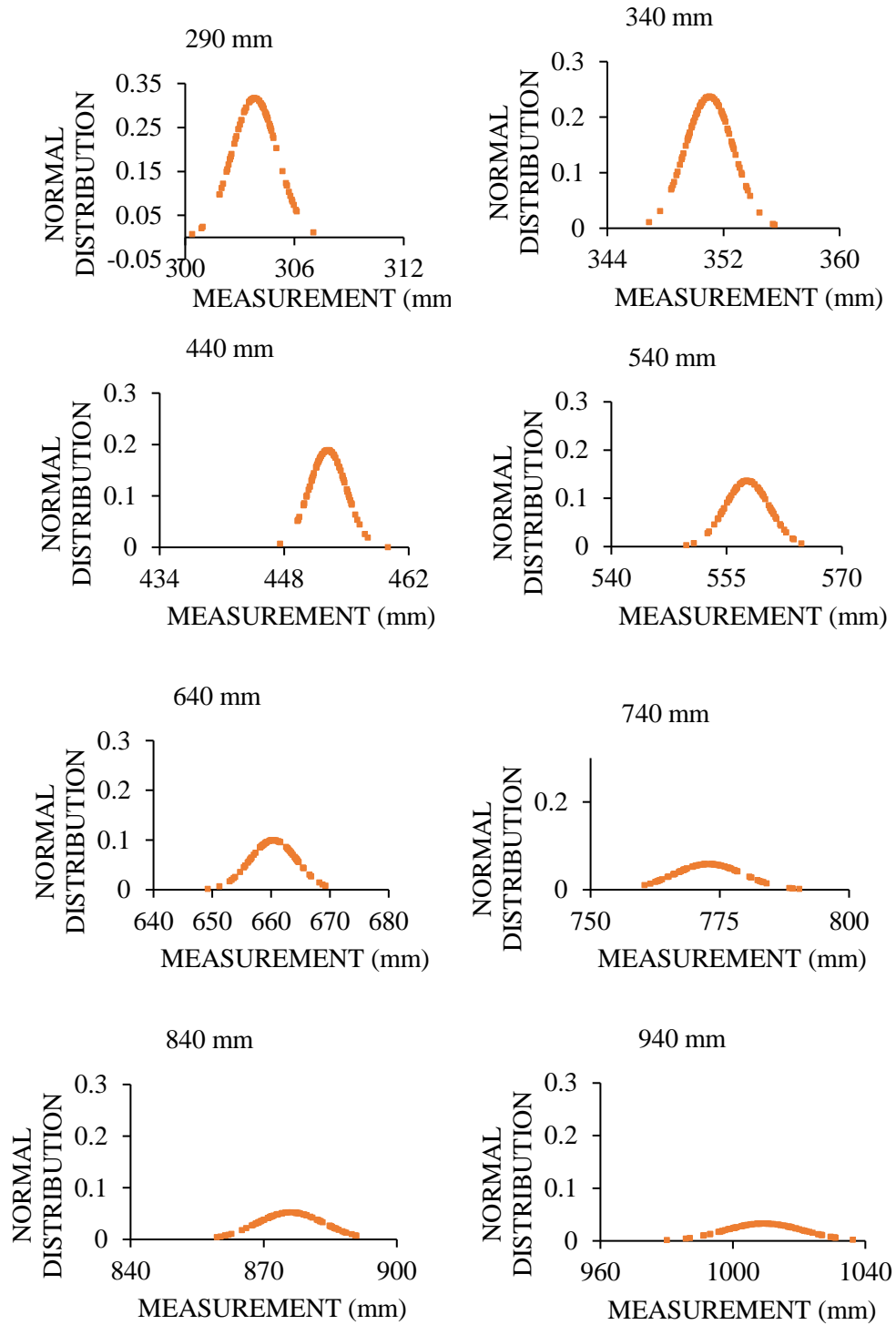


Figure 5-13. The normal distribution function of VL53L0X for tests with no excessive ambient light.

Table 5-4. Statistical analysis of VL53L0X for tests with no excessive ambient light.

Steel measurement pattern	Mean	Variance	Standard Deviation	Shapiro-Wilk P-value	Kurtosis Z-value
290	319	2.11	1.45	0.36	-0.22
340	367	3.29	1.81	0.19	2.02
440	472	6.82	2.61	0.79	-0.15
540	575	13.43	3.67	0.82	-0.51
640	679	23.27	4.82	0.21	0.59



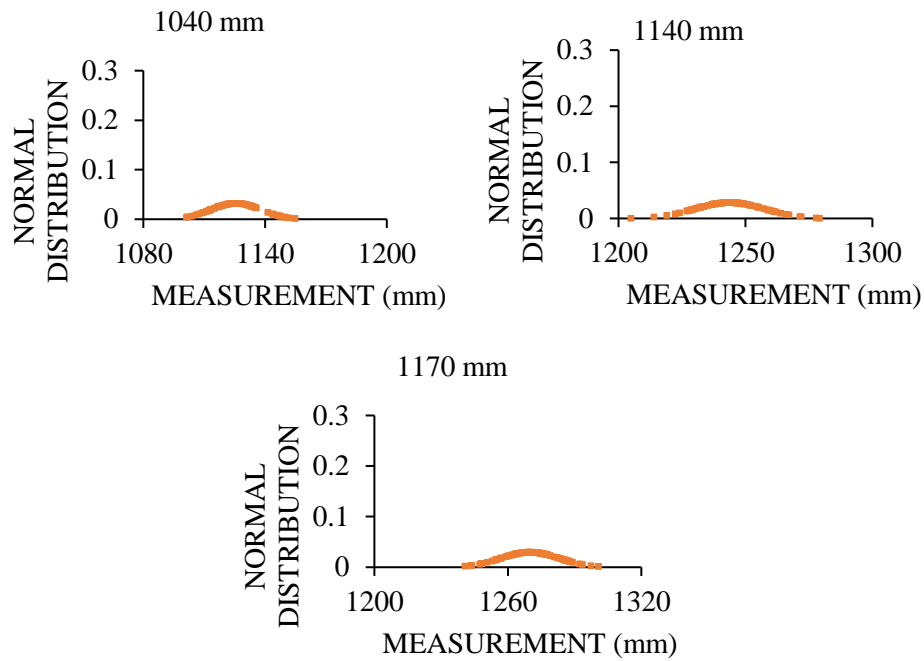
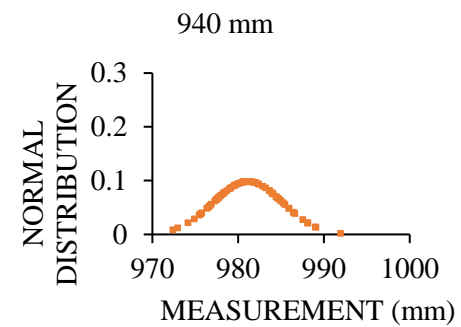
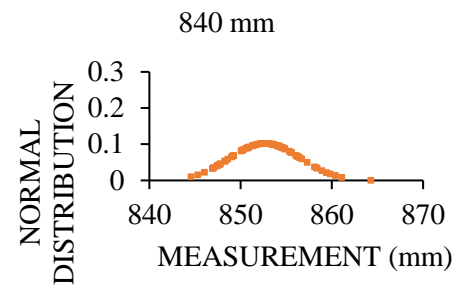
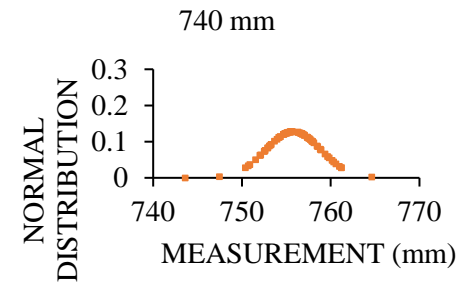
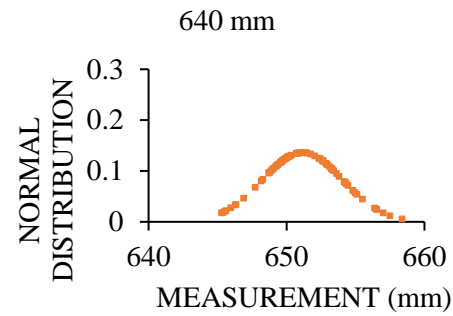
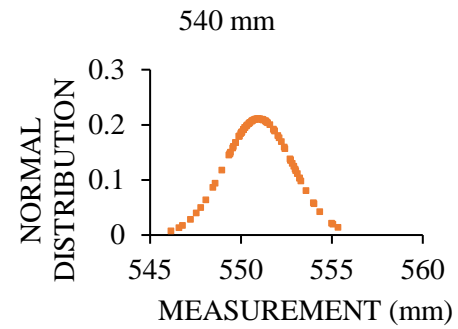
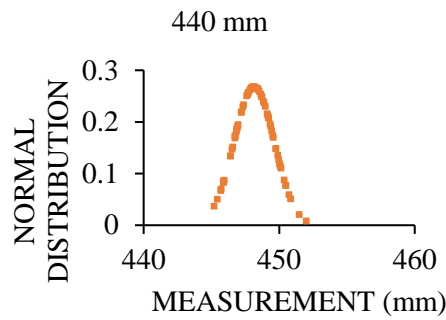
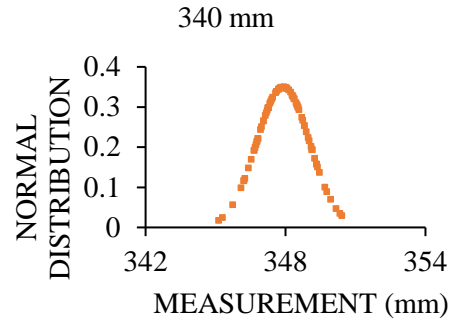
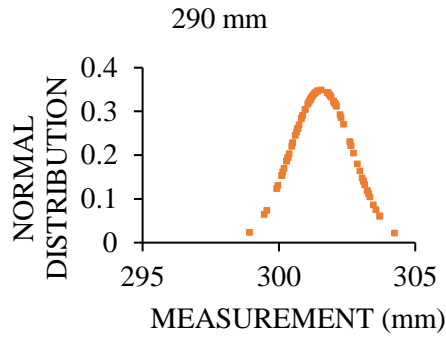


Figure 5-14. The normal distribution function of VL53L1X for tests with ambient light.

Table 5-5. Statistical analysis of VL53L1X for tests with ambient light.

Steel measurement pattern	Mean	Variance	Standard Deviation	Shapiro-Wilk P-value	Kurtosis Z-value
290	304	1.60	1.27	0.73	0.36
340	351	2.86	1.69	0.81	0.12
440	453	4.47	2.11	0.58	0.67
540	558	8.58	2.93	0.99	0.02
640	660	16.09	4.01	0.87	-0.06
740	773	46.12	6.79	0.05	-0.12
834	876	58.18	7.63	0.28	-1.13
940	1009	145.54	12.06	0.66	-1.05
1040	1126	151.65	12.31	0.06	-0.56
1140	1244	194.23	13.94	0.74	0.60
1170	1270	174.50	13.21	0.73	-0.80



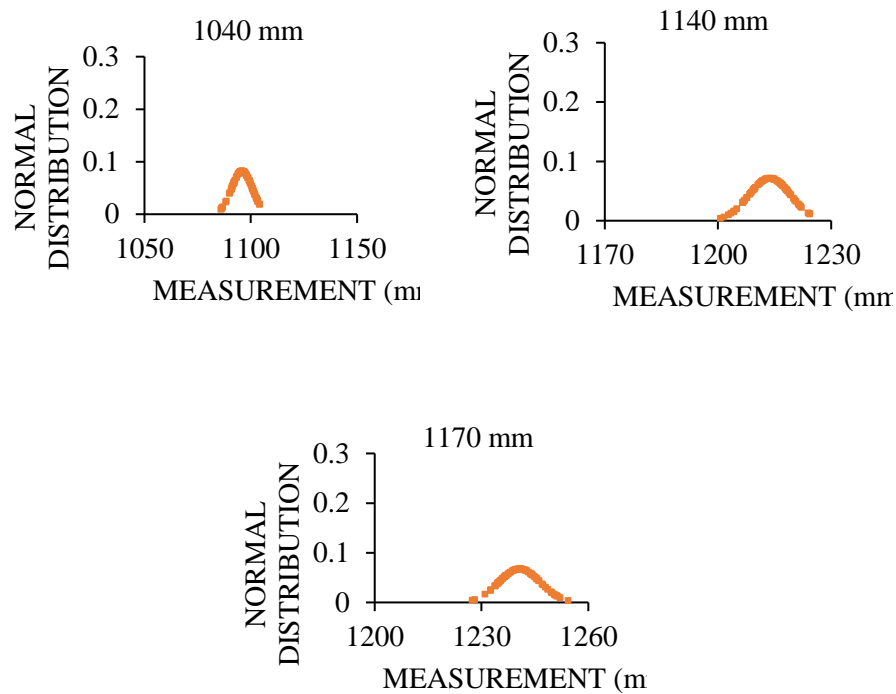


Figure 5-15. The normal distribution function of VL53L1X for tests with no excessive ambient light.

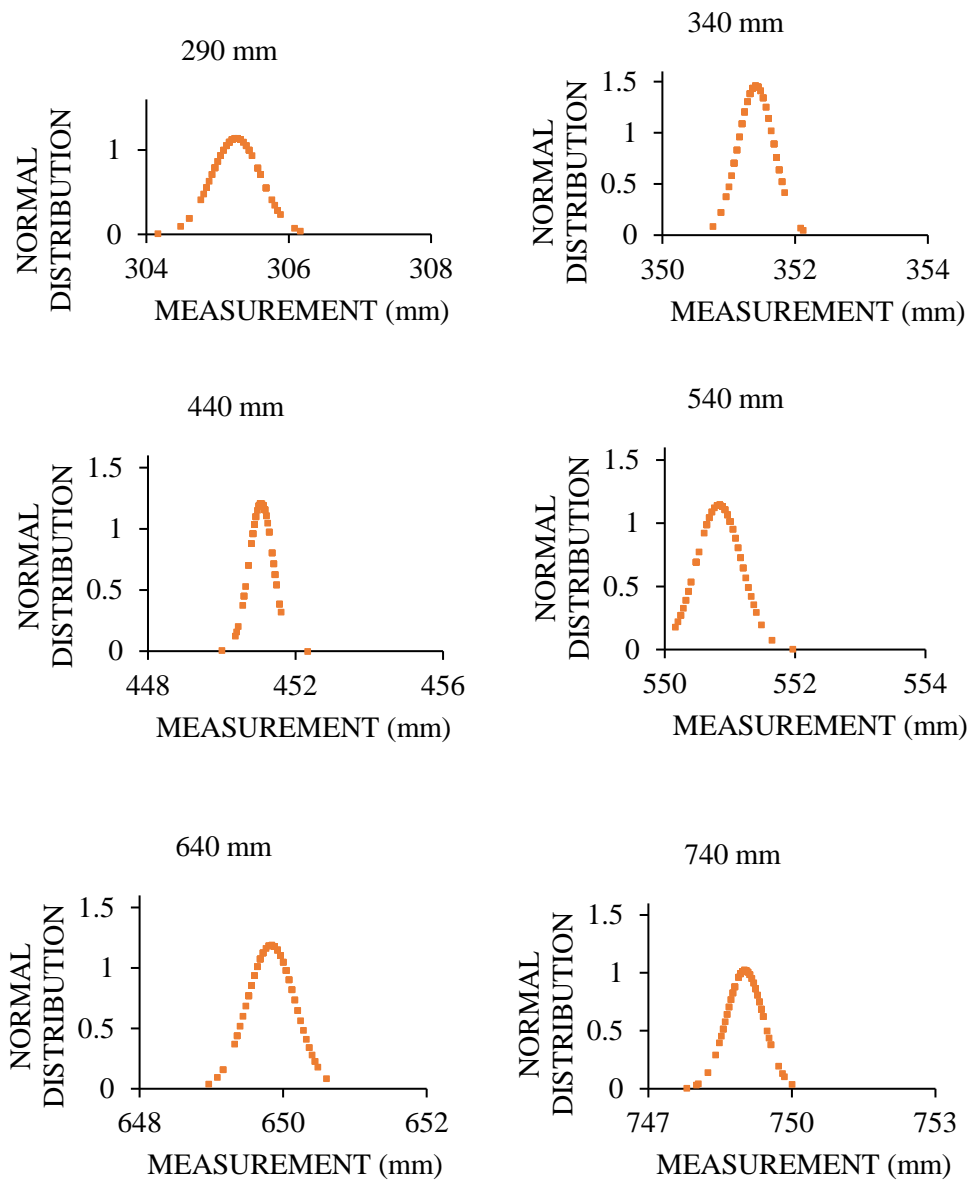
Table 5-6. Statistical analysis of VL53L1X for tests with no excessive ambient light.

Steel measurement pattern	Mean	Variance	Standard Deviation	Shapiro-Wilk P-value	Kurtosis Z-value
290	302	1.32	1.15	0.24	-1.22
340	348	1.31	1.14	0.93	-0.62
440	448	2.23	1.49	0.57	-0.86
540	551	3.60	1.90	0.43	0.44
640	651	8.60	2.93	0.18	-0.40
740	756	9.81	3.13	0.02	4.75
834	853	15.09	3.88	0.67	0.14
940	981	16.41	4.05	0.74	-0.67
1040	1096	23.59	4.86	0.04	-1.49
1140	1214	31.14	5.58	0.52	-0.91
1170	1241	34.78	5.90	0.30	-0.95

84

The analysis of Figure 5-12, Figure 5-13, Figure 5-14, and, Figure 5-15, shows that the distribution function value for ToF sensors decreases when the target object is located further away from the distance sensor. The area under the graph increases with the target object located further away. The presence of ambient light makes this area even bigger. These indicators mean that the probability of estimating the right answer by the ToF sensors decreases as the distance increases, or when ambient light exists.

Careful inspection of Table 5-3, Table 5-4, Table 5-5, and, Table 5-6 illustrate that the distributions of VL53L0X and VL53L1X in both the presence and absence of excessive ambient light are normal.



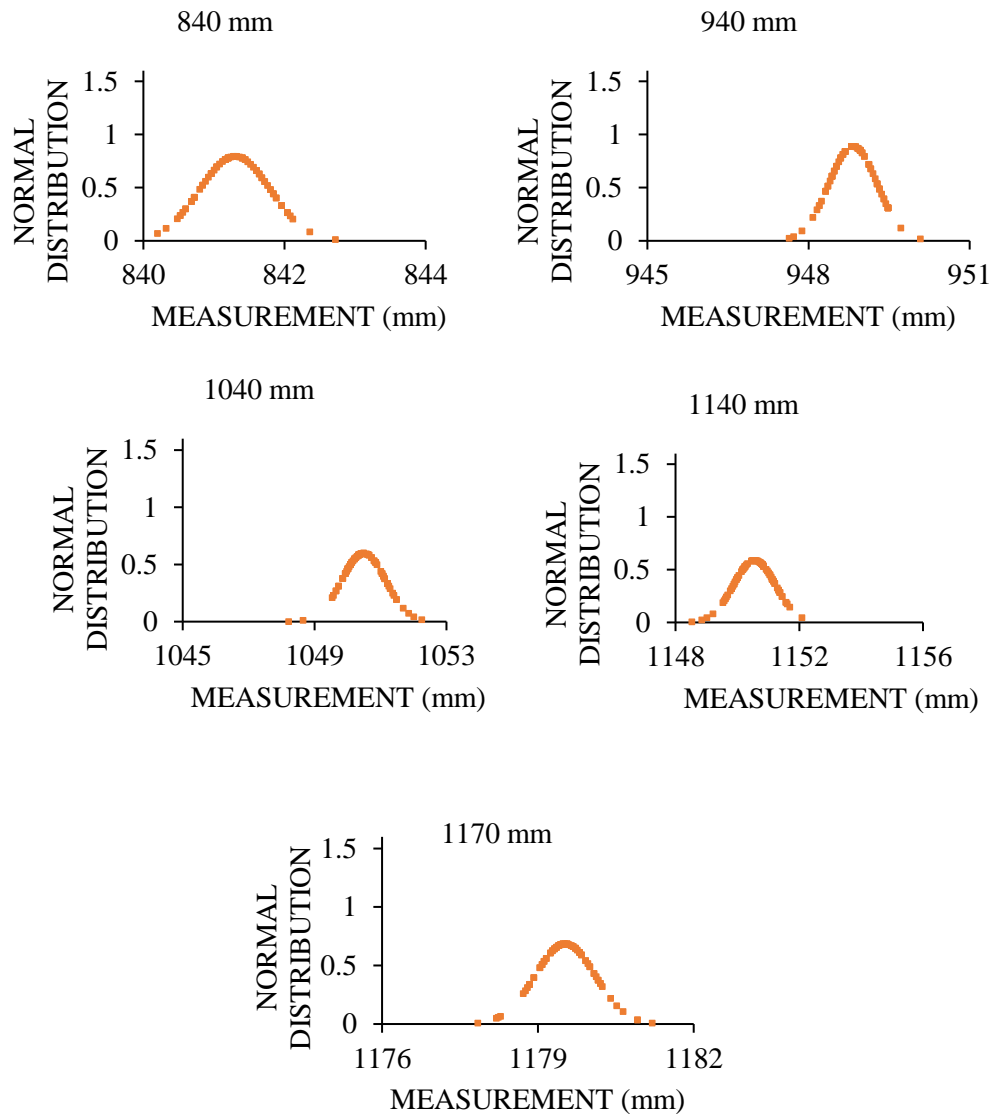


Figure 5-16. The normal distribution function of HC-SR04 for various distance measurements.

Analysis of Figure 5-16 shows that some of the distributions are not following the regular pattern. In fact, the information in Table 5-7 helps check the normal distribution of HC-SR04 outputs for the performed laboratory experiments.

Table 5-7. Statistical analysis of HC-SR04 values.

Steel measurement pattern	Mean	Variance	Standard Deviation	Shapiro-Wilk P-value	Kurtosis Z-value
290	305	0.12	0.35	0.60	1.30
340	351	0.07	0.27	0.58	-0.42
440	451	0.11	0.33	0.01	4.67
540	551	0.12	0.35	0.20	0.67
640	650	0.11	0.34	0.93	-0.24
740	749	0.15	0.39	0.18	2.04
834	841	0.25	0.50	0.71	-0.59
940	949	0.20	0.45	0.80	0.40
1040	1050	0.45	0.67	0.04	2.64
1140	1151	0.47	0.68	0.32	0.44
1170	1180	0.34	0.58	0.10	2.31

Analysis of Table 5-7 shows that most of the estimations follow a normal distribution. In fact, the assessments that are not following normal distribution may appear because of the lack of electrical current necessary for the sensors to perform accurately.

Table 5-8 shows the price of devices made from combining similar sensors for an experimental test. In this test, sensors have estimated a distance of 540mm in the absence of excessive ambient light.

Table 5-8. price comparison of the devices made from coupled sensors.

Sensor name	Sensor type	Number of needed sensors	Error (%)	Price (€)
HC-SR04	Ultrasonic	2	1.85%	5.0
V15310x	ToF	8	8.55%	43.2
V15311x	ToF	2	3.70%	25.0
HC-SR04	Ultrasonic	1	2.40%	2.5
V15310x	ToF	1	10.17%	5.4
V15311x	ToF	1	4.10%	12.5

Analysis of Table 5-8 shows that the accuracy of V15310X is so low that even after combining eight sensors, the error is still higher than V15311X and HC-SR04. In fact, by using only two V15311X sensors, the benefits of sensor combinations, such as a smoother standard deviation and having a backup sensor in case one sensor is faulty can be reached with a lower price. The ultrasonic sensor has the highest accuracy, but it cannot be used in places with high ambient

87

temperature variations. A commercial non-contact distance sensor acquisition resolution is extracted from its datasheet to show the cost efficiency of the systems in this study. O1D100 in the distance range of 200mm to 1,000mm has an 18mm accuracy (1.8%). The price of O1D100 is 383 €[174].

Further analysis of Table 5-8 suggests no need to combine 25 similar sensors to improve the accuracy of data acquisition. By using two combined HC-SR04, the estimation error will be already less than two percent. The same number of combined VL53L1x will also result in accurate distance estimation. In fact, based on the required sensitivity, more sensors can be combined. The final number of sensor combinations depends on some variables) such as the size of the understudy object and its movements).

Chapter 6 : Low-Cost Wireless Structural Health Monitoring of Bridges

6.1 Introduction

Nowadays, low-cost accelerometers are getting more attention from civil engineers to make Structural Health Monitoring (SHM) applications affordable and applicable to a broader range of structures. The present accelerometers based on Arduino or Raspberry Pi technologies in the literature share some of the following drawbacks: (1) high Noise Density (ND), (2) low sampling frequency, (3) not having the Internet's timestamp with microsecond resolution, (4) not being used in experimental eigenfrequency analysis of a flexible and a less flexible bridge and (5) synchronization issues. To solve these problems, a new low-cost triaxial accelerometer based on Arduino technology is presented in this work (Low-cost Adaptable Reliable Accelerometer-LARA). Laboratory test results show that LARA has a ND of $51 \mu\text{g}/\sqrt{\text{Hz}}$, and a frequency sampling speed of 333 Hz. In addition, LARA has been applied to the eigenfrequency analysis of a short-span footbridge and its results are compared with those of a high precision commercial sensor. Finally, a highway bridge is instrumented using two LARA accelerometers and three uniaxial commercial accelerometers (PCB 607A61). The modal analysis of LARA is compared with those of the commercial ones using Modal Assurance Criterion (MAC). It is reported that the MAC value of the first three mode shapes has a value of higher than 0.93.

This Chapter is organized as follows: In Subsection 2, LARA (the updated version proposed by this Chapter) is presented with its detailed characteristics. In Subsection 3, the validating laboratory tests of CHEAP, LARA and MPU9250 are presented together with their results. Finally, in Subsection 4, the validation of eigenfrequency and modal analysis of LARA on a short-span footbridge and a highway bridge are presented.

6.2 Triaxle wireless Low-cost Adaptable Reliable Accelerometer (LARA) with the post-synchronization capability

In this section, the main features and innovations of the Low-cost Adaptable Reliable Accelerometer (LARA) in terms of software and hardware are detailed.

LARA is an updated CHEAP version, a wireless triaxial accelerometer that can be controlled, monitored, and programmed wirelessly.

This new accelerometer has a frequency sampling of 333 Hz, an acceleration range of $\pm 2.0\text{g}$, and effective bandwidth of 165 Hz. LARA is built into two parts: (1) A sensing part: Contains the aligned accelerometers and the multiplexor, which is shown in Figure 6-1.a. It should be noted that like CHEAP, LARA consists of five aligned low-cost MEMS accelerometers. It is due to the fact that when the results of a few accelerometers with unique inherent dynamic noises are averaged, the signal under study remains invariable. However, the dynamic noises of individual sensors are divided by the square root of the number of averaged sensors, and (2) an acquisition part:

Consisting of an Arduino and a Raspberry Pi. The sensing and acquisition parts of LARA are shown in Figure 6-1.b. In addition to the CHEAP components, LARA includes:

- **A Raspberry Pi:** Raspberry Pi is a small size Linux-based computer that can be connected to Arduino microcontrollers. This way, the operator can access the Arduino codes for modifying or upgrading purposes. To save and acquire provided data of the accelerometers, a python code was written to save the acquisition data on the Raspberry Pi memory card. For synchronizing different LARAs for future SHM applications, the Arduino's acquired data were saved with an accurate timestamp. The timestamp is reported from the inner clock of the Raspberry pi. For constantly synchronizing the inner clock of the Raspberry Pi with the accurate time of the Internet, the Raspberry Pi's NTP protocol was activated. Figure 6-1.c shows the connection between the Arduino and the Raspberry Pi. Arduino gets its needed power from a USB port of the Raspberry Pi. Raspberry Pi can be powered up by using an adaptor or a power bank. It is also noteworthy to mention that the time keeping accuracy when using a Raspberry Pi model 3b+ with a NTP server was already published in the literature [73]. In this work, an overall deviation of 0.01 seconds was measured after a 40-hours test. This value corresponds to a time accuracy of 0.07 Parts Per Million (PPM).
- **A PCB board:** A Printed Circuit Board (PCB) was used to place the sensors in the targeted location with all their axes aligned. The sensors used the shortest possible wire lengths for connections between the multiplexor the accelerometers. In Figure 6-1.a, the adjustment of sensors on LARA by the PCB is shown. In fact, it can be seen in Figure 6-1.a and Figure 6-1.c that the PCB board has aligned X, Y and Z axes of the MPU9250 accelerometers.

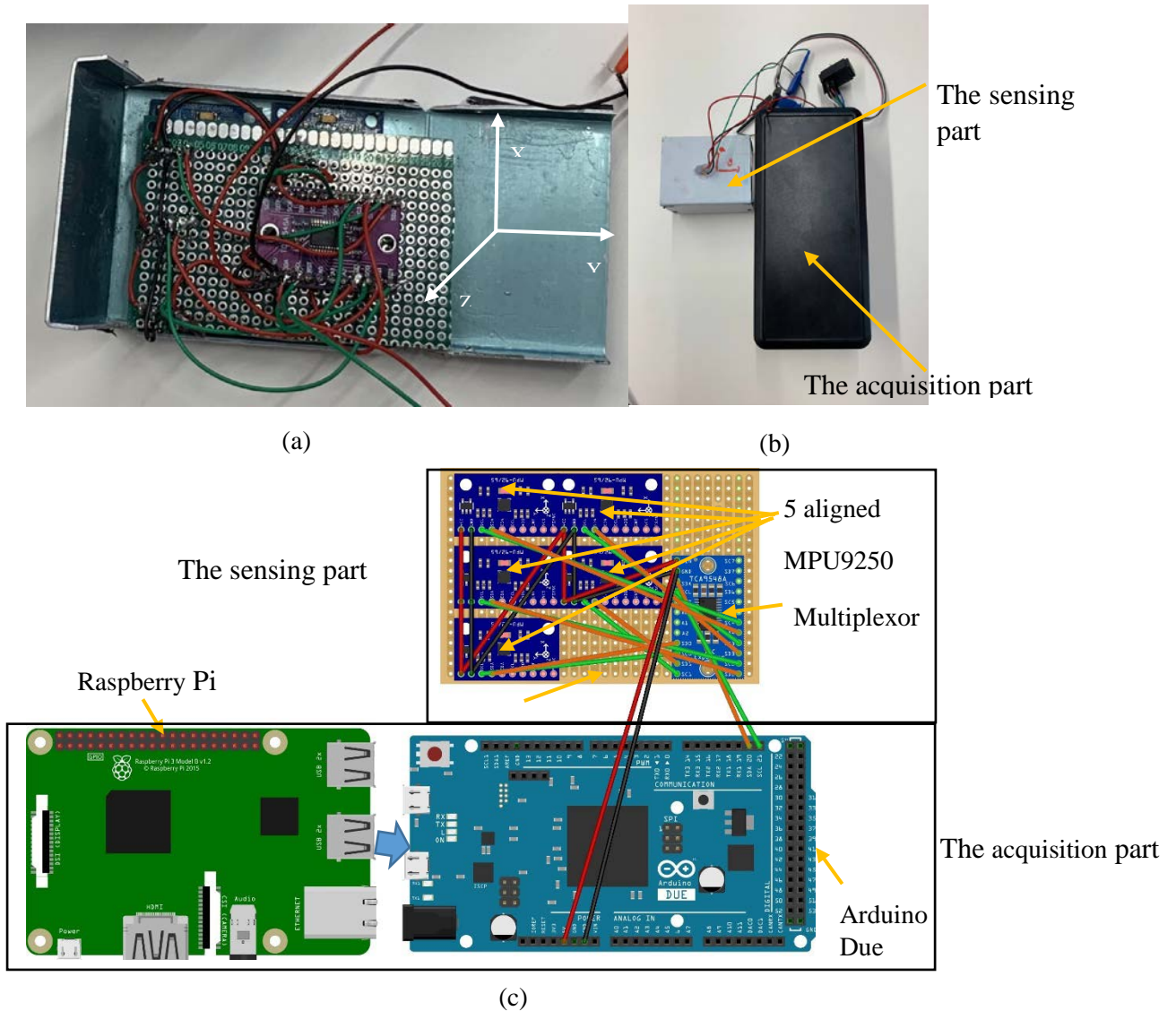


Figure 6-1. LARA elements: (a) the adjustments and wire connections of the sensing part, (b) the sensing and acquisition part and (c) LARA in detail.

- An aluminum box: The sensors are placed inside a box to preserve the accelerometers from environmental conditions (such as humidity, dust, and environmental activities). A very rigid and stiff material was needed to reach the same input signal to all the accelerometers [141]. Aluminum material was chosen to hold the accelerometers because it is very stiff, but, at the same time, it is a very light and conductive material. The conductivity helps the sensor's grounding. Besides, in Figure 6-1.b, the boxing of LARA is illustrated. The dimensions of this element are 52*72*44 millimeters.
- A USB 4G dongle: This device included a modem with an internet connection connected to the Raspberry Pi that was used for the following purposes: (1) Providing the accurate time of the internet for the data acquisition time stamp, (2) Controlling remotely the data

acquisition process, and (3) Transferring wirelessly the acquired data from the memory card of the Raspberry Pi to another computer.

- A plastic box for the acquisition equipment: A plastic box was used to preserve the Arduino, Raspberry Pi part and the internet dongle. The connection between two boxes is within four sets of wires. The red, black, green and orange wires connect the 5-volt Voltage Common Controller (VCC), GrouND (GND), Serial Clock Line (SCL) and Serial Data Line (SDA) of the sensing part to the acquisition part.

Besides the extra hardware parts that LARA possesses compared with CHEAP, LARA uses a new code and a library code that makes it faster and triaxial. The software enhancement of LARA refers to:

- Increasing sampling frequency: Frequency sampling of LARA is increased by rewriting the old library code and using a faster communication clock along with the main code.
- No coding error: Increasing the frequency sampling of a system can result in error reporting, interruptions, data loss, or fluctuation in the frequency sampling speed. In an experiment, LARA worked for an entire week and saved data with no errors or interruptions or data loss.
- Schedule data acquisition: A code has been prepared on python to schedule and end vibration acquisition. This scheduling has two benefits. Firstly, it makes wireless sensor synchronization possible with free software. Secondly, it can be used for OMA applications. It should be noticed that when a structure is heavily excited by ambient causes, the accelerometers can extract more valuable data. Therefore, an accelerometer with schedule capability can help acquire data only when the structure is under high traffic or extreme activity.
- Internal sensor synchronization lag enhancement: The accelerometers inside each LARA are not 100% synchronized. In fact, the Arduino executes codes one line at a time. When the main code is executed, the Arduino opens the library code and uses the information to get the first sensor's acceleration, and after the second one, and so on. This operation takes time. In the CHEAP, the lag between each sensor-print was about 2200 microseconds. By the hardware and software improvement, the corresponding lag of LARA is decreased to 210 microseconds, which is 10.47 less than the lag of CHEAP. In fact, a lower lag time contributes to a better sensitivity of LARA for acquiring higher frequencies.
- Post synchronization of several LARAs: To use LARA's outputs in the OMA application, various accelerometers' data must first be synchronized and have the same sampling frequency. Since LARA has access to the accurate time of the internet, the acquired data can be stamped with the precise time of the Internet with microsecond resolution. This timestamp helps calculate the sampling frequency of each LARA precisely and, more importantly, the fluctuation of the vibration acquisition process. Even though the reported sampling frequency of each LARA is calculated by measuring the number of acquired data during the acquisition process, the fluctuation is calculated by measuring the needed time for saving 100 data. It is seen through laboratory experiments that when the input power is insufficient, the fluctuation is unsteady. This insufficient input power can be due to low-

speed of the used USB wire, the long length of the USB cable, the imperfection of the used power bank, or simply using a power source that can not provide 2.5 A and 5 V [120].

6.3 Laboratory tests and results

This section aims to validate the performance of LARA. Firstly, the resolution, sensitivity, and ND of a single MPU9250, CHEAP and LARA are presented. For that, an extended duration test was performed in an office. Secondly, a test has been carried out on the hydraulic jack of the laboratory. In that test, LARA was validated and compared with CHEAP. Next, the performed tests for validating LARA's accuracy in terms of various frequencies are investigated. Finally, the acceleration amplitude evaluation is shown.

It should be noted that the performance of CHEAP was validated using two high-precision accelerometers (PCB 393A03 and 356B18) [29] in several laboratory experiments for a range of frequencies from 0.5 to 10 Hz. These tests were performed on the same shaking platform used in this work. This platform is an INSTRON 8803 model located at the Structural Laboratory Lluís Agulló of Technical University of Catalonia (Barcelona, Spain). In addition, it is essential to mention that LARA was calibrated in the laboratory of the Applus company. In that certification, the acceleration amplitude accuracy of LARA was studied in several experiments with a fixed RMS acceleration amplitude of 0.5 g within the range of 5 to 160 Hz. This certification is shown in Figure 6-2. It should be noted that the name of the developed solution used to be Super Adaptable Reliable Accelerometer (SARA). This name is changed to LARA, due to the fact that there is a company entitled SARA that produces accelerometers.



CERTIFICADO DE CALIBRACIÓN
Certificate of calibration

Número
Number 21/34549626

Página
Page 1 de 3 páginas
pájes

21/34549626

pág. 2 de 3



ENAC (Ente Nacional de Acreditació), S.A. (ENAC) -
Campus IRI4 - Rovella de la Font del Comaró -
08191 Bellaterra (Barcelona) - Spn
T +34 (91) 567 20 00
F +34 (91) 567 20 01
www.enac.es



OBJETO
Item Medidor de vibraciones

MARCA
Mark UPC

MODELO
Model SARA

IDENTIFICACIÓN
Identification --
3

SOLICITANTE
Applicant UNIVERSITAT POLITÈCNICA DE CATALUNYA
Carrer Jordi Girona, 1
08034 - BARCELONA

FECHA/S DE CALIBRACIÓN
Date/s of calibration 01/10/2021

SIGNATARIO/S AUTORIZADO/S
Authorized signatory/ies

Responsable Técnico / Technical Manager Técnico / Technician

JORDI GIL DEL RIO 13/10/2021 09:59:31 Dani Riu Solà
Código Seguro de Verificación (CSV): 2020X03031FV2 06/10/2021 10:10:06

Este documento ha sido firmado electrónicamente según la Ley 59/2003 e identificado mediante un Código Seguro de Verificación (CSV).
Consulte la validez del documento en el servicio Web de verificación https://appplus.com/finanzas/

Este certificado no puede ser reproducido parcialmente, excepto cuando se haya obtenido previamente permiso por escrito de Applus.
Los resultados que se indican se refieren únicamente al objeto sometido a calibración, en el momento y en las condiciones en que se realizaron los m.
Este Certificado may not be partially reproduced, except with the prior written permission of Applus.
The results stated in this document refer only to the samples submitted to calibration, in the moment and conditions where measurements were m.
This Certificate may not be partially reproduced, except with the prior written permission of Applus.

PROCEDIMIENTO DE CALIBRACIÓN

La calibración se ha efectuado por comparación entre la cadena de medida de referencia y la cadena a ensayar mediante procedimiento interno C2622002 Ed.7.

CONDICIONES DE CALIBRACIÓN

Temperatura: 20,6 ± 2 °C
 Humedad relativa: 62 ± 10 %
 Presión atmosférica: 100,64 ± 0,5 kPa

TRAZABILIDAD

Los siguientes patrones fueron utilizados en la calibración del equipo y tienen garantizada su trazabilidad al SI a través de los laboratorios de calibración de referencia, acreditados o integrados en la EA (European co-operation for Accreditation):

Inventario	Descripción	Marca	Modelo
102967	Acelerómetro	BRUEL & KJAER	8305
102966	Acordionador	BRUEL & KJAER	2692
102977	Multímetro	Agilent	34401A

INCERTIDUMBRE DE CALIBRACIÓN


Las incertidumbres expresadas en este documento corresponden a la incertidumbre expandida de calibración, obtenida multiplicando la incertidumbre típica de medida por el factor de cobertura k=2 que, para una distribución normal, corresponde a una probabilidad de cobertura de aproximadamente el 95%. La incertidumbre típica de medida se ha determinado conforme al documento EA-4/02 M.

OBSERVACIONES

El medidor de vibraciones se compone de una placa electrónica y un software adquiridor de desarrollo propio con una frecuencia de muestreo de 333 Hz. Cada uno de los valores RMS reportados en el apartado de resultados se obtuvo a partir de un tiempo de adquisición de 60 segundos. Los ejes se definieron de acuerdo con la serigrafía de la placa (ver imágenes).



pág. 3 de 3



21/34549626

RESULTADOS

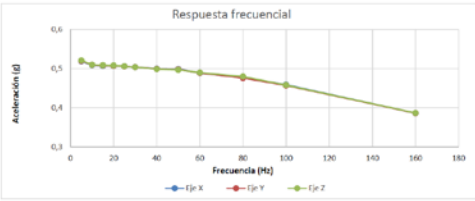
Los resultados expresados se refieren a la cadena completa de medida, y no son válidos para su utilización con un acelerómetro distinto del identificado en este certificado.
 Los resultados de las mediciones se obtienen en las condiciones ambientales en el momento del ensayo, tal como aparecen reflejadas en el apartado Condiciones de Calibración.

Respuesta frecuencial

Aceleración RMS patrón: 0,5 g (Conversión al SI: 1 g = 9,80665 m/s²)

Lecturas RMS del equipo (valores en g):

Frecuencia (Hz)	eje X (g)	eje Y (g)	eje Z (g)	U en %
5	0,519	0,520	0,521	1,5
10	0,506	0,510	0,510	1,5
15	0,507	0,508	0,509	1,5
20	0,507	0,507	0,508	1,5
25	0,508	0,506	0,508	1,5
30	0,504	0,504	0,504	1,5
40	0,500	0,499	0,499	1,5
50	0,499	0,498	0,497	1,5
60	0,489	0,489	0,490	1,5
80	0,477	0,476	0,480	1,5
100	0,459	0,457	0,458	1,5
160	0,396	0,396	0,397	1,5



Este certificado no puede ser reproducido parcialmente, excepto cuando se haya obtenido previamente permiso por escrito de Applus.
 Los resultados que se indican se refieren únicamente al objeto sometido a calibración, en el momento y en las condiciones en que se realizaron los m.
 This Certificate may not be partially reproduced, except with the prior written permission of Applus.
 The results stated in this document refer only to the samples submitted to calibration, in the moment and conditions where measurements were m.

Figure 6-2. Calibration certificate of the developed accelerometer.

6.3.1 Sensitivity, ND and resolution evaluation

This section compares the sensitivity, ND, and resolution of a single MPU9250 accelerometer with CHEAP and LARA.

The accelerometers' sensitivity can be defined as the ratio of the input (induced vibrations of the shaking table) to the output (the information reported by the accelerometer). This concept is measured and calculated differently for analog and MEMS sensors. Although an analog accelerometer usually produces electronic pulses related to the input vibrations, MEMS accelerometers convert these electronic pulses into digital signals. While the sensitivity of analog sensors is reported as V/g (Voltage per gravitational acceleration), MEMS accelerometers report their sensitivity in the Least Significant Bit per gravitational acceleration (LSB/g) [10]. Since this value is a characteristic of a sensor, it should be the same for MPU9250, CHEAP and LARA. The Data-sheet of MPU9250 reports a sensor sensitivity for the acceleration amplitude range of ± 2.0 g of 16384 LSB/g. MPU9250 accelerometers work with an operating voltage of 2.5 volts and its scale for converting data from analog to digital (Analog to Digital Converter ADC) is 16 bits [67]. The ADC formula for calculating the LSB is shown in Eq.6-1 [10].

$$LSB = \frac{\text{Input voltage}}{2^{(\text{number of bits})}} \quad (6-1)$$

In Eq.6-1, with an input voltage of 2.5 and an ADC scale of 16, each unit of LSB is equivalent to 0.03814 mv. In this way, with 16384 LSB/g for acceleration amplitude range of ± 2.0 g, the comparable sensitivity of MPU9250, CHEAP and LARA is calculated as 625 mV/g.

To calculate ND and resolution of the devices, a long-term test was performed. The ND results of the different accelerometers, are calculated using Eq.6-2 [160]. It should be noted that CHEAP was located to read the signals from the Z direction. For validating this test and the used formula, an MPU9250 accelerometer was tested. In addition, the reported results of its data sheet are compared with the results of the tests. It should be noted that the presented noise density measurement of this work is a standard procedure to characterize the noise of the developed accelerometer [175]. This typically appears on the datasheet of commercial accelerometers [176]. However, it should be noted that those applications that aim to characterize the noises throughout time (such as Allan variance or Allan deviation) are out of the scope of this Chapter. Typically, these applications are used to investigate the noises of sensors (such as gyroscopes) which data drift throughout time in the time-domain series.

$$ND = \sqrt{\frac{\sum_{i=1}^N (x_i - \mu)^2}{N * f}} \quad (6-2)$$

In Eq.6-2, the x_i is the reported values of the accelerometers in the time-domain, μ is the average of all x_i values, N is the number of used samples and f is the sampling frequency of the accelerometer.

The calculated ND of MPU9250, CHEAP and LARA for the Z-directions are 390, 162 and 81 $\mu\text{g}/\sqrt{\text{Hz}}$, respectively. In addition, the ND of LARA for both X and Y directions is 51 $\mu\text{g}/\sqrt{\text{Hz}}$.

The data-sheet of MPU9250 reports its ND as $300 \mu\text{g}/\sqrt{\text{Hz}}$. In fact, the illustrated information of data-sheets is usually acquired under the best possible circumstances. It can be deduced from the calculated ND that using shorter wires and better connections made LARA 50% less noisy than CHEAP by reducing the ND value from 162 to $81 \mu\text{g}/\sqrt{\text{Hz}}$ in the Z-direction. The calculated ND values also shows that LARA has almost 79% less ND on the Z axes than a single MPU9250 accelerometer by reducing the ND value from 390 to $81 \mu\text{g}/\sqrt{\text{Hz}}$. Further studying of these values shows a lower ND of LARA on the X and Y axes. These two axes do not measure the gravitational acceleration of the earth; subsequently, the ND of LARA is $51 \mu\text{g}/\sqrt{\text{Hz}}$.

Since the evaluation of the accelerometer's resolution depends on the number of samples [177], for a fair comparison between devices with various sampling frequencies, the same number of the acquired samples were used in the test. For illustrating the resolution of the accelerometers, their reported data have been transformed from time-domain to frequency-domain by a Fast Fourier Transform (FFT). The results for different sensors are reported in Figure 6-3.

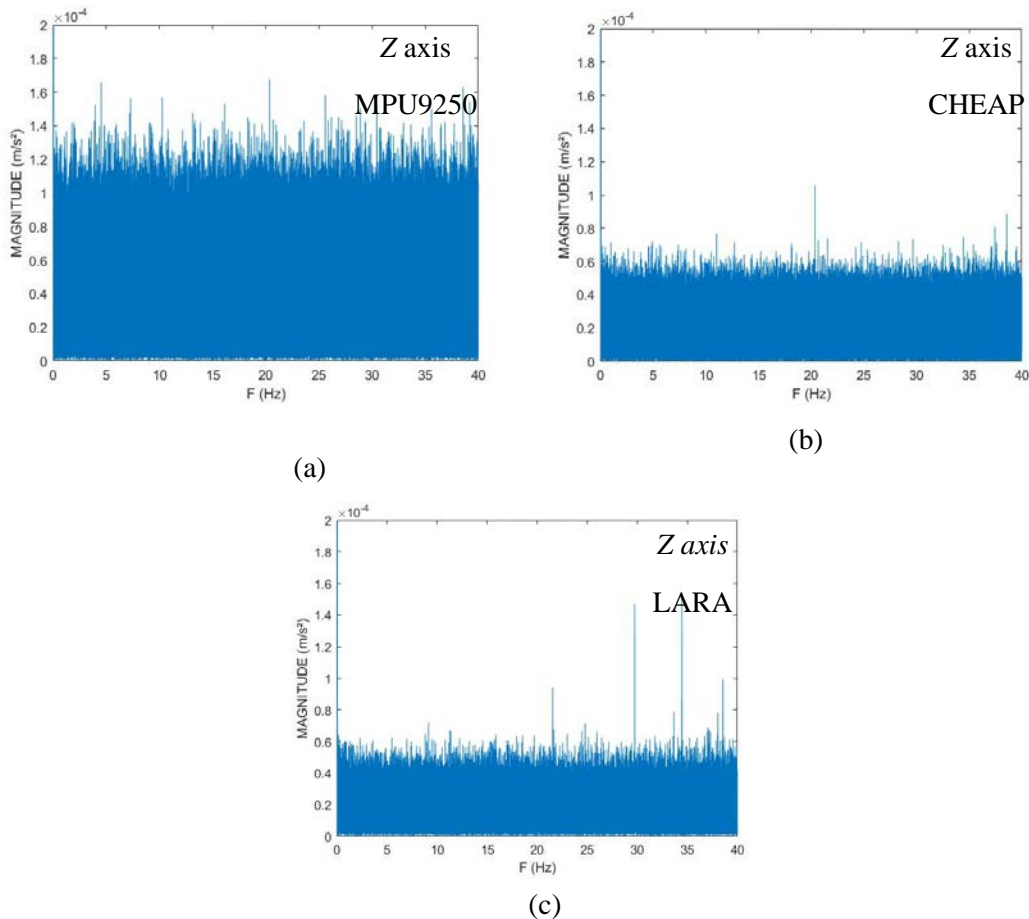


Figure 6-3. Frequency domain diagrams for Z axis of: (a) MPU9250, (b) CHEAP, (c) LARA.

Analysis of Figure 6-3 shows that while LARA and CHEAP resolution are almost equal, the resolution of a single MPU9250 is almost twice as the CHEAP or LARA. By studying Figure 6-3, MPU 9250's resolution, CHEAP and LARA for the Z-axis are reported as 0.00016 m/s^2 , 0.00009

and 0.00009 and respectively. It is to be considered that this test needed a long duration of data capture; consequently, it was done in an office at midnight. The FFT method reports more accurate outputs when it has a higher number of inputs [177]. For a fair comparison between MPU 9250, CHEAP and LARA, the same number of data had to be evaluated by the FFT method. Although sampling two million sets of data took MPU9250 and CHEAP 6.5 hours, LARA acquired two million sets of data in about 1.7 an hour. Figure 6-4 shows the frequency domain diagrams of acquired data of LARA for all the axes.

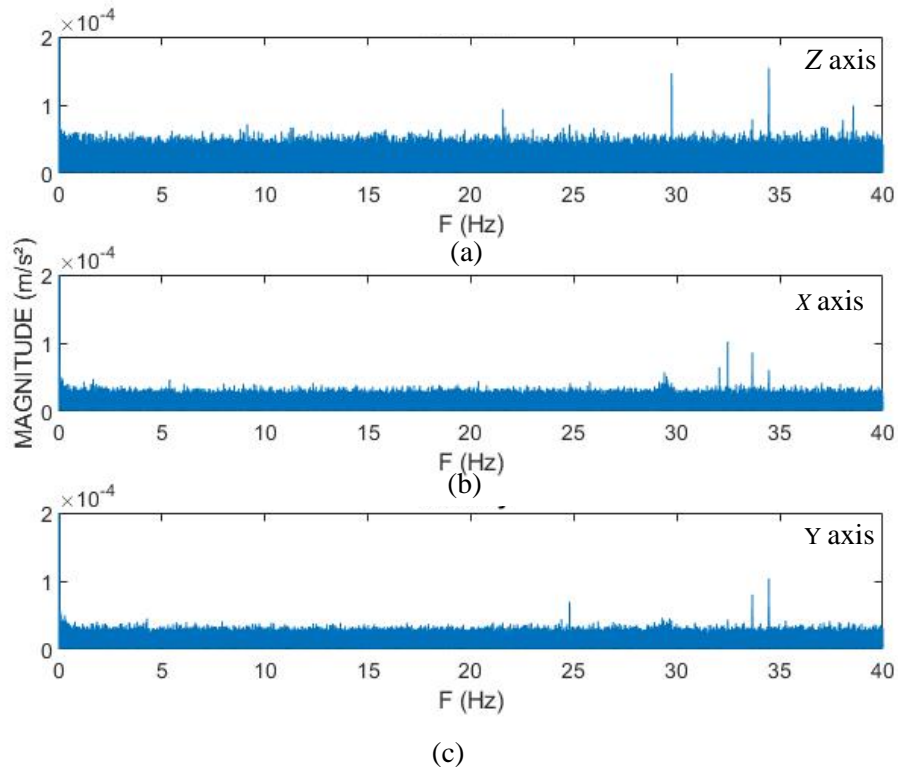


Figure 6-4. Frequency domain diagrams of LARA for: (a) Z, (b) X and (c) Y-axis.

Analysis of Figure 6-4 shows that the resolution of LARA for X and Y axes is 0.00005 m/s^2 . The resolution for X and Y-directions is 44% better than the Z-axis because of the absence of gravitational acceleration of the earth in those directions. As a result, the resolution of this accelerometer is evaluated as 0.00005 m/s^2 .

After calculating LARA's sensitivity, ND, and resolution, LARA can be compared with instrument-graded accelerometers. In Table 6-1, various commercial triaxial MEMS applications are presented. The contents of this table are ordered by the noise density of the accelerometers. This table includes the following information, which is reported by the data sheets provided by the producers or measured in this work, organized in columns: (1) sensor number, (2) sensor name, (3) acceleration range, (4) sampling frequency speed, (5) Noise Density (ND): The RMS resolution can be calculated by multiplying the ND by the square root of the sampling frequency, (6) sensitivity: For a better comparison, the analog converted sensitivities by the producer companies

are reported for each product, (7) price of the sensor (VAT excluded): Prices are based on the recent declaration of the producer. The reported price of LARA, CHEAP and MPU9250 refers to research prototypes and includes the used inceptions (such as accelerometer, Arduino, wires, multiplexor and Arduino) in them. It should be noted that the rest of the sensors are commercial solutions. The information in this column is to illustrate the price ranges and not to compare the price of the prototype sensors with the commercial ones, and (8) acquisition equipment.

Table 6-1. comparison of commercial triaxial MEMS accelerometers with LARA.

No.	Name	Acceleration Range (G)	Sampling Frequency (Hz)	Spectral Noise ($\mu\text{g}/\sqrt{\text{Hz}}$)	Sensitivity (V/G)	Price (€)	Acquisition System
1	IAC-Hires [178]	± 2.0	800	8	2.000	1192	Recovib Monitor
2	3713F112G [179]	± 2.0	500	10	0.675	2130	482C27
3	Unquake [180]	± 2.0	500	25	0.400	2500	Independent
4	Recovib Tiny [181]	± 2.0	500	30	0.600	1125	Independent
5	LARA	± 2.0	333	51	0.625	¹ 140	Independent
6	CHEAP	± 2.0	85	162	0.625	² 84	A computer
7	MPU9250	± 2.0	85	390	0.625	³ 50	A computer

Analysis of Table 6-1 shows that noise level of the commercial solutions (IAC-Hires [178] , 3713F112G [179], Unquake [180], and Recovib Tiny [181]) ranges from 8 to 30 $\mu\text{g}/\sqrt{\text{Hz}}$. In addition, analyzing Table 6-1 indicates that LARA has a more comparable ND with the introduced commercial accelerometers in Table 6-1 than with any of the low-cost accelerometers [5-7] presented in Table 2-2. The noise level of the commercial solutions (IAC-Hires [178] , 3713F112G [179], Unquake [180], and Recovib Tiny [181]) ranges from 8 to 30 $\mu\text{g}/\sqrt{\text{Hz}}$.

It is shown in Table 6-1 that 3713F112G and IAC-Hires need extra data acquisition equipment for acquiring the vibrations. In fact, 3713F112G needs a signal conditioner such as 482C27 with a price of 5070 € with four channels, and the IAC-Hires requires a data acquisition such as Recovib Monitor with a price of 3700 € which can provide up to eight reading channels. Moreover, CHEAP and MPU9250 are dependent on an attached computer for their signal monitoring and saving.

However, Unquake, Recovib Tiny, and LARA do not need any acquisition system for their data acquisition. Accelerometer Unquake, samples internally, and the measurements are timestamped with absolute time from GPS. The measurements are synchronized in the post-processing stage based on the timestamps by using the software that comes for free from the company. In addition, Recovib Tiny and LARA are both wireless sensors.

¹ Research prototype

² Research prototype

³ Research prototype

Further analysis of Table 6-1 shows a wide range of prices (varying between 1192€ up to 2500 €) of commercial solutions. In fact, as stated in [28], the cost of accelerometers is known to be one of the critical limitations of SHM analysis and long-term monitoring.

6.3.2 Frequency validation

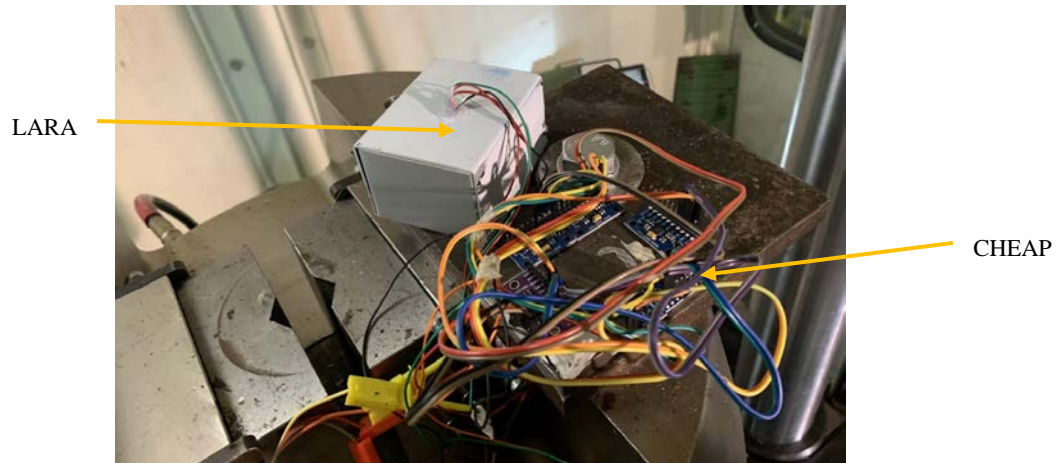
This subsection illustrates the experiments aiming at the frequency measurement accuracy of MPU9250, CHEAP and LARA on a vibration platform.

An experiment to validate the frequency report of LARA is presented in this section. A jack that could induce displacements with a known frequency was used. Although the jack is very accurate in reproducing a specific frequency, its performance is limited in movement. Therefore, for every experiment, the jack presents a report. This report is the time domain information of the activities of its lower jaw.

It should be noted that the vibration platform used in this work (INSTRON 8803) was programmed using WaveMatrix2 Dynamic Software. This jack can create various waveform types with the frequency range of 0.1 to 100 Hz and its resonant frequency is 134 Hz. The movement direction of this vibration platform (Z-direction) is shown in Figure 4.b.

In this work, the waveform is set to a sin wave. All the additional technical features of this hydraulic jack, its programming software, and its datasheets are presented in [29].

Figure 6-5.b shows the placement of the CHEAP and LARA on the hydraulic jack.



(a)



(b)

Figure 6-5. Laboratory validation of LARA: a) mounting CHEAP and LARA to the shaking part of the jack, b) The used vibrating platform (INSTRON 8803).

It can be seen from Figure 6-5.a that both CHEAP and LARA are attached to a rigid metal plate. This attachment was carried out by using an industrial adhesive (X60). X60 made by HBM company, is a two-component methyl-methacrylate adhesive that is widely used for accelerometer mounting [140]. Moreover, the metal plate containing CHEAP and LARA is bolted to the shaking

table. For validating the accelerometers' accuracy, eleven tests with various frequency ranges (from 0.1 Hz to 32 Hz) were performed. For finding the frequency report of the accelerometers, the accelerometers' time-domain raw data were converted to the frequency domain by an FFT program written in the MATLAB software. To show the methodology of the calculation of the accelerometer's frequency errors from the jack's results, four frequency domain plots of LARA for 0.1 Hz (Figure 6-6.a), 0.2 Hz (Figure 6-6.b), 0.3 Hz (Figure 6-6.c) and 0.5 Hz (Figure 6-6.d) are presented in Figure 6-6.

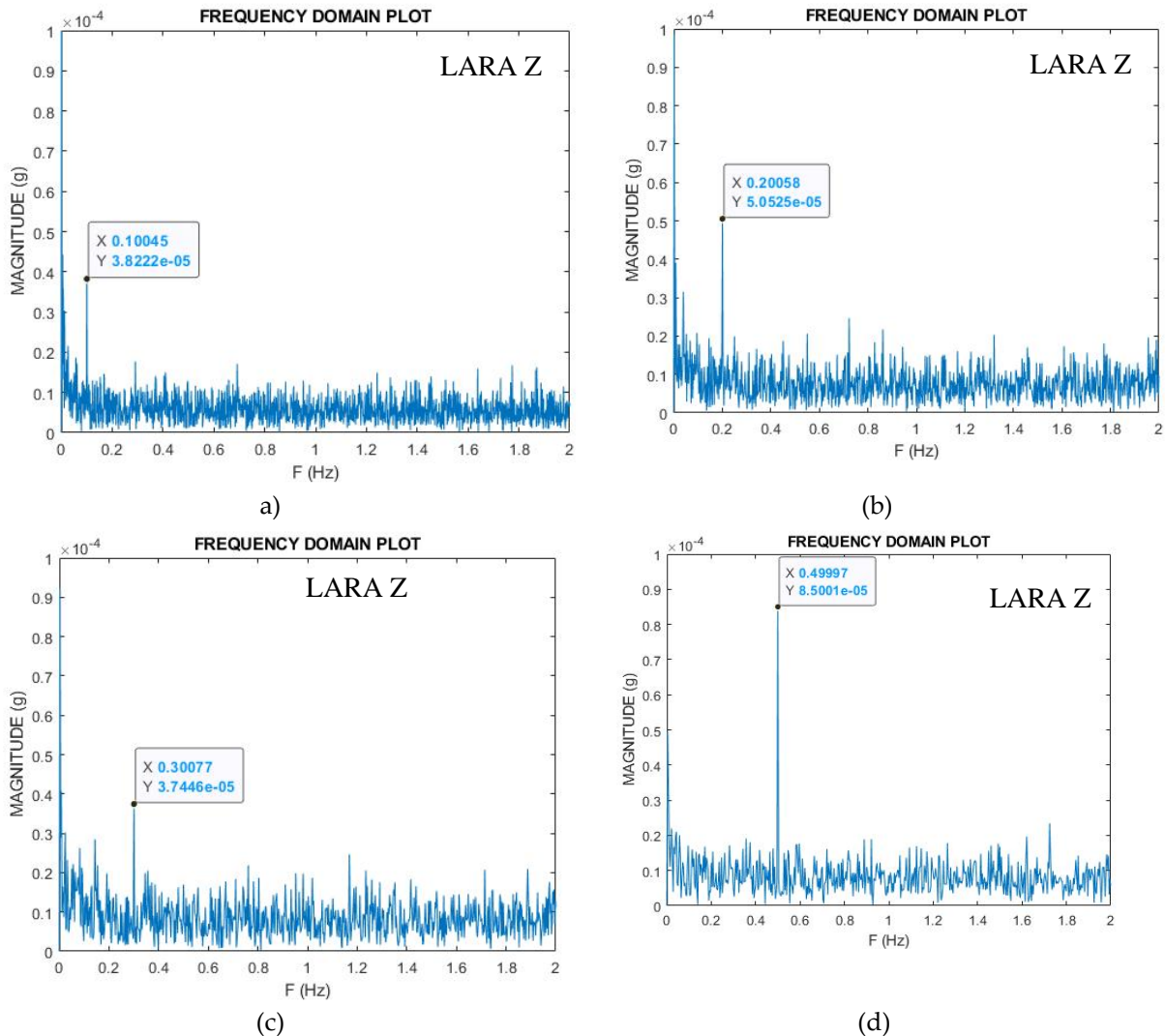


Figure 6-6. FFT representation of the low-frequency signals: a) 0.1 Hz, b) 0.2 Hz, c) 0.3 Hz, and d) 0.5 Hz.

The accelerometer's frequency error is estimated by calculating the percentage error of the plot value from the reference value of the excitation device. Table 6-2 compares the frequency errors of LARA, CHEAP and MPU9250 with the jack's reference values. Table 6-2 is organized in columns: (1) Frequency (Hz): The reference value of the excitation device, (2) LARA's error (%), (3) CHEAP's error (%), and (4) MPU9250's error (%).

Table 6-2. Frequency validation of the accelerometers

Frequency (Hz)	LARA's Error (%)	CHEAP's Error (%)	MPU9250's Error (%)
0.1	0.450		
0.2	0.295		
0.3	0.260		
0.4	0.050	0.470	
0.5	0.006	0.011	
2	0.005	0.025	0.025
4	0.000	0.000	0.000
8	0.003	0.003	0.003
10	0.004	0.004	0.004
16	0.001	0.001	0.001
32	0.003	0.003	0.003

Analysis of Table 6-2 shows that a single MPU9250 is reporting the same frequency error as the CHEAP from 2 Hz on. Since this particular MPU9250 is one of the CHEAP accelerometers, its frequency report is synchronized with CHEAP. It can also be deduced from this table that a single MPU9250 has not enough resolution for frequencies smaller than 2 Hz. Further analysis of Table 6-2 shows that CHEAP cannot visualize signals with a frequency smaller than 0.4 Hz either. In fact, LARA has a broader range of frequency than MPU9250 and CHEAP and can locate signals up to 0.1 Hz with 0.5 % of error. In fact, the frequency range of LARA, based on the presented information, is between 0.1 Hz and its bandwidth (165 Hz).

Further investigation of Table 6-2 illustrates that MPU9250, CHEAP and LARA have similar errors for signals with frequencies bigger than 2 Hz, but the error is still not 0.000%. In fact, the FFT evaluation can be influenced by irregularities such as the number of sampled data and the sampling frequency speed [177]. However, controlling all the data for such accuracy is not the aim of this work.

6.3.3 Acceleration amplitude validation

This subsection first compares the acceleration amplitude accuracy of MPU925, CHEAP and LARA using a sine wave with a known frequency and acceleration amplitude. Then, to check the ultimate acceleration range of LARA, a laboratory experiment using a sin wave with the RMS value of 1g was performed.

An experiment was carried out with the jack to compare the acceleration acquisition of MPU925, CHEAP and LARA. The jack was calibrated to move with a frequency of 4 Hz and a displacement range of 0.1 millimeters from its null axis. During each test, the jack reported its time-domain information with a sampling frequency of 500 Hz. Figure 6-7 illustrates jack's report for this experiment in the frequency-domain diagram.

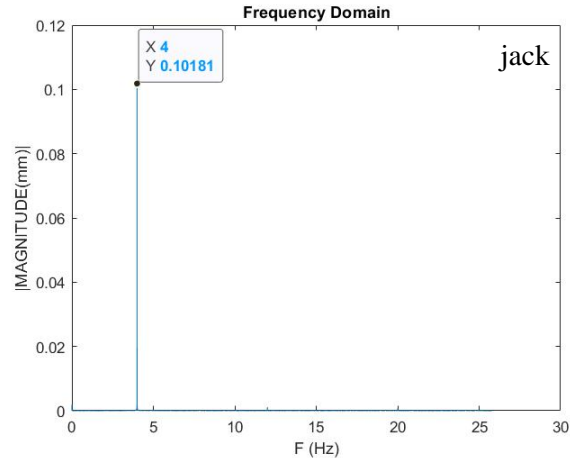


Figure 6-7. displacement report of the jack in a frequency-domain diagram.

Analyzing Figure 6-7 shows that the jack was moving with a frequency of 4Hz and an averaged displacement of 0.10181 millimeters; consequently, the jack was working with a 1.81% error rate from 0.1 millimeters that the programmed displacements.

For validating the accelerometers' accuracy, their acceleration amplitude report of the sensors was converted to displacements. Then, high-pass and low-pass filters removed signals with frequencies smaller than 0.1 Hz and bigger than 1/10 of the accelerometer's bandwidth. These filters are MATLAB functions that can filter the signals out of the interest range.

Finally, the FFT analysis was carried out, and obtained results are presented in Figure 6-8. Figure 6-8.a, Figure 6-8.b and Figure 6-8.c show the reported displacement of MPU9250, CHEAP and LARA, respectively. It should be noted that the accuracy of the accelerometers for measuring the magnitude of the induced vibration is analyzed in the frequency domain representation. It is due to the fact that making a unique noiseless signal on a shaking table or an actuator is significantly challenging [182]. In addition, for the OMA of bridges, accelerometers are mounted to measure the structural response of the bridges under ambient vibrations, such as those induced by traffic, wind and temperature variation. Therefore, this sum of ambient vibrations is usually evaluated in the frequency domain representation [35].

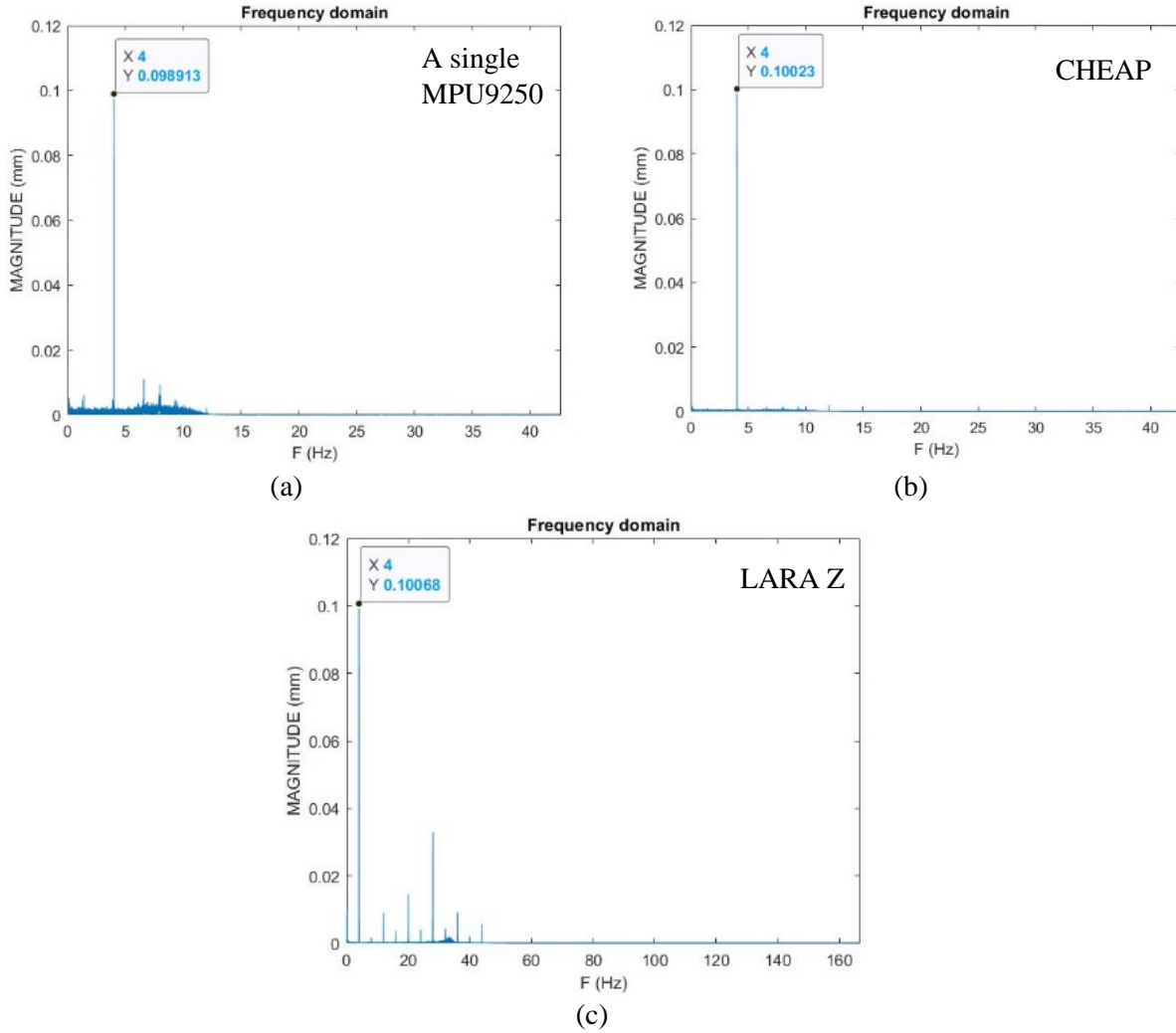


Figure 6-8. Displacement report of the accelerometers: (a) MPU9250, (b) CHEAP and (c) LARA.

Analysis of Figure 6-8 shows that even though all accelerometers are reporting the same frequency, they measure the induced signal's magnitude inconsistently. MPU9250, CHEAP and LARA have measured the jack's displacement as 0.098913, 0.10023 and 0.10068 millimeters. The MPU9250's displacement measurement is off by 1.31% from the CHEAP's report and 2.85% off from jack's report (Figure 6-7). Further analysis of Figure 6-8 shows that CHEAP and LARA's magnitude report has less than 0.5% error from each other. In fact, CHEAP and LARA have measured the jack's displacements with 1.55% and 1.2% errors from the introduced displacement measurement of the jack in Figure 6-7.

It should be pointed out that the shown displacement magnitude of Figure 6-8.c corresponds to a measured acceleration amplitude of 0.006 g. Furthermore, for measuring the top acceleration amplitude range of LARA, another test is carried out on a dynamic actuator. This time, the used dynamic actuator was programmed to induce vibrations with a Root Mean Square (RMS) value of one g. This test was performed for one minute, and after that, the RMS value of the acquired

vibrations was calculated. The time-domain representation of this test for a time duration of one second is presented in Figure 6-9. The calculated RMS value of the acquired data of LARA for one minute is 0.991 g. This value shows a 0.9% error from the reference RMS value of the test.

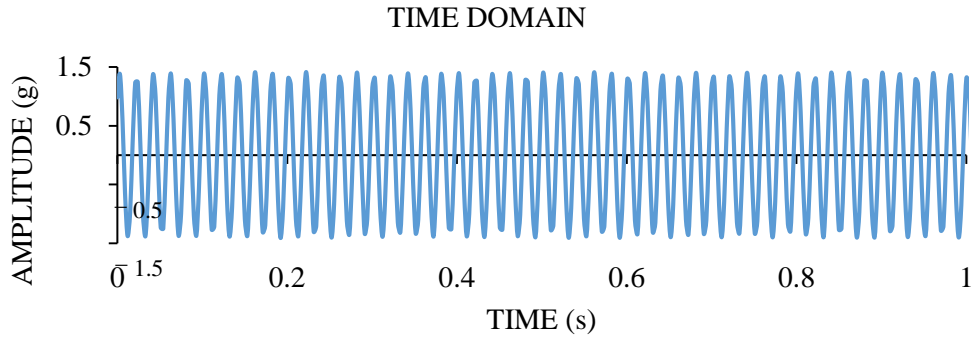


Figure 6-9. The time-domain presentation of a vibration acquisition with RMS value of one g by LARA.

It should be noted that LARA, like any other accelerometer, has an acceleration amplitude range for each of its axes. The sensor gets overloaded when a signal has an acceleration amplitude that exceed a certain range. It should be noted that when MEMS accelerometers reach their saturation level (get overloaded) [183], they are not able to measure the magnitude of the impact anymore [184]. In fact, LARA, unlike piezoelectric solutions, does not require a parametric analysis as it does not experience a drift after saturation [21]. More information about the saturation of MEMS accelerometers can be found in [183].

LARA is set to have an acceleration amplitude range of $\pm 2g$. It should be noted that the LARA was calibrated in Applus [185] under RMS acceleration amplitude of 0.5 g and frequency range of between 5 and 160 Hz. In addition, Figure 6-9 presented acceleration amplitude verification of LARA for 1g where the maximum measured impact was 1.42g. In order to investigate its theoretical saturation level ($\pm 2g$), an experiment with an acceleration amplitude higher than 2g was performed. Figure 6-10 presents the time domain representation of this experiment.

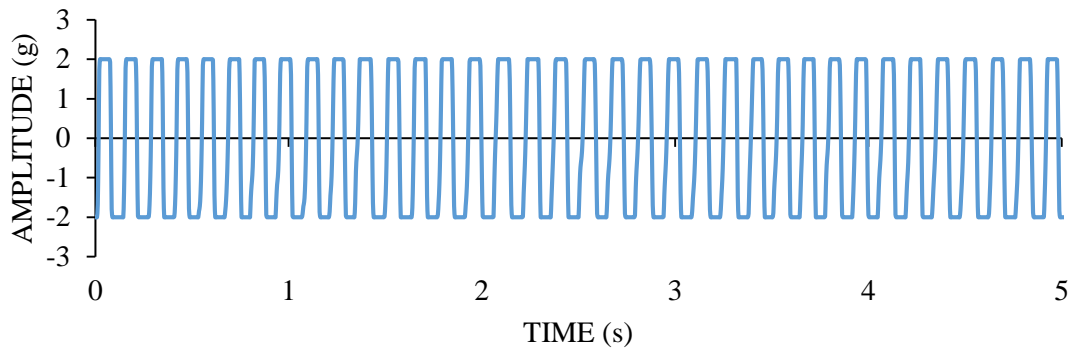


Figure 6-10. The time-domain presentation of acceleration amplitude saturation of LARA

The analysis of Figure 6-10 shows that LARA could not measure the acceleration amplitude of the produced signal beyond the $\pm 2g$ magnitude as the top and bottom of the signal are cut. This means that LARA is overloaded. It is also noted in the literature that when substantial impact happens, the output voltage of MEMS accelerometers (such as LARA) reach a fixed value that does not vary (saturation) [186]. To decrease the chance of overloading of accelerometers (saturation), low-pass filters are traditionally recommended [187].

To summarize the collected information of the laboratory tests in subsections 3.2 and 3.3, LARA accurately measured frequencies of sine waves within the range of 0.4 and 32 Hz. Furthermore, LARA accurately measured the acceleration amplitude of a sine wave with a magnitude of 0.006 g. Moreover, LARA's maximum acceleration amplitude measurement was investigated using an induced sine wave with a RMS acceleration amplitude of 1 g.

6.4 Real structure test and results

This section first presents a field test aiming to validate the eigenfrequency analysis of LARA. Then, to compare the modal analysis of LARA with those of commercial accelerometers, another field test performed on a bridge located in Donostia-San Sebastian, Spain is illustrated.

6.4.1 Eigenfrequency validation of a footbridge

This subsection presents a field test carried out on a short-span bridge (Pasarela Polvorín) in Barcelona for comparing the measured eigenfrequencies of LARA with those of a high-precision sensor. The noted coordinates of this bridge from the Google Maps are 41.363677, 2.139906. The location of this bridge is shown in Figure 6-11.

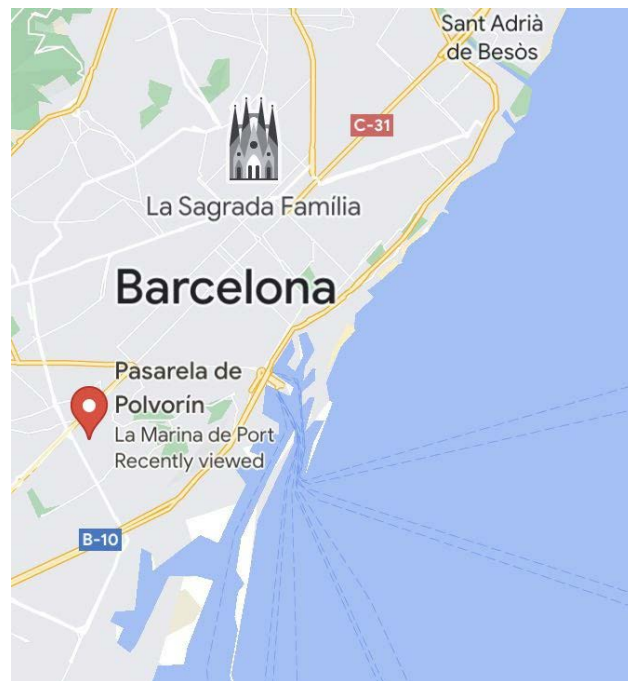


Figure 6-11. The location of the Pasarela Polvorín footbridge in Barcelona, Spain.

106

In the first place, the footbridge is shown in Figure 6-12.a. As shown, it is connected to an elevator box and from the other side, it is located on an abutment. Figure 6-12.b and Figure 6-12.c show the plan and section of the bridge, respectively.

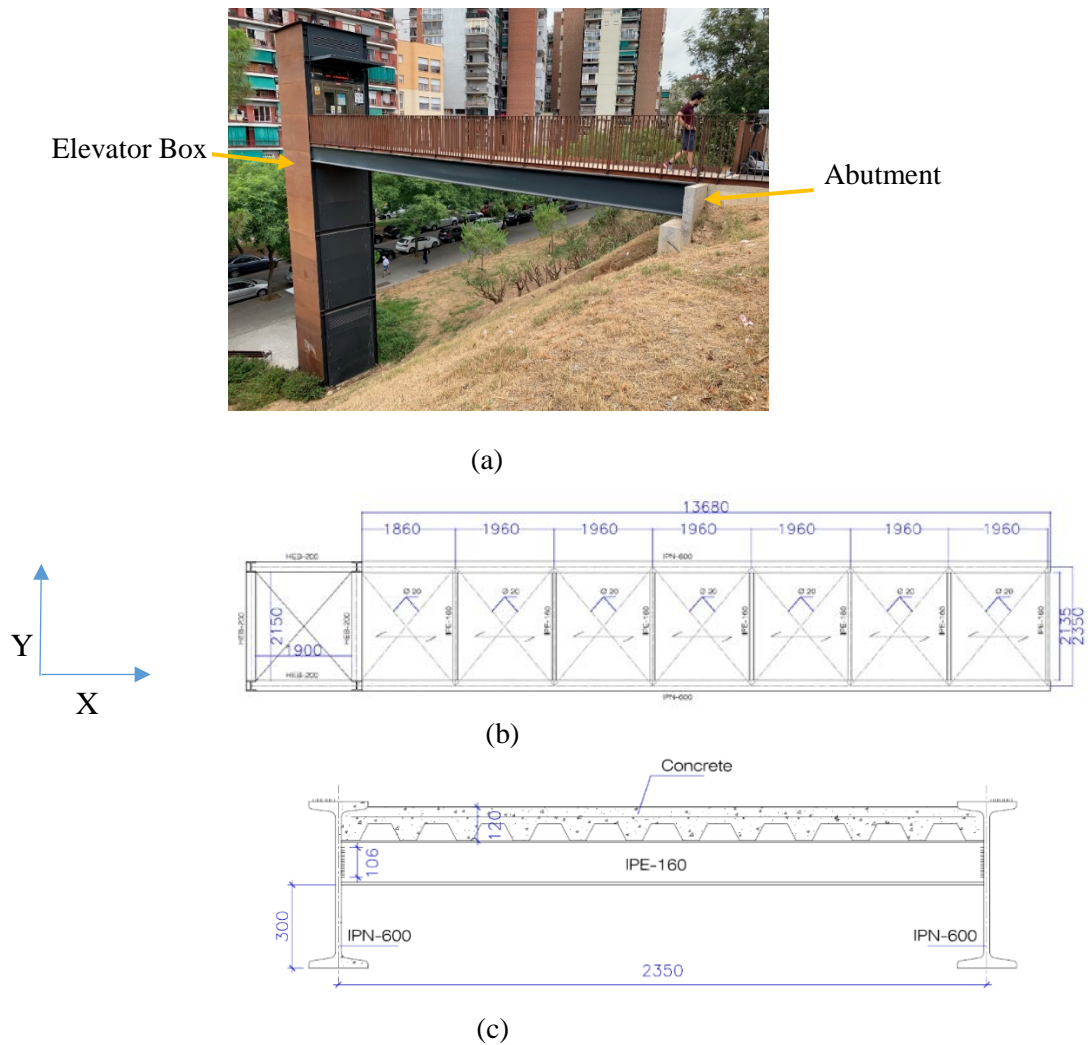
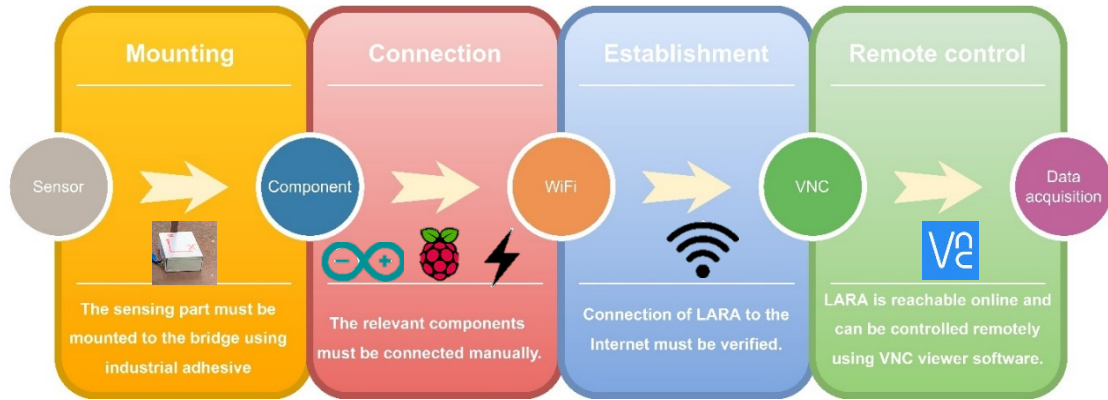
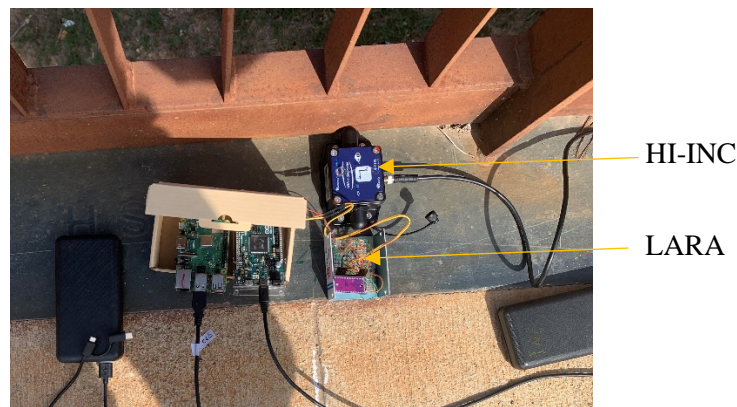


Figure 6-12. (a) A picture of the Footbridge (Pasarela Polvorín), (b) plan of the bridge and (c) section of the pass way bridge (all units are in mm).

After mounting the sensors to the bridge, they were connected to the rest of the monitoring components (power bank, USB 4G dongle, Arduino and Raspberry Pi) manually. It is important to highlight that to enable its communication throughout the internet, the Raspberry Pi was previously configured with a WiFi hotspot. In fact, after its assemblage on site the Raspberry Pi was used to initiate the data acquisition process remotely, using the Virtual Network Computing (VNC) software [188]. The acquired data was first collected on the memory card of the Raspberry Pi. Then, when the data acquisition process finished, the obtained data were moved to a computer using the VNC software. Figure 6-13.a presents the diagram of LARA setup on the bridge. The location of the commercial dynamic sensor (HI-INC) and LARA on the mid-span of the bridge is shown in Figure 6-13.b.



(a)



(b)

Figure 6-13. Mounting the sensors to the mid span of the bridge under study: a) Mounting diagram of LARA to the bridge and b) Photo of the mounted LARA and HI-INC sensors.

It is also important to mention that the cables shown in Figure 6-13.b are not for connecting LARA or HI-INC to a laptop. Both systems were controlled remotely. These cables are either for power source connection or for connecting the Arduino and the Raspberry Pi.

The outputs of the eigenfrequency analysis of LARA is shown in Figure 6-14.a, Figure 6-14.b and Figure 6-14.c. for X, Y and Z axis, respectively.

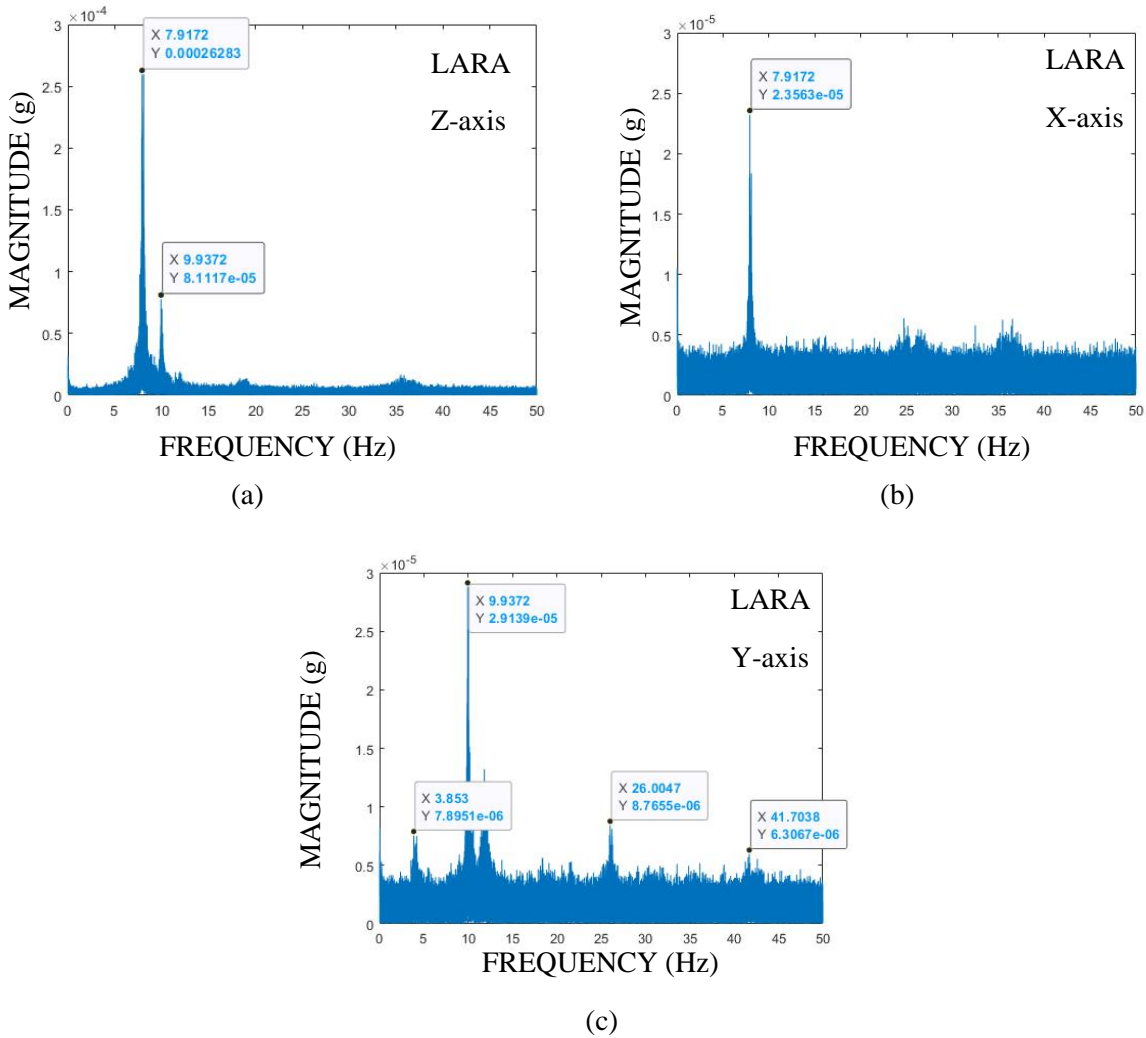


Figure 6-14. Eigenfrequency analysis of a footbridge using LARA for (a) Vertical, (b) Longitudinal, and (c) Transversal directions of the footbridge.

Analysis of Figure 6-14 shows that the bridge is not significantly excited about its X-axis (longitudinal direction). It is appeared that the bridge is excited very well about Y and Z axes.

Table 6-3 presents results of the eigenfrequency analysis of LARA and the used high precision inclinometer dynamic (HI-INC). This table also presented the difference percentage of the measured frequencies with LARA from those of the HI-INC sensor.

Table 6-3. Comparison of the first three mode steps frequencies of LARA with HI-INC.

Mode number	HI-INC	LARA	Difference
1	3.90 Hz	3.85 Hz	1.28 %
2	7.91 Hz	7.91 Hz	0.20 %
3	9.94 Hz	9.93 Hz	0.88 %
4	26.25 Hz	26.01 Hz	0.91 %
5	42.81 Hz	41.70 Hz	0.27 %

Comparing the measured eigenfrequencies of LARA with those of HI-INC, shows a maximum error of 1.28%.

6.4.2 Modal analysis validation of a Bridge

To validate the modal analysis of LARA, two LARA accelerometers and three uniaxial commercial accelerometers (PCB 607A61) were attached on a Bridge (Puente de Andoian) located in Donostia-San Sebastian, Spain. The noted coordinates of this bridge from the Google Maps are 43.219019, -2.024778. The location of this bridge is shown in Figure 6-15.



Figure 6-15. The location of the Andoain bridge in Donostia-San Sebastian, Spain.

In the first place, the bridge before instrumentation is shown in Figure 6-16.a. The blue circles show the approximate location of the accelerometers. For operational modal analysis of this bridge, the center point and one forth-span of its middle girder were instrumented. The plan of this bridge is illustrated in Figure 6-16.b. It should be noted that all dimensions are in meters. The original blueprint of this bridge is shown in Figure 6-16.c. The location of the installation of the sensors are shown on this Figure. Sensor number 1 corresponds to the accelerometer located on the mid-

span and 2 indicates the mounting location of the accelerometer situated on one-fourth span of the girder length.

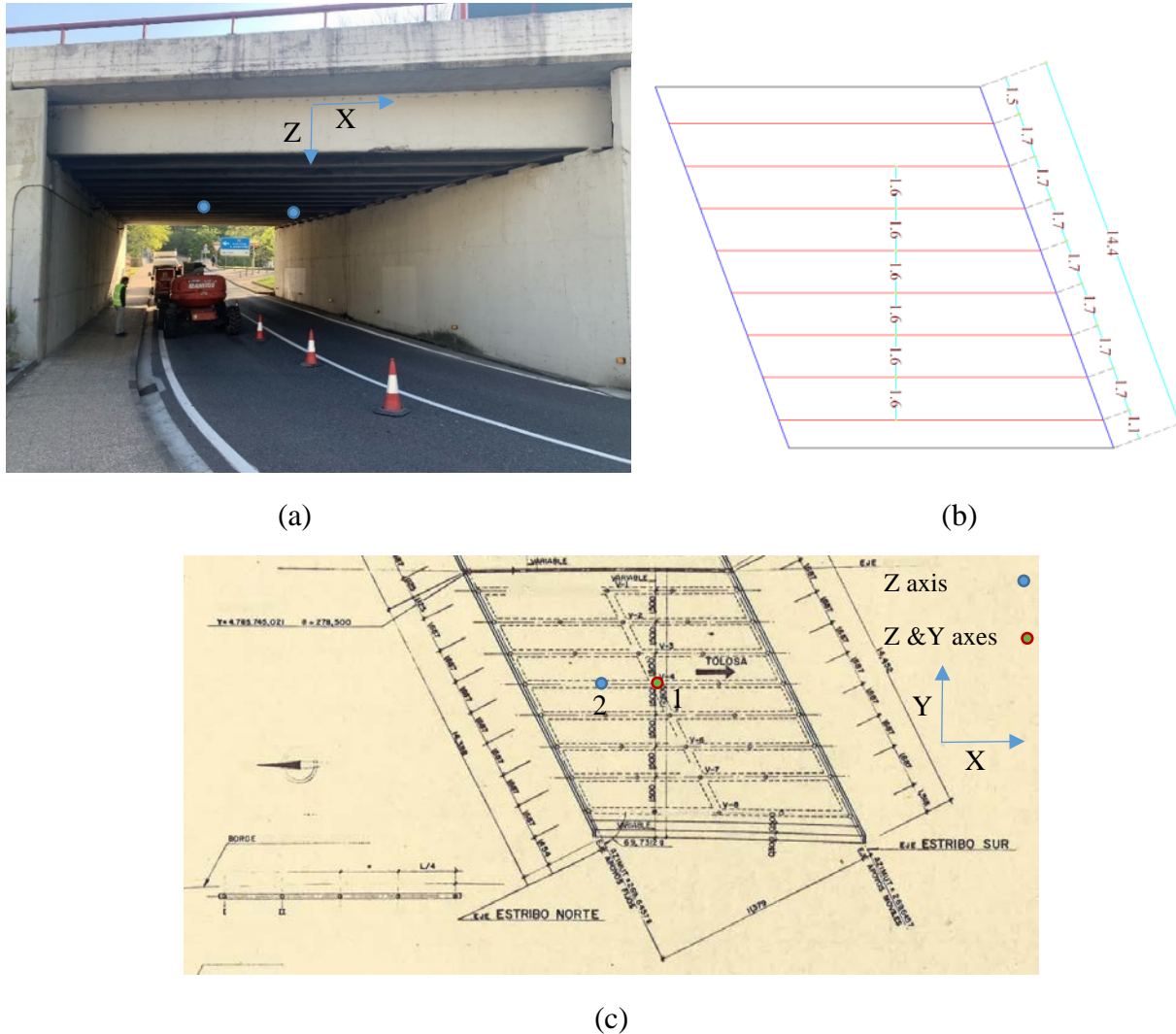


Figure 6-16. Andoin Bridge: a) A photo of the bridge before instrumentation, b) The dimensions of the bridge under study.

It should be noted that the middle point of the under study girder was instrumented using two perpendicular uniaxial (PCB 607A61) accelerometers. This was done to monitor this bridge's vertical (Z direction) and transversal (Y direction) movements. One-fourth of span length of this girder was instrumented using only a PCB 607A61 accelerometer to monitor this point's vertical movement. This way, three channels were available: Z and Y direction of the mid-span and Z direction of the one-fourth of span length (Figure 6-16.c). These accelerometers were mounted for monitoring of the dynamic performance of this bridge. Subsequently, two triaxial LARA accelerometers were mounted next to the points where the commercial accelerometers were situated.

111

To perform this monitoring, LARA had to be specially boxed. This bridge does not have constant access to electricity. In fact, only during the night, the light bulbs of the bridge are connected to the city's main electricity source. For that, the implemented sensors needed enough battery to acquire data during the day and have fast chargers to charge their batteries during the night. It should also be noted that this instrumentation was done during the summer, so it was assumed that nights would be shorter than normally. Figure 6-17.a illustrates the designed box. This box includes three fast charging power banks with 2000 mA capacity. This box also includes fast chargers dedicated to charging the power banks. This way, these power banks can be fully charged in less than two hours. The USB 4G dongle wireless modem provides Internet for remotely controlling the sensors. Figure 6-17.b shows the location of the installation of the data acquisition box on the Andoain bridge.

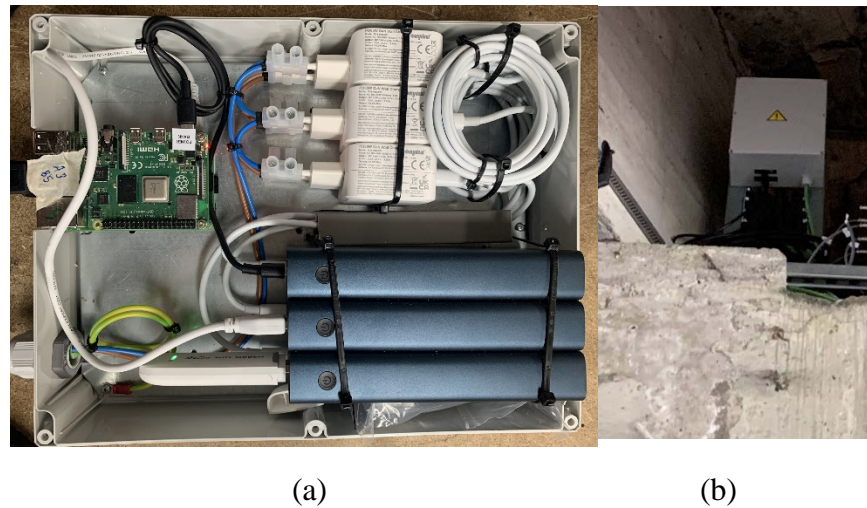


Figure 6-17. Data acquisition part of LARA: a) Box of the data acquisition equipment of LARA, b) The installation of the box on the bridge

Finally, the sensing part of LARA was mounted on the bridge. The sensing part was connected to the acquisition box using special USB cables with signal amplifiers. It was observed in the laboratory tests that standard USB cables can be used up to 3 meters for attaching the sensing part to the acquisition part. However, this range can be extended to 18 meters using USB cables with amplifiers. Figure 6-18 presents the Andoain bridge instrumentation.



Figure 6-18. Instrumentation of Andoain bridge using two LARA (sensing part only) mounted next to the PCB 607A61 accelerometers.

In order to compare the results of the commercial and LARA sensors, the vibration acquisition data of the day 22nd of May 2022 between 11:00 and 11:30 am (CEST) are compared with those of LARA accelerometers. The modal analysis of the acquired data of both solutions is done using the Frequency Domain Decomposition (FDD) method. This analysis was done using an open-access MATLAB code [189]. It should be noted that the comparison of the results of the other days of structural monitoring is not included in this current work. It is because the commercial sensors were not acquiring data due to some technical issues on some days. After three months of system troubleshooting, the company in charge of installing and maintaining the commercial sensors decided to terminate the monitoring.

The Modal Assurance Criterion (MAC) value was used to compare the mode shapes of the commercial sensors and LARA accelerometers for three channels. The vertical and transversal direction of the girder midspan and vertical direction of the girder on-fourth span. The MAC value is calculated using the formula presented in Eq. 6-3:

$$MAC(r, q) = \frac{|\{\varphi_C\}^T \{\varphi_L\}|^2}{(\{\varphi_C\}^T \{\varphi_C\})(\{\varphi_L\}^T \{\varphi_L\})} \quad (6-3)$$

Where $\{\varphi_C\}$ and $\{\varphi_L\}$ are the extracted mode shape matrices from FDD analysis of the commercial and LARA accelerometers, respectively. The MAC number for each mode shape must be between 0.8 and 1 to show a remarkable resemblance of the mode shapes [78]. Table 6-4 shows the modal and eigenfrequency analyses of PCB 607A61 and LARA accelerometers for the first three mode shapes of the bridge under study. This table includes the following information: (1) Mode number, (2) LARA: These number corresponds to the location of the accelerometers, (3) Mode shape Y: the normalized value of the mode shape value of the transversal axis of the bridge, (4) Mode shape Z: the normalized value of the mode shape value of the vertical axis of the bridge, and (5) Frequency: The results of the eigenfrequency analysis of the acquired data of LARA. It should be noted that the descriptions of columns 6, 7, 8 and 9 are as precisely as those for columns 2, 3, 4 and 5, respectively. The only difference is that they correspond to the PCB 907A61 accelerometers.

Table 6-4. Modal analysis outputs of LARA and the PCB 907A61 accelerometers.

Mode number	LARA	Mode shape		Frequency	PCB 607A61	Mode shape		Frequency
		Y	Z			Y	Z	
1	1	0.11	-1.00	12.27	1	0.06	-1.00	12.14
	2		-0.62		2		-0.56	
2	1	-0.19	-1.00	13.73	1	-0.19	-1.00	13.66
	2		-0.60		2		-0.53	
3	1	0.27	-1.00	14.99	1	0.27	-1.00	14.89
	2		-0.63		2		-0.57	

Analysis of Table 6-4 shows that the values generated from both data acquisition systems are very close. It can be seen that the highest difference between the estimated eigenfrequencies of LARA accelerometers from those of the commercial accelerometers is 0.13 Hz for the first eigenfrequency which corresponds to 1.13% of difference.

To better compare the eigenfrequency and modal analyses of these systems, Table 6-5 is presented.

Table 6-5 compares the modal and frequency analyses of these two solutions using MAC value and the percentage of eigenfrequency difference. This table is organized in the following columns: (1) Mode number, (2) MAC 2D: This value compares the mode shapes of three channels. It is 2D because two of the channels correspond to the bridge's vertical (Z direction) vibrations and one channel corresponds to those of the transversal (Y direction) axis, and (3) Frequency difference: The percentage difference of the eigenfrequencies calculated from the data acquisition information of LARA from those of the PCB 907A61 accelerometers.

Table 6-5. Comparing the modal and eigenfrequency analysis of LARA and PCB 907A61 accelerometers

Mode number	MAC 2D	Frequency difference (%)
1	0.996505	1.13
2	0.997242	0.56
3	0.998601	0.62

Analysis of Table 6-5 shows that the difference of the eigenfrequency analysis of LARA and PCB 607A61 accelerometers is less than 1.2 %. In addition, it can be seen that the MAC value comparing three channels of the commercial solution and the LARA accelerometer is more than 0.99. This value can very well demonstrate the high accuracy of the presented solution.

Chapter 7 : Conclusions and future research

7.1 Conclusions

Structural Health Monitoring (SHM) applications are typically required to identify maintenance applications, reduce repair costs, and ensure the safety of the structures. SHM systems are generally based on traditional commercial sensors and additional data acquisition equipment. The high price tag of these instruments is considered a significant drawback because currently, many structures do not have a sufficient monitoring budget, or the available budget is insufficient to comply with all the deficient and old ones. Consequently, the development and validation of low-cost sensors and equipment for decreasing the instrumentation cost of structures with a low available SHM budget is essential. Moreover, low-cost sensors can enable engineers to afford long-term SHM applications without considering leaving expensive equipment on the site.

- I. Firstly, to tackle the high price of the available commercial accelerometers for SHM applications, this thesis developed and validated a Cheap Hyper-Efficient Arduino Product (CHEAP). CHEAP is constructed from five synchronized MEMS chipsets (MPU9250). Through laboratory experiments, it was detected for the first time in the literature that averaging the outputs of synchronized low-cost accelerometers improves the system's resolution and accuracy. This achievement is the most significant contribution of this thesis.

CHEAP is designed to be a uniaxial accelerometer based on Arduino technology with a sampling frequency of 85 Hz. The eigenfrequency analysis and acceleration amplitude measurement of CHEAP were compared with those of two commercial seismic accelerometers (393A03, and 356B18). It was concluded that only CHEAP could accurately measure induced vibrations with acceleration amplitude of lower than 14.5 milli-g. This was conducted through laboratory experiments on an actuator located at the Laboratory of Technology of Structures & Materials "Lluís Agulló" (LATEM) The laboratory experiments with low magnitude vibrations revealed that CHEAP, 393A03 and 356B18 accelerometers were able to detect signals with acceleration amplitudes of 0.06, 0.5 and 1.6 milli-g, respectively. The eigenfrequency analysis of all accelerometers in the frequency range of 2 Hz until 10 Hz was acceptable. It is essential to mention that CHEAP was the only accelerometer that could detect frequencies below 2 Hz.

Conclusively, CHEAP can be used for SHM of conventional structures with low eigenfrequencies with low monitoring budgets.

- II. Secondly, to improve the sampling frequency of the currently available inclinometers used for SHM applications and decrease their price tag, a Low-cost Adaptable Reliable Angle-meter (LARA) with a sampling frequency of 250 Hz was developed and validated. LARA comprises five synchronized accelerometers, five synchronized gyroscopes, a multiplexor and an Internet of the Thing (IoT) based microcontroller (NODEMCU). The main novelty of LARA is combining the measurements of 5 low-cost accelerometers and 5 gyroscopes using a complementary filter to decrease the inherent noise density of the used chipsets. The Printed Circuit Board of LARA was designed and constructed using machinery assembly to align the synchronized chipsets. It should

be noted that this thesis also presents an easy way of building LARA out of five MPU9250 chipsets in a laboratory which can help SHM researchers to construct their low-cost inclinometer.

Four laboratory tests were conducted to verify the hypothesis of noise reduction and signal improvement of inclination measurements using the averaged results of multiple aligned inclinometers. In fact, it is established that a system made up of five aligned inclinometers has substantially better Allan variance and deviation than a single inclinometer.

Furthermore, an experimental test was conducted to assess the measurement of LARA in a rotation range of 0.0 to 4.0 degrees (it should be noted that most bridges rarely experiment with a slope of more than 0.5 degrees). In this experiment, the values of a commercial inclinometer (HI-INC) were compared to the data collected by LARA. LARA was observed to present up to 0.04 and 0.07 degrees of error in tests with one and four degrees of inclination.

A load test on a beam was also conducted to compare the accuracy of LARA and the commercial inclinometer (HI-INC). In this test, LARA's results were contrasted with those of the commercial inclinometer and hand calculations. As a result, it was demonstrated that the theoretical slope computed by LARA differed from the hand-determined values by less than 0.003 degrees. In addition, HI-INC illustrated precision with a magnitude of 0.005° that complied with the accuracy reported in its datasheet.

In conclusion, LARA has sufficient accuracy and resolution for being implemented in SHM applications aiming for bridge damage detection methods.

- III. Thirdly, it was suggested in this thesis that combining the measurements of several aligned sensors can also improve the distance estimations of low-cost sensors. Moreover, this thesis presented the distribution functions and standard deviation of HC-SR04, VL53L0X and VL53L1X sensors under various environmental conditions. To investigate the impact of combining the measurements of low-cost distance sensors, a measuring device consisting of 75 analog and digital sensors (25 HC-SR04, 25 VL53L0X and 25 VL53L1X) was designed and examined in the LATEM laboratory.

The data assessment demonstrated that, regardless of the ambient lighting conditions, the sensor combination was advantageous for both analog and digital sensors. The combination of 25 identical sensors revealed a substantial improvement in estimated accuracy and data fluctuation for all sensor types. Additionally, it was demonstrated that the worst sensor combination still had a lower estimation error than a single sensor. Further examination of the obtained data revealed that, in laboratory tests conducted in LATEM laboratory with and without excessive ambient light, the inexpensive analog distance sensor HC-SR04 had higher estimation accuracy than the pricey Time of Flight (ToF) sensors (VL53L0X and VL53L1X). Additionally, the sensor combination approach for this type of sensor can be justified by the HC-SR04's reduced cost compared to the other employed ToF sensors.

It is concluded that by averaging the outputs of a few combined uncalibrated sensors, the accuracy of the distance estimation improves. Additionally, throughout the data acquisition process, the sensitivity and accuracy of individual sensors may be evaluated by comparing the measurement of each sensor with the sum of the findings of a few sensors. Moreover, rather than only relying on a

116

single measuring tool's outputs in the event of a sensor failing or malfunctioning, the acquisition process may still proceed due to the availability of several coupled sensors.

- IV. Finally, this thesis presented a data acquisition equipment based on the Raspberry Pi technology with remote control. This system has an activated Network Time Protocol (NTP) that can access the Internet's accurate time. In addition, the developed data acquisition system can attach a timestamp with microsecond resolution to the streamed data of the sensors attached to its channels. The time stamp and the accurate time of the internet can enable post-synchronizing the vibration acquisition of several sensors located in various locations of a structure connected to different data acquisition systems.

Additionally, CHEAP accelerometer was upgraded to be triaxial and had a sampling frequency of 333 Hz. Several lab studies were conducted to assess the upgraded accelerometer's performance, resolution, and ND.

The upgraded accelerometer and the developed data acquisition equipment were used in a field test on a footbridge in Barcelona with a span of 14 meters. The eigenfrequency analysis of the developed solution was then compared with those of a commercially available high-precision sensor (HI-INC). This comparison shows a maximum difference of 1.3 % in eigenfrequency analysis between the developed prototype and the commercial solution.

Moreover, the upgraded accelerometer was used for monitoring of a bridge in Donostia-San Sebastian, Spain. To do that, the mid-span and one-fourth span of the middle girder of the Andoian bridge was instrumented using LARA and commercial accelerometers (PCB 607A61). The comparison of the modal and eigenfrequency analyses of LARA accelerometers with those of the PCB 607A61 shows a Modal Assurance Criterion (MAC) value of almost 1 for the first three mode shapes of the bridge and an eigenfrequency difference of less than 1.2 %.

In closing, the upgraded version of CHEAP with the newly developed data acquisition equipment can revolutionize the structural health monitoring of bridges through low-cost accurate and remote monitoring. It should be noted that this developed system's remote access, data management, data control and post synchronization capability are only available as long as the Internet connection is provided.

7.2 Future steps

The proposed future lines drawn from this thesis can be organized as the following:

- 1- One of the essential future plans is to use the developed accelerometer (Chapter 3) and the data acquisition system (Chapter 6) for operational modal analysis of a bridge and compare the results with those of an analytical model and commercial accelerometers. The novelty of this new system is the auto synchronization program written in Matlab for synchronizing the data acquisition of a number of accelerometers located at different locations of the understudy bridge.
- 2- It is also interesting to validate the accuracy of the developed accelerometer (Chapter 3) on structures with low eigenfrequency range (such as long-span bridges). In this case, instead

of having onsite data acquisition equipment, an offsite computer is planned to be combined with several sensors located on a long-span bridge. The acquired vibration of the sensors will be uploaded to a server that is linked to the offsite computer. The computer automatically saves the data, synchronizes them and performs a modal analysis. The modal analysis results will then be published on an IoT-based platform. It should be noted that in case of a steady abnormality, an error can be sent to the person in charge of monitoring the bridge understudy. This solution is made to deal with Big Data concept and is capable of finding the abnormal structural responses together with overall structural behavior trend of the structure.

- 3- Use the developed sensor combination system (Chapter 3) for developing different accelerometers, such as seismic accelerometers and accelerometers with higher acceleration amplitude ranges.
- 4- Using this thesis's designed inclinometer (Chapter 4), a low-cost portable deformation measurement device will be built for a damage detection application. To build this system, the acquired data of the developed inclinometer must be synchronized with those of a range sensor. First, the influence line of the understudy structure is needed to locate the damage. It should be noted that this influence line must be estimated for the undamaged structure. Then, the influence line of the damaged structure can be drawn using the range detector, the developed inclinometer, and a passing vehicle with a steady speed. By comparing the influence lines of the damaged and the undamaged structure, the location and severity of the damage can be estimated.
- 5- It should be noted that, as reviewed in the state of the art of this thesis, the ultimate aim of SHM applications is to evaluate the health state of a structure and detect damages if possible. To do that, it is planned to use a structural system identification method such as dynamic observability application and the developed system of Chapter 6 to create an efficient structural system identification and damage detection solution.
- 6- It should be noted that the performance of sensors, like any system or structure, needs to be monitored and, in case of a hitch, must be diagnosed or reported. To automatically monitor the health state of the developed system in Chapter 6, A Robotic Process Automation (RPA) application is developed through collaboration with another researcher. Furthermore, this developed system must be deployed on a structure for a long-term SHM application. During this monitoring, the RPA will check the developed sensors' performance during a long-term field test.
- 7- It is planned to develop a Modular system integrated that can acquired parameters such as acceleration, inclination, corrosion and temperature. This IoT-based Automated device is built for long-term offsite structural health monitoring bridges.

7.3 Related works and publications

This thesis resulted in several publications. The following four journal publications directly resulted from Chapters 3, 4, 5 and 6, respectively:

1. **Seyedmilad Komarizadehasl**, Behnam Mobaraki, Ma Haiying, Jose Antonio Lozano-Galant and Jose Turmo. Development of a low-cost system for the accurate measurement

of structural vibrations, Published at Sensors journal (Q2), September 2021. <https://doi.org/10.3390/s21186191>

2. **Seyedmilad Komarizadehasl**, Fidel Lozano, Jose Antonio Lozano-Galant, Gonzalo Ramos and Jose Turmo. Low-Cost Wireless Structural Health Monitoring of Bridges, Published at Sensors journal (Q2), July 2022. <https://doi.org/10.3390/s22155725>
3. **Seyedmilad Komarizadehasl**, Mahyad Komary, Ahmad Alahmad, Jose Antonio Lozano-Galant, Gonzalo Ramos and Jose Turmo. A Novel Wireless Low-Cost Inclinometer Made from Combining the Measurements of Multiple MEMS Gyroscopes and Accelerometers, Published at Sensors journal (Q2), July 2022. <https://doi.org/10.3390/s22155605>
4. **Seyedmilad Komarizadehasl**, Behnam Mobaraki, Ma Haiying, Jose Antonio Lozano-Galant and Jose Turmo. Accuracy Enhancement of Various Low-Cost Distance Sensors, Published at Applied sciences (Q2), March 2022. <https://doi.org/10.3390/app12063186>

Using the developed and presented data acquisition system and the accelerometer of this thesis (Chapter 6), a collaboration has been done with a researcher from Pontificia Universidad Católica de Valparaíso in Chile. Through this collaboration, a Robotic Process Automation (RPA) system is developed and validated for monitoring the performance of sensors and automatic self-diagnosis of the data acquisition equipment in case of an error.

Robotic Process Automation (RPA) is gaining traction in a variety of industries, both as a standalone technology and as a supplement to other technologies. RPA enables the automation of human operations on a computer, particularly those that are repetitive and large in volume. RPA reduces labor hours while increasing process productivity. The use of RPA in civil engineering is still in its early stages, and there has been little published work on the issue.

This paper is an application of research that manages and controls the functional capability of a low-cost prototype accelerometer (Chapter 6). This case study is being produced in civil engineering for the first time. Furthermore, this article suggests an RPA installation workflow. This workflow is extended to make it repeatable for other projects and encourage scholars, civil engineering experts, and the maker community to explore this technological area. The sensors' control, administration, and system troubleshooting require a large number of man-hours. RPA reduces this workflow by increasing the capability of continuous system monitoring and automatic self-troubleshooting. One of the primary benefits of RPA is its ease of programming.

The following paper illustrates this collaboration:

5. Edison Atencio, **Seyedmilad Komarizadehasl**, José Antonio Lozano-Galant and Matías Aguilera, Using RPA for Performance Monitoring of Dynamic SHM Applications, Published at Buildings (Q2), August 2022. <https://doi.org/10.3390/buildings12081140>

Another successful collaboration has been done with a researcher from Universidad de Castilla La Mancha (UCLM). Through sharing the knowledge of connecting several similar sensors (Chapter 5 of this thesis) to Arduino-based microcontrollers, thermometers consisting of several synchronized sensors have been developed and validated. Furthermore, the development and validation of the constructed devices resulted in two journal articles. These papers are as followings:

6. Behnam Mobaraki, **Seyedmilad Komarizadehasl**, Francisco Javier Castilla Pascual, Jose Antonio Lozano-Galant and Rocio Porras Soriano, A Novel Data Acquisition System for Obtaining Thermal Parameters of Building Envelopes, Published at Buildings (Q2), May 2022. <https://doi.org/10.3390/buildings12050670>
7. Behnam Mobaraki, **Seyedmilad Komarizadehasl**, Francisco Javier Castilla Pascual and Jose Antonio Lozano-Galant, Application of Low-cost Sensors for Accurate Ambient Temperature Monitoring in Buildings, Published at Buildings (Q2), September 2022, <https://doi.org/10.3390/s22186762>

The following papers are published in the international conference as a consequence of this thesis:

1. **Seyedmilad Komarizadehasl**, Behnam Mobaraki, Jose Antonio Lozano-Galant and Jose Turmo. A comprehensive description of a low-cost wireless dynamic real-time data acquisition and monitoring system, XV International Conference on Durability of Building Materials and Components DBMC, Barcelona, Spain, 2020.
2. **Seyedmilad Komarizadehasl**, Behnam Mobaraki, Jose Antonio Lozano-Galant and Jose Turmo. Practical application of low-cost sensors for static tests , XV International Conference on Durability of Building Materials and Components DBMC, Barcelona, Spain, 2020.
3. **Seyedmilad Komarizadehasl**, Behnam Mobaraki, Jose Antonio Lozano-Galant and Jose Turmo. Comparison of different low-cost sensors for Structural Health Monitoring, 10th international conference on Bridge management, safety and management IABMAS, Sapporo, Japan, 2020.
4. **Seyedmilad Komarizadehasl**, Behnam Mobaraki, Jose Antonio Lozano-Galant and Jose Turmo. A comprehensive description of a low-cost angular data monitoring system, 7th international symposium on life-cycle Civil Engineering IALCCE , Shanghai, China, 2020.
5. **Seyedmilad Komarizadehasl**, Behnam Mobaraki, Jose Antonio Lozano-Galant and Jose Turmo. Detailed Evaluation of Low-Cost Ranging Sensors for Structural Health Monitoring Applications, recent trends in constructions engineering and education RTCEE, Brisbane, Australia, 2020.
6. **Seyedmilad Komarizadehasl**, Behnam Mobaraki, Jose Antonio Lozano-Galant and Jose Turmo. Evaluation of Low-cost Angular Measuring Sensors, recent trends in geotechnical and geo-environmental engineering and education, Brisbane, Australia, 2020.
7. **Seyedmilad Komarizadehasl**, Fidel Lozano, Mahyad Komary, Jose Antonio Lozano-Galant and Jose Turmo, Development of an accurate low-cost device for structural vibration acquisition, IABSE Symposium on Challenges for Existing and Oncoming Structure, Prague, Czech Repub, 2022.
8. **Seyedmilad Komarizadehasl**, Fidel Lozano, Mahyad Komary, Jose Antonio Lozano-Galant and Jose Turmo, Resolution improvement of Low-Cost MEMS accelerometer by aligning simulations sensors, IABSE Symposium on Challenges for Existing and Oncoming Structure, Prague, Czech Repub, 2022.
9. **Seyedmilad Komarizadehasl**, Mahyad Komary, Fidel Lozano, Victor Torralba, Jose Antonio Lozano-galant and Jose Turmo, Using Few Accelerometer for Improving the Resolution and Accuracy of Low- Cost Accelerometers, Proceedings of the Eleventh

International Conference on Bridge Maintenance, Safety and Management (IABMAS 2022), Barcelona, Spain, 2022.

10. **Seyedmilad Komarizadehasl**, Mahyad Komary, Fidel Lozano, Victor Torralba, Jose Antonio Lozano-galant and Jose Turmo, Low-Cost Accurate Acceleration Acquisition Sensor, Proceedings of the Eleventh International Conference on Bridge Maintenance, Safety and Management (IABMAS 2022), Barcelona, Spain, 2022.
11. **Seyedmilad Komarizadehasl**, Ahmad Alahmad, Jose Antonio Lozano-Galant, Victor Torralba, Gonzalo Ramos and Jose Turmo, Beneficial Effect of Combining Similar Low-Cost Accelerometer to improve the overall Accuracy and Noise Density, IABSE Symposium on Bridges and structures: Connection, Integration and Harmonization, Nanjing, China, 2022.
12. **Seyedmilad Komarizadehasl**, Ahmad Alahmad, Jose Antonio Lozano-Galant, Victor Torralba, Gonzalo Ramos and Jose Turmo, Experimental Verification of A Novel Accelerometer Intended For Structural Health Monitoring of Bridges, IABSE Symposium on Bridges and structures: Connection, Integration and Harmonization, Nanjing, China, 2022.

Bibliography

- [1] T. Peng, “Structural system identification by dynamic observability technique,” UPC, Barcelona, 2021.
- [2] M. R. Kaloop, M. Eldiasty, and J. W. Hu, “Safety and reliability evaluations of bridge behaviors under ambient truck loads through structural health monitoring and identification model approaches,” *Measurement*, vol. 187, p. 110234, Jan. 2022, doi: 10.1016/J.MEASUREMENT.2021.110234.
- [3] ASCE infrastructures, “Structurally Deficient Bridges Infrastructure Report Card,” 2021. <https://infrastructurereportcard.org/wp-content/uploads/2020/12/Bridges-2021.pdf> (accessed Jun. 02, 2022).
- [4] Pablo González, “El ADIF detecta 448 puentes con deficiencias en la red ferroviaria gallega,” *La voz de Galicia*, 2019. Accessed: Nov. 25, 2021. [Online]. Available: https://www.lavozdegalicia.es/noticia/galicia/2019/02/05/adif-detecta-448-puentes-deficiencias-red-ferroviaria-gallega/0003_201902G5P6991.htm
- [5] Jesús Escudero, “Adif localiza 270 puentes, túneles y vías con daños de alto riesgo por nula conservación,” *El Confidencial*, 2020. Accessed: Nov. 25, 2021. [Online]. Available: https://www.elconfidencial.com/espana/2020-03-05/estado-puentes-tuneles-red-ferroviaria-espana_2480212/
- [6] T. Peng, M. Nogal, J. R. Casas, and J. Turmo, “Role of sensors in error propagation with the dynamic constrained observability method,” *Sensors*, vol. 21, no. 9, p. 2918, May 2021, doi: 10.3390/s21092918.
- [7] S. Emadi, J. A. Lozano-Galant, Y. Xia, G. Ramos, and J. Turmo, “Structural system identification including shear deformation of composite bridges from vertical deflections,” *Steel and Composite Structures*, vol. 32, no. 6, pp. 731–741, Sep. 2019, doi: 10.12989/scs.2019.32.6.731.
- [8] D. Proske, “Fatalities due to bridge collapse,” *Proceedings of the Institution of Civil Engineers - Bridge Engineering*, vol. 173, no. 4, pp. 1–24, Jun. 2020, doi: 10.1680/jbren.20.00001.
- [9] F. N. Çatbaş, T. Kijewski-Correa, and A. E. Aktan, *Structural Identification of Constructed Systems*. American Society of Civil Engineers, 2013. doi: 10.1061/9780784411971.
- [10] A. Elhatab, N. Uddin, and E. OBrien, “Extraction of Bridge Fundamental Frequencies Utilizing a Smartphone MEMS Accelerometer,” *Sensors*, vol. 19, no. 14, pp. 3143–3163, Jul. 2019, doi: 10.3390/s19143143.
- [11] Y. Xia, X. Lei, P. Wang, and L. Sun, “A data-driven approach for regional bridge condition assessment using inspection reports,” *Struct Control Health Monit*, vol. 29, no. 4, p. e2915, Apr. 2022, doi: 10.1002/STC.2915.
- [12] C. R. Farrar and K. Worden, “An introduction to structural health monitoring,” *Philosophical Transactions of the Royal Society A: Mathematical, Physical and Engineering Sciences*, vol. 365, no. 1851, pp. 303–315, Feb. 2007, doi: 10.1098/rsta.2006.1928.

- [13] S. Komarizadehasl and M. Khanmohammadi, "Novel plastic hinge modification factors for damaged RC shear walls with bending performance," *Advances in Concrete Construction*, vol. 12, no. 4, pp. 355–365, 2021, doi: 10.12989/ACC.2021.12.4.355.
- [14] Y. Xia, X. Lei, P. Wang, G. Liu, and L. Sun, "Long-term performance monitoring and assessment of concrete beam bridges using neutral axis indicator," *Struct Control Health Monit*, vol. 27, no. 12, p. e2637, Dec. 2020, doi: 10.1002/STC.2637.
- [15] S. Dixit and K. Sharma, "A Review of Studies in Structural Health Monitoring (SHM)," in *Creative Construction Conference 2019*, Jul. 2019, pp. 84–88. doi: 10.3311/CCC2019-013.
- [16] J. Farré-Checa, S. Komarizadehasl, H. Ma, J. A. Lozano-Galant, and J. Turmo, "Direct simulation of the tensioning process of cable-stayed bridge cantilever construction," *Autom Constr*, vol. 137, p. 104197, May 2022, doi: 10.1016/J.AUTCON.2022.104197.
- [17] P. C. Lallana *et al.*, "Sensing Applications in Aircrafts Using Polymer Optical Fibres," *Sensors*, vol. 21, no. 11, p. 3605, May 2021, doi: 10.3390/s21113605.
- [18] S. Khan *et al.*, "SSVM: An Ultra-Low-Power Strain Sensing and Visualization Module for Long-Term Structural Health Monitoring," *Sensors*, vol. 21, no. 6, p. 2211, Mar. 2021, doi: 10.3390/s21062211.
- [19] X. Lei, Y. Xia, S. Komarizadehasl, and L. Sun, "Condition level deteriorations modeling of RC beam bridges with U-Net convolutional neural networks," *Structures*, vol. 42, pp. 333–342, Aug. 2022, doi: 10.1016/J.ISTRUC.2022.06.013.
- [20] Y. Xia *et al.*, "Artificial Intelligence Based Structural Assessment for Regional Short- and Medium-Span Concrete Beam Bridges with Inspection Information," *Remote Sensing 2021, Vol. 13, Page 3687*, vol. 13, no. 18, p. 3687, Sep. 2021, doi: 10.3390/RS13183687.
- [21] D. Straub *et al.*, "Value of information: A roadmap to quantifying the benefit of structural health monitoring," in *ICOSSAR – 12th International Conference on Structural Safety & Reliability*, Aug. 2017, no. 12, pp. 3018–3029.
- [22] R. S. Panah and M. Kioumars, "Application of building information modelling (BIM) in the health monitoring and maintenance process: A systematic review," *Sensors (Switzerland)*, vol. 21, no. 3. MDPI AG, pp. 1–26, Feb. 01, 2021. doi: 10.3390/s21030837.
- [23] J. Biliszczyk, P. Hawryszków, and M. Teichgraber, "SHM System and a FEM Model-Based Force Analysis Assessment in Stay Cables," *Sensors*, vol. 21, no. 6, p. 1927, Mar. 2021, doi: 10.3390/s21061927.
- [24] B. Mobaraki, S. Komarizadehasl, F. Javier, C. Pascual, A. Lozano-Galant, and R. P. Soriano, "A Novel Data Acquisition System for Obtaining Thermal Parameters of Building Envelopes," *Buildings 2022, Vol. 12, Page 670*, vol. 12, no. 5, p. 670, May 2022, doi: 10.3390/BUILDINGS12050670.
- [25] J. Lei, D. Xu, and J. Turmo, "Static structural system identification for beam-like structures using compatibility conditions," *Struct Control Health Monit*, vol. 25, no. 1, pp. 1–15, Jan. 2018, doi: 10.1002/STC.2062/ABSTRACT.
- [26] G. Morgenthal *et al.*, "Framework for automated UAS-based structural condition assessment of bridges," *Autom Constr*, vol. 97, pp. 77–95, Jan. 2019, doi: 10.1016/j.autcon.2018.10.006.

- [27] S. Sony, S. Laventure, and A. Sadhu, “A literature review of next-generation smart sensing technology in structural health monitoring,” *Struct Control Health Monit*, vol. 26, no. 3, pp. e2321–e2343, Mar. 2019, doi: 10.1002/STC.2321.
- [28] D. Feng and M. Q. Feng, “Experimental validation of cost-effective vision-based structural health monitoring,” *Mech Syst Signal Process*, vol. 88, pp. 199–211, May 2017, doi: 10.1016/j.ymssp.2016.11.021.
- [29] S. Komarizadehasl, B. Mobaraki, H. Ma, J.-A. Lozano-Galant, and J. Turmo, “Development of a Low-Cost System for the Accurate Measurement of Structural Vibrations,” *Sensors*, vol. 21, no. 18, pp. 6191–6213, Sep. 2021, doi: 10.3390/S21186191.
- [30] G. Lacidogna *et al.*, “Automatic Detection of Real Damage in Operating Tie-Rods,” *Sensors 2022, Vol. 22, Page 1370*, vol. 22, no. 4, p. 1370, Feb. 2022, doi: 10.3390/S22041370.
- [31] G. Villanueva, V. Meruane, S. J. Yanez, L. Quinteros, and E. I. Saavedra Flores, “Damage Detection in Steel–Concrete Composite Structures by Impact Hammer Modal Testing and Experimental Validation,” *Sensors 2022, Vol. 22, Page 3874*, vol. 22, no. 10, p. 3874, May 2022, doi: 10.3390/S22103874.
- [32] A. Aktan, N. Catbas, K. Grimmelsman, and M. Pervizpour, “Development of a model health monitoring guide for major bridges,” *Federal Highway Administration Research and Development*, 2002. https://www.researchgate.net/profile/Necati-Catbas/publication/267839627_Development_of_a_Model_Health_Monitoring_Guide_for_Major_Bridges/links/54732e720cf216f8cfaeae7d/Development-of-a-Model-Health-Monitoring-Guide-for-Major-Bridges.pdf (accessed Jan. 24, 2022).
- [33] Michael A. Grubb *et al.*, “Load and Resistance Factor Design (LRFD) for Highway Bridge Superstructures,” 2007. <https://www.fhwa.dot.gov/bridge/pubs/nhi15047.pdf> (accessed Jan. 24, 2022).
- [34] C. Costa, D. Ribeiro, P. Jorge, R. Silva, R. Calçada, and A. Arêde, “Calibration of the Numerical Model of a Short-span Masonry Railway Bridge Based on Experimental Modal Parameters,” *Procedia Eng*, vol. 114, pp. 846–853, Jan. 2015, doi: 10.1016/J.PROENG.2015.08.038.
- [35] C. Bedon, E. Bergamo, M. Izzi, and S. Noè, “Prototyping and Validation of MEMS Accelerometers for Structural Health Monitoring—The Case Study of the Pietratagliata Cable-Stayed Bridge,” *Journal of Sensor and Actuator Networks*, vol. 7, no. 3, pp. 30–48, Jul. 2018, doi: 10.3390/JSAN7030030.
- [36] H. Tran-Ngoc, S. Khatir, G. De Roeck, T. Bui-Tien, L. Nguyen-Ngoc, and M. Abdel Wahab, “Model Updating for Nam O Bridge Using Particle Swarm Optimization Algorithm and Genetic Algorithm,” *Sensors 2018, Vol. 18, Page 4131*, vol. 18, no. 12, p. 4131, Nov. 2018, doi: 10.3390/S18124131.
- [37] S. Kavitha, R. Joseph Daniel, and K. Sumangala, “Design and Analysis of MEMS Comb Drive Capacitive Accelerometer for SHM and Seismic Applications,” *Measurement*, vol. 93, pp. 327–339, Nov. 2016, doi: 10.1016/J.MEASUREMENT.2016.07.029.
- [38] G. Gaultschi, “Piezoelectric Sensors,” in *Piezoelectric Sensorics*, Berlin, Heidelberg: Springer Berlin Heidelberg, 2002, pp. 73–91. doi: 10.1007/978-3-662-04732-3_5.
- [39] Á. Cunha and E. Caetano, “Experimental modal analysis of civil engineering structures,” 2006.

125

- [40] R. S. Khandpur, “accelerometer,” in *Compendium of Biomedical Instrumentation*, Wiley, 2020, pp. 1–8. doi: 10.1002/9781119288190.ch1.
- [41] S. Komarizadehasl, F. Lozano, J. A. Lozano-Galant, G. Ramos, and J. Turmo, “Low-Cost Wireless Structural Health Monitoring of Bridges,” *Sensors 2022, Vol. 22, Page 5725*, vol. 22, no. 15, p. 5725, Jul. 2022, doi: 10.3390/S22155725.
- [42] “3713B112G data-sheet.”
https://www.pcb.com/contentstore/docs/PCB_Corporate/Vibration/Products/Manuals/3713B112G.pdf%0A
- [43] M. Botz, S. Oberlaender, M. Raith, and C. U. Grosse, “Monitoring of Wind Turbine Structures with Concrete-steel Hybrid-tower Design.”
- [44] “356B08 data-sheet.”
https://www.pcb.com/contentstore/docs/PCB_Corporate/Vibration/Products/Manuals/356B08.pdf%0A
- [45] F. Keilpflug, R. Kamenzky, D. J. Alarcón, T. Mallareddy, and P. Blaschke, “Structural Health Monitoring on Industrial Structures Using a Combined Numerical and Experimental Approach,” *Springer*, pp. 263–277, 2020, doi: 10.1007/978-3-030-12684-1_27.
- [46] “356A45 data-sheet.”
https://www.pcb.com/contentstore/docs/PCB_Corporate/Vibration/Products/Manuals/356A45.pdf%0A
- [47] V. Handojo, Y. M. Meddaikar, J. K. S. Dillinger, J. Sodja, and R. De Breuker, “International Forum on Aeroelasticity and Structural Dynamics INVESTIGATION OF GUST LOADS ON A FLEXIBLE FORWARD SWEEP WING.”
- [48] PCB Piezotronics, “356B18 data-sheet,” 2007.
https://www.pcb.com/contentstore/docs/PCB_Corporate/Vibration/Products/Manuals/356B18.pdf (accessed Aug. 01, 2020).
- [49] K. Gr̄ Ebowski, M. Rucka, and K. Wilde, “Non-Destructive Testing of a Sport Tribune under Synchronized Crowd-Induced Excitation Using Vibration Analysis,” *materials*, doi: 10.3390/ma12132148.
- [50] “3711B1110G data-sheet.”
https://www.pcb.com/contentstore/docs/PCB_Corporate/Vibration/Products/Manuals/3713B1110G.pdf%0A
- [51] A. Ozdagli, B. Liu, and F. Moreu, “Real-time low-cost wireless reference-free displacement sensing of railroad bridges,” in *Conference Proceedings of the Society for Experimental Mechanics Series*, 2019, no. 213429, pp. 103–109. doi: 10.1007/978-3-319-74642-5_12.
- [52] M. Str, “KS48C and KB12VD-MMF data-sheet.” <http://www.mmf.de/pdf/1-5.pdf%0A> (accessed Mar. 03, 2020).
- [53] A. Pierdicca, F. Clementi, P. Mezzapelle, ... A. F.-P., and undefined 2017, “One-year monitoring of a reinforced concrete school building: Evolution of dynamic behavior during retrofitting works,” *Elsevier*.
- [54] “393b12 data-sheet.”
https://www.pcb.com/contentstore/docs/PCB_Corporate/Vibration/Products/Manuals/393B12.pdf%0A

- [55] R. Aguilar, L. Ramos, P. L.-3rd I. O. Modal, and undefined 2009, “Wireless sensor technology for structural health monitoring of historical masonry structures,” *iomac.eu*.
- [56] J. de SEBASTIÁN, I. Díaz, C. C.- Proc., 4th Int. Conf, and undefined 2011, “Environmental and crowd influence on the dynamic behaviour of an in-service footbridge,” *researchgate.net*.
- [57] “393A03 data-sheet.”
https://www.pcb.com/contentstore/docs/PCB_Corporate/Vibration/Products/Manuals/393A03.pdf
- [58] N. Makoond, L. Pelà, C. Molins, and L. Pei, “Dynamic elastic properties of brick masonry constituents Autoaprenentatge del formigó estructural View project Seismic strength of multi storey masonry buildings with flexible and rigid floor slabs View project Dynamic elastic properties of brick masonry constituents”, doi: 10.1016/j.conbuildmat.2018.12.071.
- [59] “352A24 data-sheet.”
https://www.pcb.com/contentstore/docs/PCB_Corporate/Vibration/Products/Manuals/352A24.pdf%0A
- [60] M. Aykan and H. N. Özgüven, “Detection of Structural Damage Through Nonlinear Identification by Using Modal Testing,” in *Conference Proceedings of the Society for Experimental Mechanics Series*, 2014, vol. 45, no. 7, pp. 461–470. doi: 10.1007/978-1-4614-6585-0_44.
- [61] “352C33 data-sheet.”
https://www.pcb.com/contentstore/docs/PCB_Corporate/Vibration/Products/Manuals/352C33.pdf%0A
- [62] Y. B. Yang, H. Xu, B. Zhang, F. Xiong, and Z. L. Wang, “Measuring bridge frequencies by a test vehicle in non-moving and moving states,” *Eng Struct*, vol. 203, no. 0, pp. 109859–109870, 2020, doi: 10.1016/j.engstruct.2019.109859.
- [63] ST, “LIS344ALH data-sheet,” 2008.
<https://www.st.com/resource/en/datasheet/lis344alh.pdf> (accessed Aug. 01, 2020).
- [64] A. Girolami, F. Zonzini, L. De Marchi, D. Brunelli, and L. Benini, “Modal Analysis of Structures with Low-cost Embedded Systems,” in *International Symposium on Circuits and Systems*, 2018, vol. 2018-May, pp. 1–4. doi: 10.1109/ISCAS.2018.8351705.
- [65] Analog Devices, “ADXL 335 data-sheet.”
<https://www.sparkfun.com/datasheets/Components/SMD/adx1335.pdf> (accessed Aug. 01, 2020).
- [66] K. A. Grimmelsman and N. Zolghadri, “Experimental evaluation of low-cost accelerometers for dynamic characterization of bridges,” in *Conference Proceedings of the Society for Experimental Mechanics Series*, 2020, pp. 145–152. doi: 10.1007/978-3-030-12115-0_19.
- [67] M. Agüero, A. Ozdagli, and F. Moreu, “Measuring reference-free total displacements of piles and columns using low-cost, battery-powered, efficient wireless intelligent sensors (LEWIS2),” *Sensors*, vol. 19, no. 7, pp. 1549–1566, 2019, doi: 10.3390/s19071549.
- [68] G. Chatterjee, L. Latorre, F. Mailly, P. Nouet, N. Hachelef, and C. Oudea, “Smart-MEMS based inertial measurement units: gyro-free approach to improve the grade,” *Microsystem Technologies*, vol. 23, no. 9, pp. 3969–3978, Sep. 2017, doi: 10.1007/s00542-015-2741-y.

- [69] InvenSense, “MPU6050 data-sheet,” 2013. <https://www.invensense.com/wp-content/uploads/2015/02/MPU-6000-Datasheet1.pdf%0A> (accessed Aug. 01, 2020).
- [70] M. Varanis, A. L. Silva, and A. G. Mereles, “On mechanical vibration analysis of a multi degree of freedom system based on arduino and MEMS accelerometers,” *Revista Brasileira de Ensino de Fisica*, vol. 40, no. 1, pp. e1304–e1314, 2018, doi: 10.1590/1806-9126-RBEF-2017-0101.
- [71] A. I. Ozdagli, B. Liu, and F. Moreu, “Low-cost, efficient wireless intelligent sensors (LEWIS) measuring real-time reference-free dynamic displacements,” *Mech Syst Signal Process*, vol. 107, pp. 343–356, Jul. 2018, doi: 10.1016/j.ymssp.2018.01.034.
- [72] Y. Shi, J. Zhang, J. Jiao, R. Zhao, and H. Cao, “Calibration Analysis of High-G MEMS Accelerometer Sensor Based on Wavelet and Wavelet Packet Denoising,” *Sensors 2021, Vol. 21, Page 1231*, vol. 21, no. 4, p. 1231, Feb. 2021, doi: 10.3390/S21041231.
- [73] Q. Meng and S. Zhu, “Developing iot sensing system for construction-induced vibration monitoring and impact assessment,” *Sensors (Switzerland)*, vol. 20, no. 21, pp. 1–24, Nov. 2020, doi: 10.3390/s20216120.
- [74] E. Atencio, S. Komarizadehasl, J. A. Lozano-Galant, and M. Aguilera, “Using RPA for Performance Monitoring of Dynamic SHM Applications,” *Buildings 2022, Vol. 12, Page 1140*, vol. 12, no. 8, p. 1140, Aug. 2022, doi: 10.3390/BUILDINGS12081140.
- [75] D. Feng and M. Q. Feng, “Model Updating of Railway Bridge Using in Situ Dynamic Displacement Measurement under Trainloads,” *Journal of Bridge Engineering*, vol. 20, no. 12, pp. 04015019–04015031, Dec. 2015, doi: 10.1061/(ASCE)BE.1943-5592.0000765.
- [76] F. L. Zhang, C. E. Ventura, H. B. Xiong, W. S. Lu, Y. X. Pan, and J. X. Cao, “Evaluation of the dynamic characteristics of a super tall building using data from ambient vibration and shake table tests by a Bayesian approach,” *Struct Control Health Monit*, vol. 25, no. 4, pp. e2121–e2139, Apr. 2018, doi: 10.1002/stc.2121.
- [77] S. Beskhyroun, L. D. Wegner, and B. F. Sparling, “New methodology for the application of vibration-based damage detection techniques,” *Struct Control Health Monit*, vol. 19, no. 8, pp. 632–649, Dec. 2012, doi: 10.1002/stc.456.
- [78] M. Pastor, M. Binda, and T. Harčarik, “Modal Assurance Criterion,” *Procedia Eng*, vol. 48, pp. 543–548, Jan. 2012, doi: 10.1016/J.PROENG.2012.09.551.
- [79] D. W. Ha, H. S. Park, S. W. Choi, and Y. Kim, “A Wireless MEMS-Based Inclinometer Sensor Node for Structural Health Monitoring,” *Sensors 2013, Vol. 13, Pages 16090-16104*, vol. 13, no. 12, pp. 16090–16104, Nov. 2013, doi: 10.3390/S131216090.
- [80] F. Huseynov, C. Kim, E. J. OBrien, J. M. W. Brownjohn, D. Hester, and K. C. Chang, “Bridge damage detection using rotation measurements – Experimental validation,” *Mech Syst Signal Process*, vol. 135, p. 106380, Jan. 2020, doi: 10.1016/J.YMSSP.2019.106380.
- [81] B. Glišić, D. Posenato, D. Inaudi, and A. Figini, “Structural health monitoring method for curved concrete bridge box girders,” in *SPIE 6932, Sensors and Smart Structures Technologies for Civil, Mechanical, and Aerospace Systems*, Mar. 2008, vol. 6932, p. 693204. doi: 10.1117/12.778643.
- [82] Y. Zhou, Z. Dongjian, C. Zhuoyan, and L. Yongtao, “Research on a novel inclinometer based on distributed optical fiber strain and conjugate beam method,” *Measurement*, vol. 153, p. 107404, Mar. 2020, doi: 10.1016/J.MEASUREMENT.2019.107404.

- [83] S. Bas, N. M. Apaydin, A. Ilki, and F. N. Catbas, "Structural health monitoring system of the long-span bridges in Turkey," <https://doi.org/10.1080/15732479.2017.1360365>, vol. 14, no. 4, pp. 425–444, Apr. 2017, doi: 10.1080/15732479.2017.1360365.
- [84] J. M. Ko and Y. Q. Ni, "Technology developments in structural health monitoring of large-scale bridges," *Eng Struct*, vol. 27, no. 12, pp. 1715–1725, Oct. 2005, doi: 10.1016/J.ENGSTRUCT.2005.02.021.
- [85] H. Pei, F. Zhang, and S. Zhang, "Development of a novel Hall element inclinometer for slope displacement monitoring," *Measurement*, vol. 181, p. 109636, Aug. 2021, doi: 10.1016/J.MEASUREMENT.2021.109636.
- [86] N. Haritos and T. J. Chalko, "Determination of abutment support conditions in an 80-year-old RC bridge," <https://doi.org/10.1117/12.259148>, vol. 2946, pp. 312–323, Nov. 1996, doi: 10.1117/12.259148.
- [87] N. A. Hoult, P. R. A. Fidler, P. G. Hill, and C. R. Middleton, "Long-Term Wireless Structural Health Monitoring of the Ferriby Road Bridge," *Journal of Bridge Engineering*, vol. 15, no. 2, pp. 153–159, Feb. 2010, doi: 10.1061/(ASCE)BE.1943-5592.0000049.
- [88] X. Hou, X. Yang, and Q. Huang, "Using Inclinometers to Measure Bridge Deflection," *Journal of Bridge Engineering*, vol. 10, no. 5, pp. 564–569, Sep. 2005, doi: 10.1061/(ASCE)1084-0702(2005)10:5(564).
- [89] Y. Robert-Nicoud, B. Raphael, O. Burdet, and I. F. C. Smith, "Model Identification of Bridges Using Measurement Data," *Computer-Aided Civil and Infrastructure Engineering*, vol. 20, no. 2, pp. 118–131, Mar. 2005, doi: 10.1111/J.1467-8667.2005.00381.X.
- [90] "ZEROTRONIC inclination sensor." <https://www.wylerag.com/en/products/inclination-measuring-sensors/zerotronic-inclination-sensor/> (accessed Aug. 24, 2022).
- [91] "JDI 100/200 Digital MEMS Inclinometer Series - Jewell Instruments." <https://jewellinstruments.com/products/inertial-tilt-sensors/inclinometer/jdi/> (accessed Aug. 24, 2022).
- [92] "DUETTO-Engineering - T935 Inclinometers." <http://www.duetto-engineering.com/en/transducer/inclinometers/t935-inclinometers/> (accessed Aug. 24, 2022).
- [93] "Dual-axis inclinometer - ACA2200-SHENZHEN RION TECHNOLOGY CO." <https://www.directindustry.com/prod/shenzhen-rion-technology-co-ltd/product-144867-2125155.html> (accessed Aug. 24, 2022).
- [94] "HI-INC dual-axis inclinometer - BeanDevice® WILOW® ." <https://www.directindustry.com/prod/beanair-gmbh/product-161641-1835299.html> (accessed Aug. 24, 2022).
- [95] Y. Yu, J. Ou, J. Zhang, C. Zhang, and L. Li, "Development of wireless MEMS inclination sensor system for swing monitoring of large-scale hook structures," *IEEE Transactions on Industrial Electronics*, vol. 56, no. 4, pp. 1072–1078, 2009, doi: 10.1109/TIE.2009.2012469.
- [96] G. Ruzza, L. Guerriero, P. Revellino, and F. M. Guadagno, "A Multi-Module Fixed Inclinometer for Continuous Monitoring of Landslides: Design, Development, and Laboratory Testing," *Sensors 2020, Vol. 20, Page 3318*, vol. 20, no. 11, p. 3318, Jun. 2020, doi: 10.3390/S20113318.

- [97] B. Andò, S. Baglio, and A. Pistorio, “A low cost multi-sensor system for investigating the structural response of buildings,” *Annals of Geophysics*, vol. 61, no. 2, p. SE217, Jun. 2018, doi: 10.4401/ag-7702.
- [98] H. S. Park, H. M. Lee, H. Adeli, and I. Lee, “A New Approach for Health Monitoring of Structures: Terrestrial Laser Scanning,” *Computer-Aided Civil and Infrastructure Engineering*, vol. 22, no. 1, pp. 19–30, Jan. 2007, doi: 10.1111/J.1467-8667.2006.00466.X.
- [99] H. Yoon, J. Shin, and B. F. Spencer, “Structural Displacement Measurement Using an Unmanned Aerial System,” *Computer-Aided Civil and Infrastructure Engineering*, vol. 33, no. 3, pp. 183–192, Mar. 2018, doi: 10.1111/MICE.12338.
- [100] R. Nasimi and F. Moreu, “A methodology for measuring the total displacements of structures using a laser-camera system,” *Computer-Aided Civil and Infrastructure Engineering*, vol. 36, no. 4, pp. 421–437, Apr. 2021, doi: 10.1111/MICE.12652.
- [101] S. Artese and G. Nico, “TLS and GB-RAR Measurements of Vibration Frequencies and Oscillation Amplitudes of Tall Structures: An Application to Wind Towers,” *Applied Sciences 2020, Vol. 10, Page 2237*, vol. 10, no. 7, p. 2237, Mar. 2020, doi: 10.3390/APP10072237.
- [102] L. Yang, X. Feng, J. Zhang, and X. Shu, “Multi-Ray Modeling of Ultrasonic Sensors and Application for Micro-UAV Localization in Indoor Environments,” *Sensors*, vol. 19, no. 8, p. 1770, Apr. 2019, doi: 10.3390/s19081770.
- [103] S. Komarizadehasl, J. Turmo, B. Mobaraki, and J. A. Lozano-galant, “Comparison of different low-cost sensors for structural health monitoring,” in *Bridge Maintenance, Safety, Management, Life-Cycle Sustainability and Innovations*, Mar. 2021, pp. 186–191. doi: 10.1201/9780429279119-21.
- [104] Z. Dong, X. Sun, W. Liu, and H. Yang, “Measurement of free-form curved surfaces using laser triangulation,” *Sensors (Switzerland)*, vol. 18, no. 10, p. 3527, Oct. 2018, doi: 10.3390/s18103527.
- [105] “Types of Distance Sensor and How to select one? - Latest open tech from seeed studio.” <https://www.seeedstudio.com/blog/2019/12/23/distance-sensors-types-and-selection-guide/> (accessed Apr. 10, 2021).
- [106] J. Yang, B. Zhao, and B. Liu, “Distance and velocity measurement of coherent lidar based on chirp pulse compression,” *Sensors (Switzerland)*, vol. 19, no. 10, p. 2313, May 2019, doi: 10.3390/s19102313.
- [107] Y. S. Suh, “Laser Sensors for Displacement, Distance and Position,” *Sensors*, vol. 19, no. 8, p. 1924, Apr. 2019, doi: 10.3390/s19081924.
- [108] “LD-OEM1000 | Sick | WIAutomation.” https://es.wiautomation.com/sick/productos-generales/fotocelulas/LDOEM1000?utm_source=shopping_free&utm_medium=organic&utm_content=ES61334&gclid=CjwKCAjwhYOFBhBkEiwASF3KGXHI78pJN2mnmvGWpjBFfrZI_exeLCdR9uW4Rkfb05AOCLs0EpddOgxocAOcQAvD_BwE (accessed May 16, 2021).
- [109] “Lite v3 datasheet.” https://www.google.com/search?q=Lite+v3+datasheet&ei=kmOnYK2II9CflwSgn5LgDw&oq=Lite+v3+datasheet&gs_lcp=Cgdnd3Mtd2l6EAMyBggAEAUQHjIICAAQBxAFEb5QjbYEWI22BGC7wARoAHACeACAAYUBiAHRAZIBAzEuMZgBAKABAqABAao

- BB2d3cy13aXrAAQE&scient=gws-wiz&ved=0ahUKEwitme24otrWAh (accessed May 21, 2021).
- [110] W. Metzler, D. Pinson, A. Hendrickson, R. Xu, and J. Henriques, “Low-cost drone system for analyzing elevation,” in *2018 Systems and Information Engineering Design Symposium, SIEDS 2018*, Jun. 2018, pp. 182–184. doi: 10.1109/SIEDS.2018.8374732.
- [111] “gp2y0a21yk0f datasheet.” https://www.google.com/search?q=gp2y0a21yk0f+datasheet&ei=jmOnYKYvOcWEacDbiYgH&oq=gp2y0a21yk0f+data&gs_lcp=Cgdnnd3Mtd2l6EAMYADICCAA6BwgAEecQsAM6BwgAELADEEM6BAgAEB5QgQhYxQ5gwhVoAXACeACAAZMBiAGEBJIBAzUuMZgBAKABAaoBB2d3cy13aXrIAQrAAQE&scient=gws-wiz (accessed May 21, 2021).
- [112] J. Chacon, J. Saenz, L. de la Torre, J. Diaz, and F. Esquembre, “Design of a low-cost air levitation system for teaching control engineering,” *Sensors (Switzerland)*, vol. 17, no. 10, p. 2321, Oct. 2017, doi: 10.3390/s17102321.
- [113] Adafruit, “Adafruit VL53L0X Time of Flight Micro-LIDAR Distance Sensor Breakout,” 2016.
- [114] K. M. Luthfi, A. Sugiana, and F. Y. Suratman, “Broken rail detection system using laser,” *IOP Conf Ser Mater Sci Eng*, vol. 1098, no. 4, p. 042045, Mar. 2021, doi: 10.1088/1757-899X/1098/4/042045.
- [115] E. F.-H.-S. datasheet and undefined 2016, “Ultrasonic ranging module hc-sr04”.
- [116] V. A. Zhmud, N. O. Kondratiev, K. A. Kuznetsov, V. G. Trubin, and L. V. Dimitrov, “Application of ultrasonic sensor for measuring distances in robotics,” in *Journal of Physics: Conference Series*, May 2018, vol. 1015, no. 3, p. 32189. doi: 10.1088/1742-6596/1015/3/032189.
- [117] J. Lei, J. A. Lozano-Galant, M. Nogal, D. Xu, and J. Turmo, “Analysis of measurement and simulation errors in structural system identification by observability techniques,” *Struct Control Health Monit*, vol. 24, no. 6, pp. 1–21, 2017, doi: 10.1002/stc.1923.
- [118] J. Lei, J. A. Lozano-Galant, D. Xu, and J. Turmo, “Structural system identification by measurement error-minimizing observability method,” *Struct Control Health Monit*, vol. 26, no. 10, pp. e2425–e2444, Oct. 2019, doi: 10.1002/stc.2425.
- [119] B. Mobaraki, F. Lozano-Galant, R. P. Soriano, and F. J. C. Pascual, “Application of Low-Cost Sensors for Building Monitoring: A Systematic Literature Review,” *Buildings 2021, Vol. 11, Page 336*, vol. 11, no. 8, p. 336, Aug. 2021, doi: 10.3390/BUILDINGS11080336.
- [120] S. Komarizadehasl, B. Mobaraki, H. Ma, J.-A. Lozano-Galant, and J. Turmo, “Low-Cost Sensors Accuracy Study and Enhancement Strategy,” *Applied Sciences 2022, Vol. 12, Page 3186*, vol. 12, no. 6, pp. 3186–3215, Mar. 2022, doi: 10.3390/APP12063186.
- [121] S. Komarizadehasl, B. Mobaraki, J. A. Lozano-Galant, and J. Turmo, “Detailed evaluation of low-cost ranging sensors for structural health monitoring applications,” in *International Conference of Recent Trends in Geotechnical and Geo-Environmental Engineering and Education. "RTCEE/RTGEE 2020*, 2020, pp. 8–12.
- [122] G. Barbon, M. Margolis, F. Palumbo, F. Raimondi, and N. Weldin, “Taking Arduino to the Internet of Things: The ASIP programming model,” *Comput Commun*, vol. 89–90, pp. 128–140, 2016, doi: 10.1016/j.comcom.2016.03.016.

- [123] R. Piedrahita *et al.*, “The next generation of low-cost personal air quality sensors for quantitative exposure monitoring,” *Atmos Meas Tech*, vol. 7, no. 10, pp. 3325–3336, 2014, doi: 10.5194/amt-7-3325-2014.
- [124] S. H. Man and C. C. Chang, “Design and performance tests of a LED-based two-dimensional wireless crack propagation sensor,” *Struct Control Health Monit*, vol. 23, no. 4, pp. 668–683, Apr. 2016, doi: 10.1002/stc.1802.
- [125] A. Mei, E. Zampetti, P. di Mascio, G. Fontinovo, P. Papa, and A. D’andrea, “ROADS—Rover for Bituminous Pavement Distress Survey: An Unmanned Ground Vehicle (UGV) Prototype for Pavement Distress Evaluation,” *Sensors*, vol. 22, no. 9, p. 3414, May 2022, doi: 10.3390/S22093414/S1.
- [126] R. Nasimi *et al.*, “Use of Remote Structural Tap Testing Devices Deployed via Ground Vehicle for Health Monitoring of Transportation Infrastructure,” *Sensors 2022, Vol. 22, Page 1458*, vol. 22, no. 4, p. 1458, Feb. 2022, doi: 10.3390/S22041458.
- [127] E. Angelini, S. Corbellini, M. Parvis, F. Ferraris, and S. Grassini, “An Arduino-based EIS with a logarithmic amplifier for corrosion monitoring,” *Conference Record - IEEE Instrumentation and Measurement Technology Conference*, pp. 905–910, 2014, doi: 10.1109/I2MTC.2014.6860873.
- [128] “Arduino - Home.” <https://www.arduino.cc/> (accessed Jan. 10, 2021).
- [129] G. Chiesa, D. Di Vita, A. Ghadirzadeh, A. H. Muñoz Herrera, and J. C. Leon Rodriguez, “A fuzzy-logic IoT lighting and shading control system for smart buildings,” *Autom Constr*, vol. 120, p. 103397, Dec. 2020, doi: 10.1016/J.AUTCON.2020.103397.
- [130] S. Komarizadehasl, M. Komary, A. Alahmad, J. A. Lozano-Galant, G. Ramos, and J. Turmo, “A Novel Wireless Low-Cost Inclinometer Made from Combining the Measurements of Multiple MEMS Gyroscopes and Accelerometers,” *Sensors 2022, Vol. 22, Page 5605*, vol. 22, no. 15, p. 5605, Jul. 2022, doi: 10.3390/S22155605.
- [131] A. G. Özcebe *et al.*, “Raspberry Shake-Based Rapid Structural Identification of Existing Buildings Subject to Earthquake Ground Motion: The Case Study of Bucharest,” *Sensors 2022, Vol. 22, Page 4787*, vol. 22, no. 13, p. 4787, Jun. 2022, doi: 10.3390/S22134787.
- [132] D. Caballero-Russi, A. R. Ortiz, A. Guzmán, and C. Canchila, “Design and Validation of a Low-Cost Structural Health Monitoring System for Dynamic Characterization of Structures,” *Applied Sciences 2022, Vol. 12, Page 2807*, vol. 12, no. 6, p. 2807, Mar. 2022, doi: 10.3390/APP12062807.
- [133] S. Jeong, Y. J. Lee, D. H. Shin, and S. H. Sim, “Automated Real-Time Assessment of Stay-Cable Serviceability Using Smart Sensors,” *Applied Sciences 2019, Vol. 9, Page 4469*, vol. 9, no. 20, p. 4469, Oct. 2019, doi: 10.3390/APP9204469.
- [134] “Buy a Raspberry Pi – Raspberry Pi.” <https://www.raspberrypi.org/products/> (accessed Jan. 11, 2021).
- [135] D. Hester, J. Brownjohn, F. Huseynov, E. O'Brien, A. Gonzalez, and M. Casero, “Identifying damage in a bridge by analysing rotation response to a moving load,” *Structure and Infrastructure Engineering*, vol. 16, no. 7, pp. 1050–1065, Jul. 2019, doi: 10.1080/15732479.2019.1680710.

- [136] A. Knörrig, R. Wettach, and J. Cohen, “Fritzing - A tool for advancing electronic prototyping for designers,” in *3rd International Conference on Tangible and Embedded Interaction*, 2009, pp. 351–358. doi: 10.1145/1517664.1517735.
- [137] InvenSense, “MPU 9250 data-sheet,” 2014. https://cdn.sparkfun.com/assets/learn_tutorials/5/5/0/MPU9250REV1.0.pdf (accessed Aug. 01, 2020).
- [138] M. Bálský, M. Kozlok, and R. Bayer, “Application of Arduino Platform for Light Field Analysis,” in *7th Lighting Conference of the Visegrad Countries (Lumen V4)*, 2018, pp. 1–4. doi: 10.1109/LUMENV.2018.8521176.
- [139] N. Davis, “An Introduction to Ground: Earth Ground, Common Ground, Analog Ground, and Digital Ground,” *Allaboutcircuits*, 2018. <https://www.allaboutcircuits.com/technical-articles/an-introduction-to-ground/> (accessed Aug. 01, 2020).
- [140] M. Cocconcelli and A. Spaggiari, “Mounting of accelerometers with structural adhesives: Experimental characterization of the dynamic response,” *J Adhes*, vol. 93, no. 8, pp. 585–598, Jul. 2017, doi: 10.1080/00218464.2015.1120197.
- [141] Alliantech, “Accelerometer Mounting Considerations,” 2014. http://www.alliantech.com/pdf/technique/vibration_montage2.pdf (accessed Aug. 01, 2020).
- [142] National Instruments, “cRIO data-sheet,” 2015. https://www.ni.com/pdf/manuals/376901a_02.pdf (accessed Aug. 01, 2020).
- [143] National Instruments, “NI-9234 data-sheet.” https://www.ni.com/pdf/manuals/374238a_02.pdf (accessed Aug. 01, 2020).
- [144] C. Elliott, V. Vijayakumar, W. Zink, and R. Hansen, “National Instruments LabVIEW: A Programming Environment for Laboratory Automation and Measurement,” *J Lab Autom*, vol. 12, no. 1, pp. 17–24, 2007, doi: 10.1016/j.jala.2006.07.012.
- [145] INSTRON, “8802 (250 kN) Fatigue Testing System,” 2017. <https://www.instron.co.hu/-/media/literature-library/products/2013/10/8803-servo-hydraulic-fatigue-testing-system.pdf?la=hu-HU> (accessed Aug. 01, 2020).
- [146] Instron, “WaveMatrix2 Dynamic Testing Software,” 2018. <https://www.instron.us/-/media/literature-library/products/2018/07/wavematrix2-brochure.pdf?la=en-US> (accessed Aug. 03, 2020).
- [147] P. Barsocchi *et al.*, “A New Tool for Monitoring and Assessing the Structural Health of Ancient Masonry Construction,” in *Civil-Comp Proceedings*, 2015, vol. 108. doi: 10.4203/ccp.108.136.
- [148] P. Barsocchi *et al.*, “Wireless Sensor Networks for Continuous Structural Health Monitoring of Historic Masonry Towers,” *International Journal of Architectural Heritage*, vol. 15, no. 1, pp. 22–44, Jan. 2021, doi: 10.1080/15583058.2020.1719229.
- [149] M. Bacco *et al.*, “Monitoring Ancient Buildings: Real Deployment of an IoT System Enhanced by UAVs and Virtual Reality,” *IEEE Access*, vol. 8, pp. 50131–50148, 2020, doi: 10.1109/ACCESS.2020.2980359.
- [150] P. Barsocchi, P. Cassara, F. Mavilia, and D. Pellegrini, “Sensing a City’s State of Health: Structural Monitoring System by Internet-of-Things Wireless Sensing Devices,” *IEEE*

- Consumer Electronics Magazine*, vol. 7, no. 2, pp. 22–31, Mar. 2018, doi: 10.1109/MCE.2017.2717198.
- [151] K. Faulkner, J. M. W. Brownjohn, Y. Wang, and F. Huseynov, “Tracking bridge tilt behaviour using sensor fusion techniques,” *J Civ Struct Health Monit*, vol. 10, no. 4, pp. 543–555, Sep. 2020, doi: 10.1007/S13349-020-00400-9/TABLES/2.
- [152] C. Yi *et al.*, “Estimating Three-Dimensional Body Orientation Based on an Improved Complementary Filter for Human Motion Tracking,” *Sensors 2018, Vol. 18, Page 3765*, vol. 18, no. 11, p. 3765, Nov. 2018, doi: 10.3390/S18113765.
- [153] X. Shen, M. Yao, W. Jia, and D. Yuan, “Adaptive complementary filter using fuzzy logic and simultaneous perturbation stochastic approximation algorithm,” *Measurement*, vol. 45, no. 5, pp. 1257–1265, Jun. 2012, doi: 10.1016/J.MEASUREMENT.2012.01.011.
- [154] “HW VSP3 - Virtual Serial Port | HW-group.com.” <https://www.hw-group.com/software/hw-vsp3-virtual-serial-port> (accessed Oct. 31, 2021).
- [155] “SerialPlot - Realtime Plotting Software | Hackaday.io.” <https://hackaday.io/project/5334-serialplot-realtime-plotting-software> (accessed Oct. 31, 2021).
- [156] “BeanDevice® Wilow® User Manual.” <https://www.wireless-iot.beanair.com/files/UM-RF-07-ENG-Wilow-Wifi-Sensor.pdf> (accessed Nov. 02, 2021).
- [157] C. Bedon and S. Noè, “Uncoupled Wi-Fi Body CoM Acceleration for the Analysis of Lightweight Glass Slabs under Random Walks,” *Journal of Sensor and Actuator Networks 2022, Vol. 11, Page 10*, vol. 11, no. 1, p. 10, Jan. 2022, doi: 10.3390/JSAN11010010.
- [158] K. Jerath, S. Brennan, and C. Lagoa, “Bridging the gap between sensor noise modeling and sensor characterization,” *Measurement*, vol. 116, pp. 350–366, Feb. 2018, doi: 10.1016/J.MEASUREMENT.2017.09.012.
- [159] N. K. *et al.*, “Noise modeling and analysis of an IMU-based attitude sensor: improvement of performance by filtering and sensor fusion,” <https://doi.org/10.1117/12.2234255>, vol. 9912, pp. 2138–2147, Jul. 2016, doi: 10.1117/12.2234255.
- [160] K.-M. Kwong, “MEMS Accelerometer Specifications and Their Impact in Inertial Applications,” *Master thesis*. http://www.eecg.utoronto.ca/~johns/nobots/theses/pdf/2017_keiming_kwong_masc.pdf (accessed Mar. 07, 2021).
- [161] K. Kwong, “MEMS Accelerometer Specifications and Their Impact in Inertial Applications,” p. 95, 2017.
- [162] J. Hidalgo, P. Poulakis, J. Köhler, J. Del-Cerro, and A. Barrientos, “Improving Planetary Rover Attitude Estimation via MEMS Sensor Characterization,” *Sensors 2012, Vol. 12, Pages 2219-2235*, vol. 12, no. 2, pp. 2219–2235, Feb. 2012, doi: 10.3390/S120202219.
- [163] C. McGeown, F. Huseynov, D. Hester, P. McGetrick, E. J. Obrien, and V. Pakrashi, “Using measured rotation on a beam to detect changes in its structural condition,” <https://doi.org.recursos.biblioteca.upc.edu/10.1080/24705314.2021.1906092>, vol. 6, no. 3, pp. 159–166, 2021, doi: 10.1080/24705314.2021.1906092.
- [164] M. Caruso *et al.*, “Analysis of the Accuracy of Ten Algorithms for Orientation Estimation Using Inertial and Magnetic Sensing under Optimal Conditions: One Size Does Not Fit All,” *Sensors 2021, Vol. 21, Page 2543*, vol. 21, no. 7, p. 2543, Apr. 2021, doi: 10.3390/S21072543.

- [165] R. C. Hibbeler, *Structural Analysis*. Pearson; 10th edition (July 28, 2017), ISBN: 0134610679, 2017.
- [166] “Wireless Industrial IOT Inclinometer Sensor | Overview - BeanAir | Wireless IOT Sensors.” <https://www.beanair.com/wireless-iot-inclinometer-sensor-overview.html> (accessed Sep. 17, 2021).
- [167] P. Kapita Mvemba, S. Kidiamboko Guwa Gua Band, A. Lay-Ekuakille, and N. I. Giannoccaro, “Advanced acoustic sensing system on a mobile robot: Design, construction and measurements,” *IEEE Instrum Meas Mag*, vol. 21, no. 2, pp. 4–9, Apr. 2018, doi: 10.1109/MIM.2018.8327971.
- [168] S. Komarizadehasl, B. Mobaraki, J. Lozano-Galant, and J. Turmo, “Practical Application of Low-Cost Sensors for Static Tests,” Sep. 2020. doi: 10.23967/dbmc.2020.207.
- [169] B. Mobaraki*, S. Komarizadehasl, F. J. C. Pascual, and J. A. L. Galant, “Open source platforms for monitoring thermal parameters of structures,” in *Bridge Maintenance, Safety, Management, Life-Cycle Sustainability and Innovations*, CRC Press, 2021, pp. 3892–3896. doi: 10.1201/9780429279119-532.
- [170] “Adafruit TCA9548A.” <https://learn.adafruit.com/adafruit-tca9548a-1-to-8-i2c-multiplexer-breakout> (accessed May 21, 2021).
- [171] Y. He, B. Liang, Y. Zou, J. He, and J. Yang, “Depth Errors Analysis and Correction for Time-of-Flight (ToF) Cameras,” *Sensors 2017, Vol. 17, Page 92*, vol. 17, no. 1, p. 92, Jan. 2017, doi: 10.3390/S17010092.
- [172] R. Baratov, Y. Chulliyev, and S. Ruziyev, “Smart system for water level and flow measurement and control in open canals,” *E3S Web of Conferences*, vol. 264, p. 04082, Jun. 2021, doi: 10.1051/E3SCONF/202126404082.
- [173] S. W. Kim and Y. K. Lee, “Accurate Water Level Measurement in the Bridge Using X-Band SAR,” *IEEE Geoscience and Remote Sensing Letters*, vol. 19, 2022, doi: 10.1109/LGRS.2021.3138396.
- [174] “Ifm electronic laser distance sensor O1D100 - O1DL... | Automation24.” https://www.automation24.es/sensor-de-distancia-laser-ifm-electronic-o1d100-o1dlf3kg?previewPriceListId=1&gclid=Cj0KCQjwqKuKBhCxAARIsACf4XuFkoS-XBv4R8wEcktYqU4f_oCW-bs1R1oGPVj5Ng7xZ2tjhHj2lnhIaApx0EALw_wcB (accessed Sep. 22, 2021).
- [175] R. R. Ribeiro and R. de M. Lameiras, “Evaluation of low-cost MEMS accelerometers for SHM: frequency and damping identification of civil structures,” *Latin American Journal of Solids and Structures*, vol. 16, no. 7, Jul. 2019, doi: 10.1590/1679-78255308.
- [176] “356A01 data-sheet.” https://www.pcb.com/contentstore/docs/PCB_Corporate/Vibration/Products/Manuals/356A01.pdf (accessed Jul. 25, 2022).
- [177] “Data Acquisition Handbook.” <https://www.mccdaq.com/support/Data-Acquisition-Handbook> (accessed Mar. 06, 2021).
- [178] “IAC-Hires data-sheet.” <https://micromega-dynamics.com/wp-content/uploads/2020/03/IAC-HiRes-I-01-EN-Rev1p2.pdf> (accessed Mar. 24, 2021).
- [179] “PCB Model 3713F112G data-sheet.” <https://www.pcb.com/products?m=3713F112G> (accessed Jul. 24, 2022).

135

- [180] “Unquake accelerometer data-sheet.” <https://www.unquake.co/en/products> (accessed Mar. 23, 2021).
- [181] “RecoVibTiny data-sheet.” <https://micromega-dynamics.com/wp-content/uploads/2020/01/RecoVibTiny-EN-Rev1p4.pdf> (accessed Jul. 24, 2022).
- [182] A. Airouche, H. Aknouche, H. Bechtoula, N. Mezouer, and A. Kibboua, “Performance of the CGS six DOF shaking table on the harmonic signal reproduction,” *Periodica Polytechnica Civil Engineering*, vol. 62, no. 1, pp. 102–111, 2018, doi: 10.3311/PPCI.9033.
- [183] Q. K. Dang and Y. S. Suh, “Sensor Saturation Compensated Smoothing Algorithm for Inertial Sensor Based Motion Tracking,” *Sensors 2014, Vol. 14, Pages 8167-8188*, vol. 14, no. 5, pp. 8167–8188, May 2014, doi: 10.3390/S140508167.
- [184] M. V. Potter, L. V. Ojeda, N. C. Perkins, and S. M. Cain, “Effect of IMU Design on IMU-Derived Stride Metrics for Running,” *Sensors 2019, Vol. 19, Page 2601*, vol. 19, no. 11, p. 2601, Jun. 2019, doi: 10.3390/S19112601.
- [185] “Acoustic and Vibration Calibration | Applus+ Laboratories.” <https://www.appluslaboratories.com/global/en/what-we-do/service-sheet/acoustic-and-vibration-calibration> (accessed Jul. 25, 2022).
- [186] S. C. Sun and G. C. Shi, “Research on the output characteristics of MEMS convective accelerometer under heavy impact,” *4th IEEE International Conference on Nano/Micro Engineered and Molecular Systems, NEMS 2009*, pp. 33–36, 2009, doi: 10.1109/NEMS.2009.5068521.
- [187] M. Lindstrom, “Written By What’s Wrong With My Piezoelectric Accelerometer? ,” *PCB* . www.pcb.com (accessed Jul. 23, 2022).
- [188] “REAL VNC Viewer | VNC® Connect.” <https://www.realvnc.com/en/connect/download/viewer/> (accessed Jul. 23, 2022).
- [189] “Frequency Domain Decomposition (FDD).” https://ww2.mathworks.cn/matlabcentral/fileexchange/50988-frequency-domain-decomposition-fdd?s_tid=ta_fx_results (accessed May 28, 2022).

Appendix 1: Publications



Article

Development of a Low-Cost System for the Accurate Measurement of Structural Vibrations

Seyedmilad Komarizadehasl ¹, Behnam Mobaraki ², Haiying Ma ^{3,*}, Jose-Antonio Lozano-Galant ² and Jose Turmo ¹

¹ Department of Civil and Environment Engineering, Universitat Politècnica de Catalunya, BarcelonaTech. C/Jordi Girona 1-3, 08034 Barcelona, Spain; milad.komary@upc.edu (S.K.); Jose.turmo@upc.edu (J.T.)

² Department of Civil Engineering, Universidad de Castilla-La Mancha, Av. Camilo Jose Cela s/n, 13071 Ciudad Real, Spain; Behnam.mobaraki@uclm.es (B.M.); Joseantonio.lozano@uclm.es (J.-A.L.-G.)

³ Department of Bridge Engineering, Tongji University, Shanghai 200092, China

* Correspondence: mahaiying@tongji.edu.cn

Abstract: Nowadays, engineers are widely using accelerometers to record the vibration of structures for structural verification purposes. The main obstacle for using these data acquisition systems is their high cost, which limits its use to unique structures with a relatively high structural health monitoring budget. In this paper, a Cost Hyper-Efficient Arduino Product (CHEAP) has been developed to accurately measure structural accelerations. CHEAP is a system that is composed of five low-cost accelerometers that are connected to an Arduino microcontroller as their data acquisition system. Test results show that CHEAP not only has a significantly lower price (14 times cheaper in the worst-case scenario) compared with other systems used for comparison but also shows better accuracy on low frequencies for low acceleration amplitudes. Moreover, the final output results of Fast Fourier Transformation (FFT) assessments showed a better observable resolution for CHEAP than the studied control systems.

Keywords: arduino; structural health monitoring (SHM); Internet of Things (IoT); accelerometer; low-cost sensors



Citation: Komarizadehasl, S.; Mobaraki, B.; Ma, H.; Lozano-Galant, J.-A.; Turmo, J. Development of a Low-Cost System for the Accurate Measurement of Structural Vibrations. *Sensors* **2021**, *21*, 6191. <https://doi.org/10.3390/s21186191>

Academic Editors: Rafal Burdzik, Minvydas Ragulskis, Maosen Cao, Radoslaw Zimroz, Chaari Fakher and Lukasz Konieczny

Received: 4 August 2021
Accepted: 13 September 2021
Published: 15 September 2021

Publisher's Note: MDPI stays neutral with regard to jurisdictional claims in published maps and institutional affiliations.



Copyright: © 2021 by the authors. Licensee MDPI, Basel, Switzerland. This article is an open access article distributed under the terms and conditions of the Creative Commons Attribution (CC BY) license (<https://creativecommons.org/licenses/by/4.0/>).





1. Introduction

Civil structures and infrastructures could be considered as the main foundation of today's modern society and, hence, their soundness is of utmost importance. However, the reports of ASCE infrastructure grades shows that in the United States: (1) 9.1% of all the bridges are not structurally efficient, (2) 188 million trips are taken every day over these deficient bridges, (3) The average age of bridges is 43 years old [1]. Monitoring and evaluating the health state of these structures are required for the maintenance applications, for minimizing the reparation costs and, eventually, for guaranteeing infrastructure safety [2–4]. Structural Health Monitoring (SHM) applications provide information on the state of structures, their functioning, and their structural response. As pointed out by many scholars (see, e.g., [5]), SHM can be used to calibrate structural models of real structures (digital twins [6]) that mimic the infrastructure performance to assess the decision-making process during the maintenance phase [7–9].

SHM systems are composed of sensors that measure the structural response (such as accelerations, rotations, strains, or deflections) over time. This information can be used to estimate changes in the structural performance of infrastructures [10–12]. The time variation of some environmental factors (such as temperature or humidity) that could produce crack opening, rotations, settlements, corrosion and other pathologies is so slow that they can be considered as quasi-static or static [13]. On the other hand, some events (such as the wave response due to earthquake ground motion, traffic-induced vibrations,

Article

Low-Cost Sensors Accuracy Study and Enhancement Strategy

Seyedmilad Komarizadehasl ¹, Behnam Mobaraki ², Haiying Ma ^{3,*}, Jose-Antonio Lozano-Galant ²
and Jose Turmo ¹

¹ Department of Civil and Environment Engineering, Universitat Politècnica de Catalunya, BarcelonaTech, C/Jordi Girona 1-3, 08034 Barcelona, Spain; milad.komary@upc.edu (S.K.); jose.turmo@upc.edu (J.T.)

² Department of Civil Engineering, Universidad de Castilla-La Mancha, Av. Camilo Jose Cela s/n, 13071 Ciudad Real, Spain; behnam.mobaraki@uclm.es (B.M.); joseantonio.lozano@uclm.es (J.-A.L.-G.)

³ Department of Bridge Engineering, Tongji University, Shanghai 200092, China

* Correspondence: mahaiying@tongji.edu.cn

Abstract: Today, low-cost sensors in various civil engineering sectors are gaining the attention of researchers due to their reduced production cost and their applicability to multiple nodes. Low-cost sensors also have the advantage of easily connecting to low-cost microcontrollers such as Arduino. A low-cost, reliable acquisition system based on Arduino technology can further reduce the price of data acquisition and monitoring, which can make long-term monitoring possible. This paper introduces a wireless Internet-based low-cost data acquisition system consisting of Raspberry Pi and several Arduinos as signal conditioners. This study investigates the beneficial impact of similar sensor combinations, aiming to improve the overall accuracy of several sensors with an unknown accuracy range. The paper then describes an experiment that gives valuable information about the standard deviation, distribution functions, and error level of various individual low-cost sensors under different environmental circumstances. Unfortunately, these data are usually missing and sometimes assumed in numerical studies targeting the development of structural system identification methods. A measuring device consisting of a total of 75 contactless ranging sensors connected to two microcontrollers (Arduinos) was designed to study the similar sensor combination theory and present the standard deviation and distribution functions. The 75 sensors include: 25 units of HC-SR04 (analog), 25 units of VL53L0X, and 25 units of VL53L1X (digital).

Keywords: Arduino; time-of-flight sensors; distribution functions; standard deviation; low-cost sensors; HC-SR04; CHEAP; accuracy enhancement; noise reduction



Citation: Komarizadehasl, S.; Mobaraki, B.; Ma, H.; Lozano-Galant, J.-A.; Turmo, J. Low-Cost Sensors Accuracy Study and Enhancement Strategy. *Appl. Sci.* **2022**, *12*, 3186. <https://doi.org/10.3390/app12063186>

Academic Editors: Yun-Kyu An and Soojin Cho

Received: 24 February 2022

Accepted: 18 March 2022

Published: 21 March 2022

Publisher's Note: MDPI stays neutral with regard to jurisdictional claims in published maps and institutional affiliations.



Copyright: © 2022 by the authors. Licensee MDPI, Basel, Switzerland. This article is an open access article distributed under the terms and conditions of the Creative Commons Attribution (CC BY) license (<https://creativecommons.org/licenses/by/4.0/>).

1. Theoretical Background

The demand for efficient and low-cost monitoring continues to increase. This matter can be the first step toward reducing the uncertainty of building monitoring by increasing the density of measurement points. Bilro et al. reviewed the potential application of optical sensors based on plastic fibers used for low-cost structural response monitoring [1]. Barrias et al. presented the theoretical background of distributed optical fiber sensors and their multiple applications in building monitoring [2]. Mobaraki et al. provided a systematic literature review of low-cost sensor applications for building monitoring [3]. Rodrigues and Li reviewed the recent achievements in low-cost Doppler radar systems for displacement measurement and Time-Doppler analysis for structural monitoring [4]. Kohler et al. installed cheap seismometers in a building in Los Angeles to assess the shaking intensity caused by earthquakes [5]. The primary objectives of the developed protocol were to compute the modal characteristics of the structure, such as mode shape and frequencies. Due to the high level of earthquake activity in New Zealand, Simkin et al. installed low-cost accelerometers in a couple of houses in Wellington to monitor the dynamic behavior of the buildings during earthquake excitations [6]. Application of low-cost accelerometers for monitoring dynamic behavior of scale structures in laboratory were



Article

A Novel Wireless Low-Cost Inclinometer Made from Combining the Measurements of Multiple MEMS Gyroscopes and Accelerometers

Seyedmilad Komarizadehasl ¹, Mahyad Komary ¹, Ahmad Alahmad ¹, José Antonio Lozano-Galant ², Gonzalo Ramos ¹ and Jose Turmo ^{1,*}

¹ Department of Civil and Environment Engineering, Universitat Politècnica de Catalunya, BarcelonaTech. C/Jordi Girona 1-3, 08034 Barcelona, Spain; milad.komary@upc.edu (S.K.); mahyad.komarizadeh@upc.edu (M.K.); ahmad.alahmad@estudiantat.upc.edu (A.A.); gonzalo.ramos@upc.edu (G.R.)

² Department of Civil Engineering, Universidad de Castilla-La Mancha, Av. Camilo Jose Cela s/n, 13071 Ciudad Real, Spain; joseantonio.lozano@uclm.es

* Correspondence: jose.turmo@upc.edu

Abstract: Structural damage detection using inclinometers is getting wide attention from researchers. However, the high price of inclinometers limits this system to unique structures with a relatively high structural health monitoring (SHM) budget. This paper presents a novel low-cost inclinometer, the low-cost adaptable reliable angle-meter (LARA), which combines five gyroscopes and five accelerometers to measure inclination. LARA incorporates Internet of Things (IoT)-based microcontroller technology enabling wireless data streaming and free commercial software for data acquisition. This paper investigates the accuracy, resolution, Allan variance and standard deviation of LARA produced with a different number of combined circuits, including an accelerometer and a gyroscope. To validate the accuracy and resolution of the developed device, its results are compared with those obtained by numerical slope calculations and a commercial inclinometer (HI-INC) in laboratory conditions. The results of a load test experiment on a simple beam model show the high accuracy of LARA (0.003 degrees). The affordability and high accuracy of LARA make it applicable for structural damage detection on bridges using inclinometers.

Keywords: low-cost sensors; NodeMCU; Allan variance; noise reduction; influence line measurement; structural health monitoring



Citation: Komarizadehasl, S.; Komary, M.; Alahmad, A.; Lozano-Galant, J.A.; Ramos, G.; Turmo, J. A Novel Wireless Low-Cost Inclinometer Made from Combining the Measurements of Multiple MEMS Gyroscopes and Accelerometers. *Sensors* **2022**, *22*, 5605. <https://doi.org/10.3390/s22155605>

Academic Editor: Shihchuan Her

Received: 30 June 2022

Accepted: 23 July 2022

Published: 27 July 2022

Publisher's Note: MDPI stays neutral with regard to jurisdictional claims in published maps and institutional affiliations.



Copyright: © 2022 by the authors. Licensee MDPI, Basel, Switzerland. This article is an open access article distributed under the terms and conditions of the Creative Commons Attribution (CC BY) license (<https://creativecommons.org/licenses/by/4.0/>).

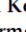



1. Introduction

Structural health monitoring (SHM) has attracted the attention of engineers over past decades as a control system to measure the structural response of structural elements to prevent future potential failures in civil infrastructures. A number of factors and situations such as construction defects, fatigue and environmental factors might decrease the structure's serviceability and safety over time [1–3]. Therefore, monitoring and assessing structures' health state throughout their life cycle is essential to minimize the future repair costs and to confirm the structural safety and serviceability [4,5]. SHM applications provide vital information about the actual structural response of infrastructures, the condition of the structures and their performance. As indicated by many scholars (such as [6,7]), SHM can be used to calibrate the simulated model of the real structures (digital-twin), which imitates the performance of the structures [8]. Digital twins can then be used to evaluate the decision-making alternatives during the maintenance phase of structures under study [9,10].

SHM measurements can be used to determine structural parameters with structural system identification techniques [11,12]. Structural system identification targets identifying

Article

Low-Cost Wireless Structural Health Monitoring of Bridges

Seyedmilad Komarizadehasl ¹, Fidel Lozano ², Jose Antonio Lozano-Galant ², Gonzalo Ramos ¹
and Jose Turmo ^{1,*}

- ¹ Department of Civil and Environment Engineering, Universitat Politècnica de Catalunya, BarcelonaTech. C/Jordi Girona 1-3, 08034 Barcelona, Spain; milad.komary@upc.edu (S.K.); gonzalo.ramos@upc.edu (G.R.)
² Department of Civil Engineering, Universidad de Castilla-La Mancha, Av. Camilo Jose Cela s/n, 13071 Ciudad Real, Spain; fidel.lozanolgalant@uclm.es (F.L.); joseantonio.lozano@uclm.es (J.A.L.-G.)
 * Correspondence: jose.turmo@upc.edu

Abstract: Nowadays, low-cost accelerometers are getting more attention from civil engineers to make Structural Health Monitoring (SHM) applications affordable and applicable to a broader range of structures. The present accelerometers based on Arduino or Raspberry Pi technologies in the literature share some of the following drawbacks: (1) high Noise Density (ND), (2) low sampling frequency, (3) not having the Internet's timestamp with microsecond resolution, (4) not being used in experimental eigenfrequency analysis of a flexible and a less-flexible bridge, and (5) synchronization issues. To solve these problems, a new low-cost triaxial accelerometer based on Arduino technology is presented in this work (Low-cost Adaptable Reliable Accelerometer—LARA). Laboratory test results show that LARA has a ND of 51 $\mu\text{g}/\sqrt{\text{Hz}}$, and a frequency sampling speed of 333 Hz. In addition, LARA has been applied to the eigenfrequency analysis of a short-span footbridge and its results are compared with those of a high-precision commercial sensor.

Keywords: Arduino Due; Raspberry Pi; accelerometers; low-cost sensors; eigenfrequency analysis; short-span footbridge



Citation: Komarizadehasl, S.; Lozano, F.; Lozano-Galant, J.A.; Ramos, G.; Turmo, J. Low-Cost Wireless Structural Health Monitoring of Bridges. *Sensors* **2022**, *22*, 5725. <https://doi.org/10.3390/s22155725>

Academic Editor: Yongbo Li

Received: 5 July 2022
 Accepted: 28 July 2022
 Published: 30 July 2022

Publisher's Note: MDPI stays neutral with regard to jurisdictional claims in published maps and institutional affiliations.



Copyright: © 2022 by the authors. Licensee MDPI, Basel, Switzerland. This article is an open access article distributed under the terms and conditions of the Creative Commons Attribution (CC BY) license (<https://creativecommons.org/licenses/by/4.0/>).

1. Introduction

Civil infrastructures and structures might be considered the leading basis of modern society; consequently, their health state is of the highest importance [1]. However, data provided by the American Society of Civil Engineers (ASCE) infrastructure indicates about 9.1% of bridges in the United States of America are structurally inefficient. Every day, over 188 million trips are taken across structurally deficient bridges. In addition, in average, a bridge in the United States of America is 43 years old, which is close to its expected life span [2].

Evaluating these structures along with their health-state assessment is needed to reduce repair costs, maintenance, and, eventually, for certifying infrastructure/structure safety [3–5]. Structural Health Monitoring (SHM) applications issue statistics on structures' functioning states and their structural responses [6–8].

For measuring the structural responses (such as deflections, strains, rotation, temperature, humidity, and accelerations) over time, sensors are widely used in SHM systems [9,10]. The recorded information of the sensors is then used for structural performance estimations [11–13]. In fact, natural phenomena can be categorized as static or quasi-static and dynamic [14–16]. On the one hand, some environmental elements (such as temperature or humidity) change very slowly, so they can be considered to perform either as quasi-static or static [17,18]. On the contrary, some events (such as traffic-induced vibrations, ambient activities, and waves from seismic activities) are considered dynamic because their changing rate is significantly affected by the time [19–21].

Accelerometers are force-sensors that are broadly used for measuring vibrations [22]. According to [23], accelerometers are frequently set up on one of the following principles: